DESIGN OF A CONTROLLABLE PITCH UNDERWATER THRUSTER SYSTEM

by

Robert W. Keefe

B.S. Ocean Engineering, United States Naval Academy, 1991

submitted in partial fulfillment of the
requirements for the dual degree of

MASTER OF SCIENCE IN OCEANOGRAPHIC ENGINEERING
at the
MASSACHUSETTS INSTITUTE OF TECHNOLOGY
and
WOODS HOLE OCEANOGRAPHIC INSTITUTION

and

MASTER OF SCIENCE IN MECHANICAL ENGINEERING
at the
MASSACHUSETTS INSTITUTE OF TECHNOLOGY
and the
WOODS HOLE OCEANOGRAPHIC INSTITUTION
August, 1993

Signature of Author_____
Department of Ocean Engineering, MIT and the
MIT-WHOI Joint Program in Oceanographic Engineering.

Certified by _____
Dr. Nathan T. Ulrich
Thesis Supervisor

Accepted by _____
Dr. Arthur B. Baggeroer
Chairman, Joint Committee for Applied Ocean Sciences and Engineering,
Massachusetts Institute of Technology - Woods Hole Oceanographic Institution

Design of a Controllable Pitch Underwater Thruster System

Robert W. Keefe

Submitted in partial fulfillment of the requirements
for the degrees of Master of Science
in Oceanographic Engineering and Master of
Science in Mechanical Engineering

at the

MASSACHUSETTS INSTITUTE OF TECHNOLOGY
and the
WOODS HOLE OCEANOGRAPHIC INSTITUTION

August, 1993

ABSTRACT

Control systems for underwater vehicles have reached the level of sophistication where they are limited by the dynamic performance of the thrust actuators. Standard fixed-pitch propellers have been shown to have very poor dynamic characteristics, particularly at low thrust levels The dynamic response of a fixed-pitch propeller is dependent upon highly non-linear transients encountered while the shaft speed approaches its steady-state value. This thesis proposes the use of a controllable pitch propeller system to address this problem. A controllable pitch propeller varies the amount of thrust produced by varying the pitch angle of the blades at a constant shaft speed. The bandwidth of this type of thrust actuator would be dependent primarily on the speed at which the pitch angle of the blades are changed. A variable pitch propeller system suitable for retrofit into an ROV is designed and built. The system is designed for maximal pitch angle bandwidth with low actuator power consumption.

ACKNOWLEDGMENTS

I owe a great debt to large number of people for the completion of this thesis and successful completion of my program. I wish to thank the U.S. Navy, and especially the office of the Oceanographer of the Navy, RADM Chesborough, for allowing me to pursue my interests in a postgraduate setting. Thanks also to Captain Fields, Commander Celotto, Captain Brown, and especially Jennifer Laible for greasing the official skids and freeing me to concentrate on my work. I eagerly look forward to paying the Navy back in the coming years.

Thanks to my advisor, Dr. Nathan Ulrich, for directing my work and being a great sounding board for ideas and designs. Without his time and concern this thesis would not have been possible.

Thanks to the crew down at DSL for showing me how science is done, for motivating me with the practical application of my work, and for being great friends, especially: Will Sellers for his experience, practical skills, and shared interest in the New Yankee Workshop, Marty Marra and John Howland for their indispensable help with the computer system, and Steve Gegg for helping me with one of the most difficult aspects of this thesis, plotting the mechanical drawings.

Thanks to Dr. Warren Seering and Dr. Alex Slocum for helping me make a quantum leap in my mechanical design skills. Their instruction, insight, and personal example were instrumental in my ability to produce a functional design.

Thanks to Commander Curt Murphy for taking me under his wing and using his nearly 30 years experience in the Navy to bring this boot Ensign up to speed. I'll miss our interesting discussions.

Thanks to my fellow students. Tad Snow has my deepest gratitude for his constant help, guidance, experience, and friendship. I often feel I learned as much from him as from any of my professors. Thanks to Hanu Singh, my fellow "Navy guys" Gary Edwards, Larry Galvin, Steve Bowen, Dennis Wojcik, Chris Willy, Dan Leader, Mike Hajosy, and the rest of my friends as Woods Hole and MIT. You have made my time here worthwhile and enjoyable.

Thanks, of course, to my parents. They may not understand all that's in this thesis, but through their support, encouragement, emphasis on education, and love, they are responsible for it.

Finally, thanks to my best friend, my wife Sheila. She was there through the best and worst times, always supportive, encouraging, and reminding me of my goal. It is to her that this thesis is dedicated.

TABLE OF CONTENTS

LIST OF FIGURES

Chapter 1
INTRODUCTION

Modern underwater remotely operated vehicles are often tasked with operations requiring precise positioning and vehicle control. Typical vehicle missions include precise survey of bottom features and artifacts where the vehicle is required to closely follow a prescribed trajectory. The vehicles may be involved with recovery of delicate biological or archaeological objects where even motion of only a few centimeters could damage or destroy the finds. In addition, commercial remotely operated vehicles, or ROV's, often are called upon to manipulate underwater machinery.

Computer algorithms of ever-increasing complexity are being developed to address the issue of precise vehicle control, but in many cases they are limited by the performance of the vehicle actuators. The standard method of providing thrust, the fixed-pitch propeller, while relatively efficient, inexpensive, and easy to maintain, is a poor dynamic actuator. The step response of a typical fixed-pitch propeller to a step torque input is highly non-linear. Indeed, the thrust bandwidth, a measure of dynamic thrust performance, actually decreases as the steady-state thrust decreases [1]. This translates

into poorer dynamic thrust response during low-thrust operations such as station-keeping and hover—the very operations requiring the best dynamic performance.

This thesis presents a thrust actuator designed to deliver vastly superior dynamic response when compared to a fixed-pitch propeller. The controllable-pitch thruster system presented relies upon high speed alterations of the pitch of its blades during operation to achieve variations in thrust. It is designed with the ability to be retrofitted into an existing ROV utilizing the ROV's thruster motor as an actuator and fitting inside a 25 cm diameter propeller shroud. The pitch actuation is accomplished electrically using minimal power.

Chapter 2 describes two different dynamic models for fixed-pitch propellers, highlighting the propeller's deficiencies as dynamic actuators.

Chapter 3 reviews a number of alternative methods of thrust actuation.

Chapter 4 examines applications of these alternative devices in improvement of dynamic performance. The controllable pitch propeller is chosen from among several options.

Chapter 5 sets forth the mechanical design of the controllable pitch propeller system. The system is modeled statically and dynamically.

Chapter 6 reviews the design of the propeller blades. A brief review of propeller theory is included.

Chapter 7 discusses the debugging process and makes recommendations regarding ultimate test and redesign of the propeller system.

Appendix A lists the symbols used in the mechanical analysis of the system in Chapter 5.

Appendix B is a listing of the mechanical drawing from which the propeller was constructed.

Chapter 2
REVIEW OF PROPELLER DYNAMIC PERFORMANCE

2.1 Current Models

In recent years, the advent of advanced ROV control schemes has led to the development of models to describe propeller dynamic performance. Two such models have been prepared by John Cooke [1] and Michael McLean [2]. Cooke's model is derived from a momentum flux analysis of the fluid through the thruster. A schematic of a typical shrouded propeller is shown in figure 2-1. The propeller is driven at an angular velocity, ω, by some torque, τ. A fluid of density, ρ, flows through the shroud or duct of area, A, and volume, V, at a volumetric flow rate, Q. A number of simplifying assumptions are made: friction is ignored, the kinetic energy of the ambient flow is negligible,

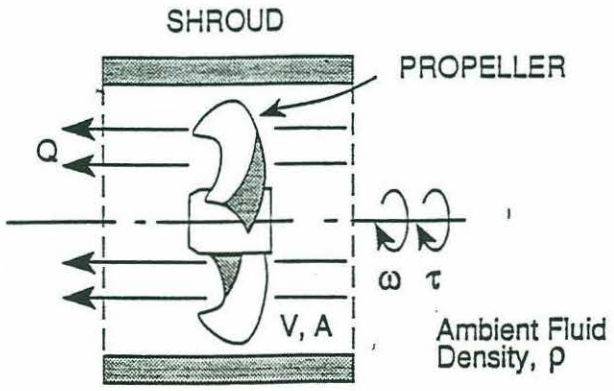

Fig. 2-1. Typical thruster schematic. [1]

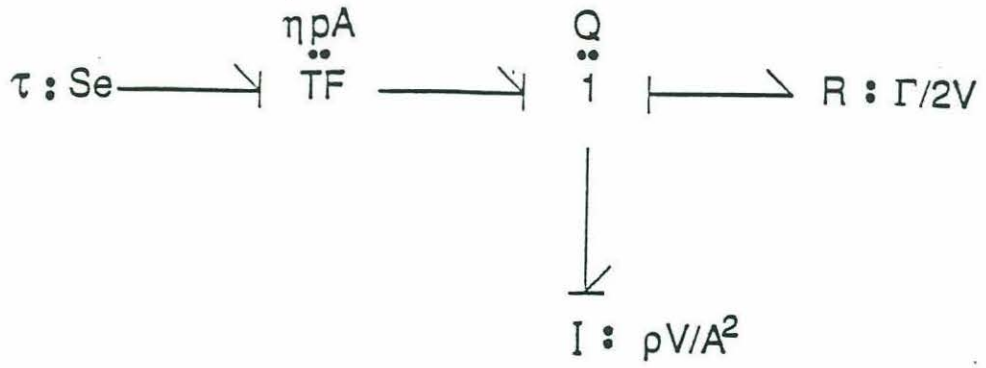

Fig.2-2 Bond graph of thruster system.[1]

compressibility is ignored, and the flow into and out of the duct is parallel and at ambient pressure. A bond graph is used to analyze the energy flux through the duct (figure 2-2). The kinetic co-energy of the fluid in the thruster, T* is related to the volumetric flow rate by

$$T^*(Q) = \frac{1}{2}\rho V\left(\frac{Q}{A}\right)^2$$

A generalized momentum, Γ, is then defined as

$$\Gamma = \frac{dT^*}{dQ} = \rho V\frac{Q}{A^2}$$

Since the energy relations are linear, the co-energy and energy have equal magnitudes[3]. The kinetic energy T can be expressed in terms of the pressure momentum,

$$T(\Gamma) = \frac{A^2}{2\rho V}\Gamma^2 = T^*(Q)$$

Performance of a power balance yields,

$$\frac{dT}{dt} = \frac{A^2}{2\rho V}\Gamma\dot{\Gamma} = \omega\tau - KQ$$

where K represents the exiting kinetic energy per unit volume. This quantity can be derived as

$$K = \frac{A^2\Gamma^2}{2\rho V^2} = \frac{\gamma^2}{2\rho}$$

where

$$\gamma \equiv \frac{A\Gamma}{V}$$

The thrust is simply the convected linear momentum.

$$Thrust \equiv \gamma Q$$

The volumetric flow rate through the duct is defined in terms of the propeller pitch, p, and the volumetric efficiency of the propeller, η_v. The propeller pitch is the axial distance advanced by the helix formed by lines tangent to the propeller blades as they move through one complete revolution. The volumetric flow rate is given by

$$Q = \eta_v p A \omega$$

Combining the above equations results in a non-linear relation between thrust and shaft speed.

$$\dot{\omega} = \frac{\tau}{\eta^2 p^2 \rho V} - \frac{\eta p A}{2V}\omega|\omega|$$

$$Thrust = A\rho\eta^2 p^2 \omega|\omega|$$

The resultant step response is shown in figure 2-3 for a representative thruster given three different torque commands.

The McLean model is developed along similar lines, but includes a term representing the acceleration of the added mass of fluid inside the thruster duct to the thrust equation. Additionally, a number of correction factors (β, α) are added to account for variations in the input and output kinetic energy across the cross-section of the thruster duct. A final correction factor, K_a, increases the effective length of the duct to account for the influence of fluid outside of the duct. The equations for the McLean model are

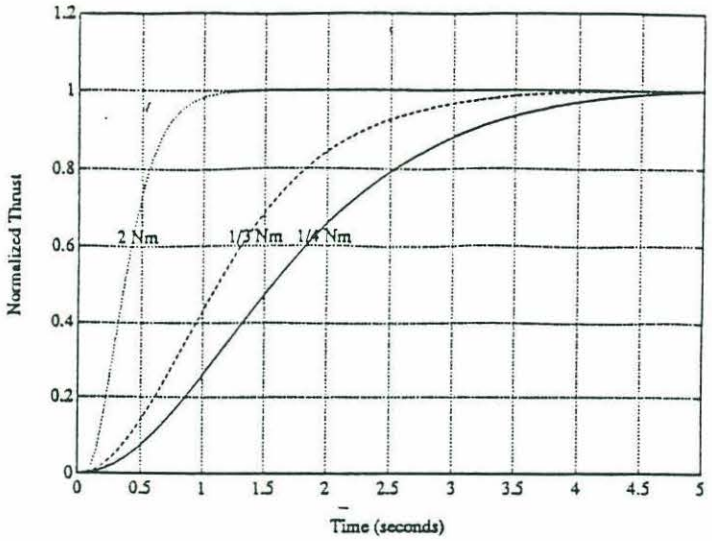

Fig. 2-3. Normalized step response of thruster model. [1]

$$\tau = (\eta p)^2 \rho A L (K_a + 1)\beta \dot{\omega} + \frac{(\eta p)^3 \rho A}{2}(\alpha_o - \alpha_i)\omega|\omega$$

$$Thrust = (\eta p)^2 \rho A L (K_a + 1)\dot{\omega} + (\eta p)^2 \rho A (\beta_o - \beta_i)\omega|\omega|$$

The step response of this model is similar to the Cooke model, but contains an acceleration term (fig. 2-4).

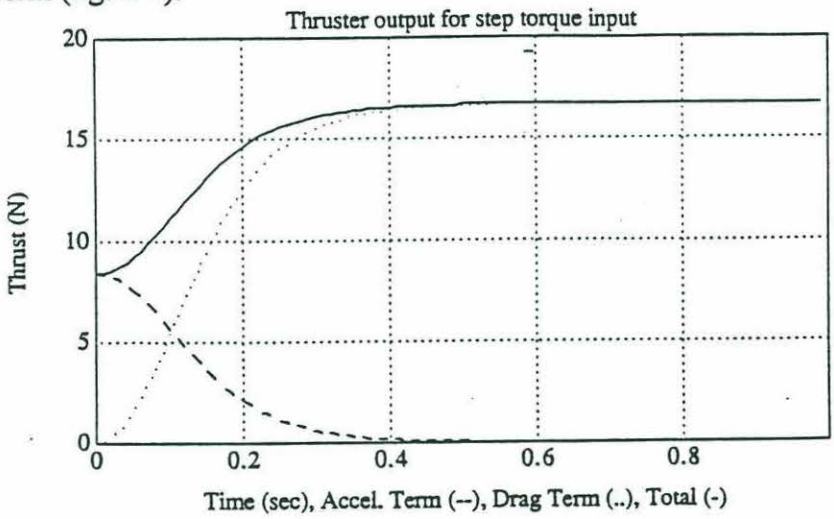

Fig. 6-4 Thrust response predicted by McLean. The step response is shown by the solid line. [2]

2.2 Comparison of models

Both models produce highly non-linear response. The Cooke model demonstrates one critical shortcoming of fixed pitch propellers—as the commanded thrust decreases, the dynamic response decreases. In practice, this means that the propeller exhibits poorer dynamic response during station-keeping and hover operations, where low thrust output is desired, than it does during normal operation. The McLean model does predict an immediate step response component to a step input torque. This response is, however, not seen in practice due to friction and lack of flow development. Typically a foil must translate at least six chord lengths before steady state flow is achieved.

The ideal thrust actuator would have infinite bandwidth and infinite range. Unfortunately, such an actuator is impossible to build. A high-performance actuator for maximum maneuverability would have three qualities.

1. Highest bandwidth at low thrust levels.
2. Ability to utilize all thrust levels within the thruster's range.
3. High repeatability.

While a fixed-pitch propeller satisfies the last two of these qualifications, it fails to meet the first. This thesis describes and attempt to design an actuator which satisfies all three requirements.

Chapter 3
ALTERNATIVE PROPULSION DEVICES

3.1 Controllable Pitch Propellers

There are a number of alternatives to fixed pitch propellers which may yield improved dynamic response. Perhaps the most promising is the controllable pitch (CP) propeller. This system allows for real-time control of the pitch angle of the propeller blades to vary the thrust produced. Using this type of system, the dynamic performance of thrust response, can be made largely independent of the startup non-linearities of a fixed pitch propeller, and instead be dependent on a comparatively high bandwidth pitch actuator.

CP propellers have been used for nearly a century on commercial ships. They are primarily used in special applications to improve efficiency. Ships encountering widely varying operating conditions, such as tugs and icebreakers, use them to maximize efficiency both when traveling in the open ocean, and when providing a pushing or pulling force at low speed. Certain types of marine engines operate efficiently only over a small

range of shaft speeds. Ships using these engines of this sort, diesel or gas turbine drives ships for example, use CP propellers to provide a wide range of thrust levels while maintaining optimum shaft speed. Other ships may lack reversing gears in their transmission to save space or weight. Inclusion of a CP propeller on these ships allows for thrust reversal through pitch change alone. Finally, CP propellers are used on vessels where rapid and frequent thrust modifications are required, most notably on military vessels.

Controllable pitch propellers are, however, not without their disadvantages. Most significant to commercial shipping is the somewhat decreased efficiency seen in CP systems when compared to conventional propellers. Fixed pitch propeller blades are optimized for the specific a pitch. Instead, CP propeller blades must operate effectively over a range of pitch settings, and are suboptimal for any given pitch. On well-designed systems the efficiency of CP systems is on the order of 5% poorer than for similar fixed-pitch propellers.

Another disadvantage is the substantial cost of a controllable pitch propeller system. These systems require special shafting, hydraulics, and bridge controls in addition to the complex propeller itself. The cost of these components can be dozens of times the cost of a simple fixed pitch propeller. These components also occupy space and contribute to the total weight of a ship. These drawbacks have prevented CP systems from becoming a common fixture in modern shipping.

CP systems on commercial vessels invariably rely on hydraulic actuation. A representative CP mechanism includes some mechanical means of converting axial force to

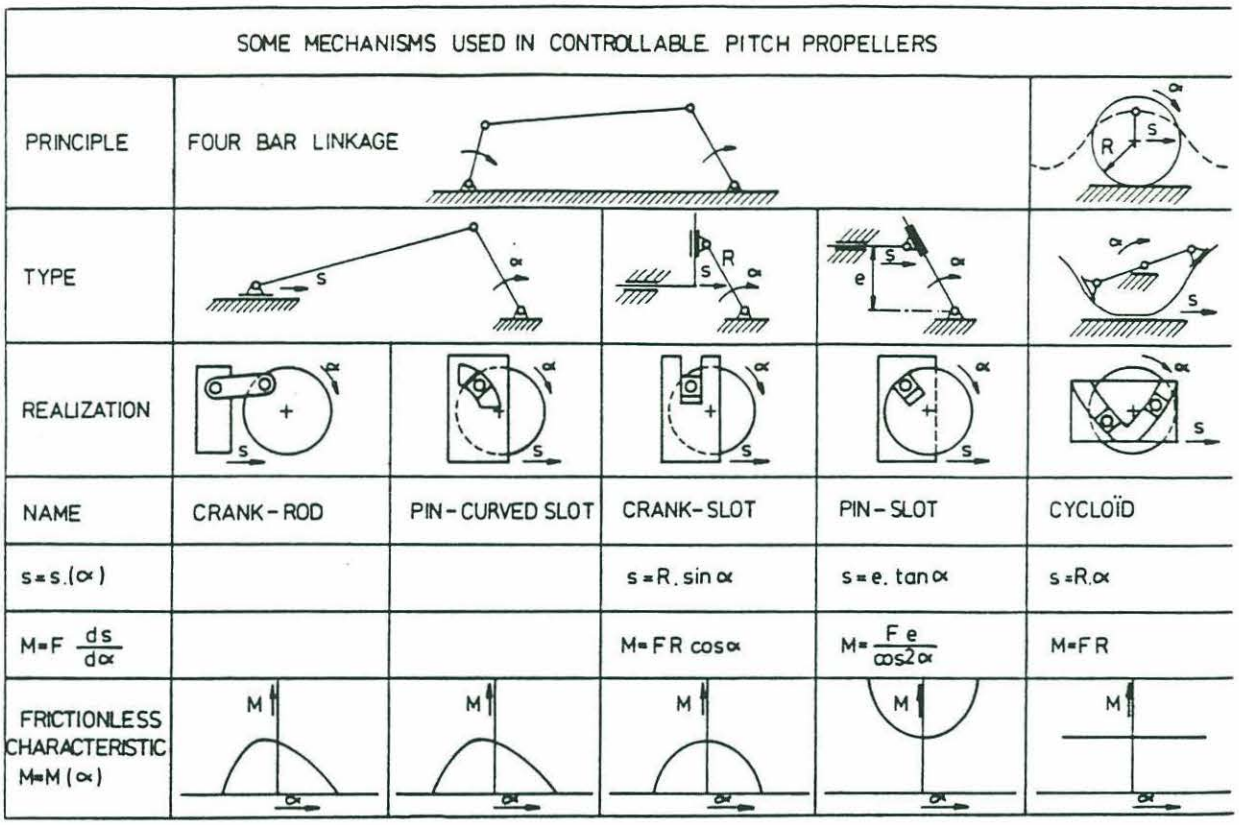

Fig. 3-1 [11]

torque, usually involving an eccentric pin and fixed axis of rotation. An axial force is applied by means of a hydraulic ram within the propeller hub. This force moves a block, usually called a crosshead, axially within the hub. Eccentric pins on the base of the shafts to which the propeller blades are connected, called the spindles, mate to the crosshead through an eccentric pin or lever. When the crosshead moves axially, the pin or lever imparts a torque on the spindle rotating the propeller blade. The rams used are double acting to achieve both advancing and reversing of blade pitch. The hydraulic oil flows from the pump located within the hull of the ship through ducts within the propeller shaft. Note that the decoupling of the rotating propeller and the stationary pumping equipment is done through the hydraulic fluid.

The blades themselves are usually bolted to their support system to allow easy change-out. Blades are produced to achieve maximum efficiency for a certain narrow range of expected operating conditions. For example, an icebreaker might be optimized for maximum thrust at speeds of 5 to 8 knots. This optimization leads to non-linear thrust response when compared to pitch angle. The icebreaker propeller in question might not achieve negative thrust until the blade pitch is -8 degrees or so. These non-linearities can be abated, but only at the cost of decreased maximum efficiency.

CP systems differ most widely in the specific mechanism for changing ram force to spindle torque. Several different mechanism are shown in figure 3-1. Each system is optimized to provide the greatest mechanical advantage at a specific operating point. One of the most common pitch changing systems is the crank-connecting rod mechanism. This design, reminiscent of old steam engine pistons, uses a rod connecting the crosshead to an ear on the spindle shaft. Another design, called the crank-slot mechanism connects sliding sockets on the crosshead to fixed pins on the spindle shaft. The sockets permit rotation but prevent translation in the direction parallel to the axis of the ram. Similar to this design is the slot-pin mechanism where the socket slides in a slot in a disk connected to the base of the spindle instead of in the crosshead [4].

The other primary distinguishing aspect of a propeller design is the mechanism by which the propeller blades are supported within the housing. There are two common ways of doing this, shown in figure 3-2. The trunnion type of blade support uses two bushings on the base of the propeller spindle exerting axial resistive forces. The other uses a large disk on the base of the propeller blade. This disk has a smaller diameter section between

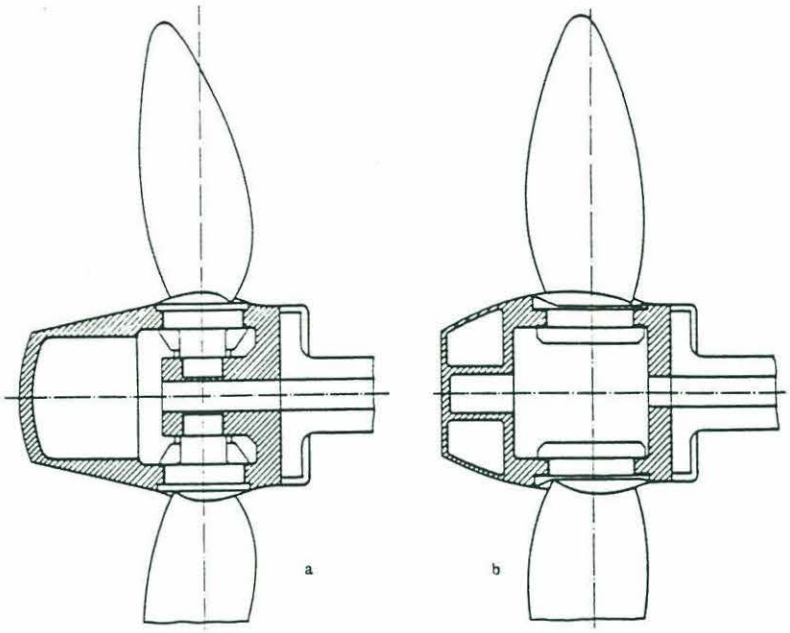

Fig. 3-2. The trunnion (a) and disk-type (b) blade support mechanisms. [4]

two larger diameter sections. A single bushing riding in this smaller diameter section resists all forces and moments on the blade. This design is often combined with the crank-slot pitch changing mechanism.

3.2 Helicopter Blade Pitch Actuation

Controllable pitch propulsor blades are not limited to marine applications. The ability to dynamically control blade pitch is essential to helicopter operation. The high bandwidth of helicopter blade pitch actuators makes the study of these systems instructive to those designing high speed marine CP mechanisms.

Helicopters must have the ability to control the pitch of each propeller blade individually. This allows the helicopter to generate differing levels of thrust at different locations on the propeller disk. This differential in thrust levels changes the direction of the

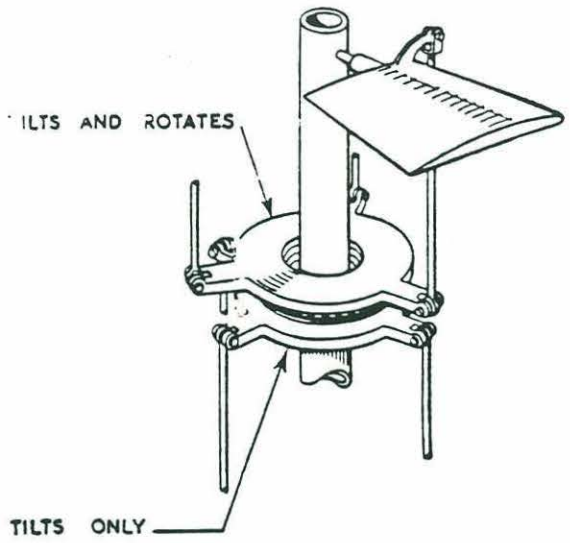

Fig. 3-3 Schematic of propeller pitch actuation system. [12]

resultant thrust vector. Since the pitch of the blades varies systematically throughout each rotation cycle, this type of control is termed *cyclic* pitch control. To increase the magnitude of the thrust vector, the baseline pitch of the blades are increased throughout the cycle. The changing of the pitch of the blades without regard to cyclic position is termed *collective* pitch control. The marine CP propellers described earlier in this chapter control the pitch of all blades equally and hence have only collective control over the blades.

Helicopter pitch control mechanisms differ from marine CP propellers primarily in their requirement for cyclic pitch control. A schematic of a helicopter pitch control system is shown in figure 3-3. Each individual blade has a mechanism nearly identical to the crank connecting rod mechanism used in marine propellers. The rods connect to protuberances on the blades near the hub called horns. Instead of connecting to a crosshead, however, the connecting rods are connected to a rodplate through spherical bearings. This rodplate rotates with the propeller blades around the propeller axis, and rides on a stationary

swashplate. The swashplate is controlled, either mechanically or hydraulically, to translate along the propeller axis or to tilt in any direction. The translation is analogous to the axial movement of the hydraulic ram in the crank connecting rod mechanism, causing a collective change in pitch. Tilting the swashplate causes the connecting rods to push and pull in a cyclic pattern giving the pilot cyclic control.

3.3 Tandem Propeller System

A marine propulsion system has been constructed utilizing both collective and cyclic control. The Tandem Propeller System (TPS) developed by Ted Haselton and John Goode at Imagineering is designed to provide 6 degree of freedom control for a cigar-shaped underwater vehicle. One propulsor is placed coaxially at each end of the vehicle. Using cyclic control to "aim" the force vectors of the propulsors, and collective control to adjust their magnitude, any combination of net force and torque can be developed (figure 3-4). The pitch of the blades is controlled in a manner similar to that of the helicopter. TPS uses a swashplate and rodplate operating in a manner similar to those of a helicopter. Instead of using connecting rods, the TPS system relies upon the friction between a rod protruding from the rodplate and a capstan drum attached to the blade's spindle. When the rod moves toward the blades, the rod rotates the capstan pitching the blade. This system has proven to be very complex and expensive and has some sealing problems.

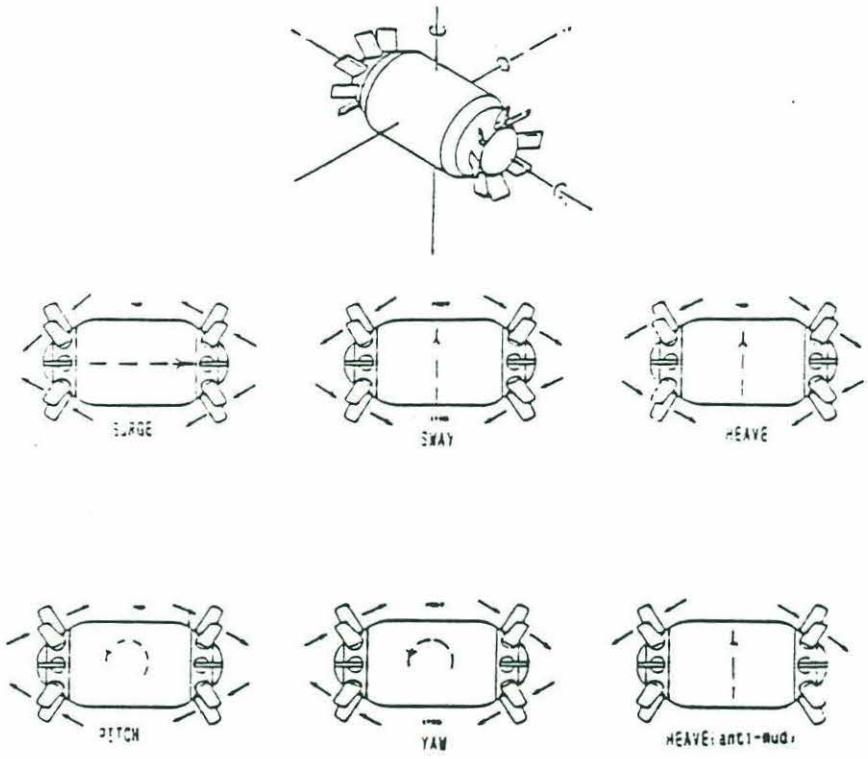

Fig. 3-4. Schematic of TPS showing different thrust modes. [5]

3.4 Vertical Axis Propeller

Another unique type of marine propulsion is the vertical axis propeller. This class of propulsor uses a disk mounted on the bottom of a ship hull from the bottom of which several blades protrude. This disk rotates at a set speed, and the blades undergo some cyclic variation in angle.

The Kirsten-Boeing type is geared such that each blade undergoes a half revolution about its axis for each revolution of the disk. If a line were drawn along each

blade these lines would intersect at some point on the circle described by the rotation of the blade axes with the disk. This is the effective center of rotation of the blade angles. The operation of this type of propeller is shown in fig. 3-5. In view (a) the net of the normal blade forces, N, produces a thrust vector, T, parallel to the direction of travel, V_O. Views (b) and (c) show a reverse and sideward thrust respectively.

A second type, the Voith-Schneider, is similar to the Kirsten-Boeing, differing only in its ability to place the effective center of blade rotation at an arbitrary point in the plane of the propeller disk. This requires each blade to undergo a complete rotation per disk rotation. The action of this propeller is shown in fig.3-6. Both types of propellers have been employed effectively in commercial shipping. They are primarily used on ships requiring precise positioning capability, such as oceanographic research and survey vessels, and vessels requiring precise positioning in restricted waters [6].

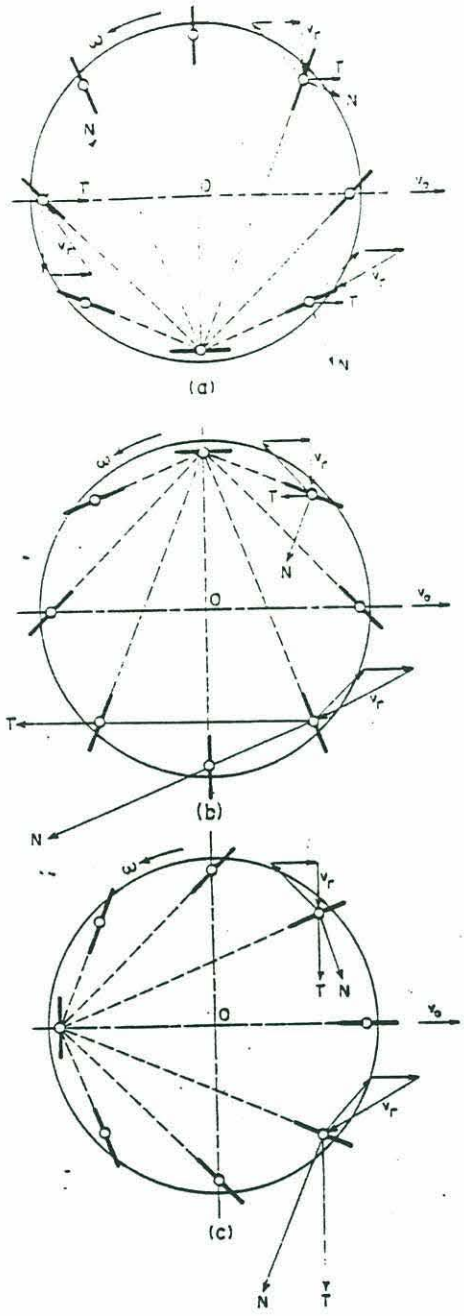

Fig. 3-5. Kirsten-Boeing Vertical Axis Propeller [13]

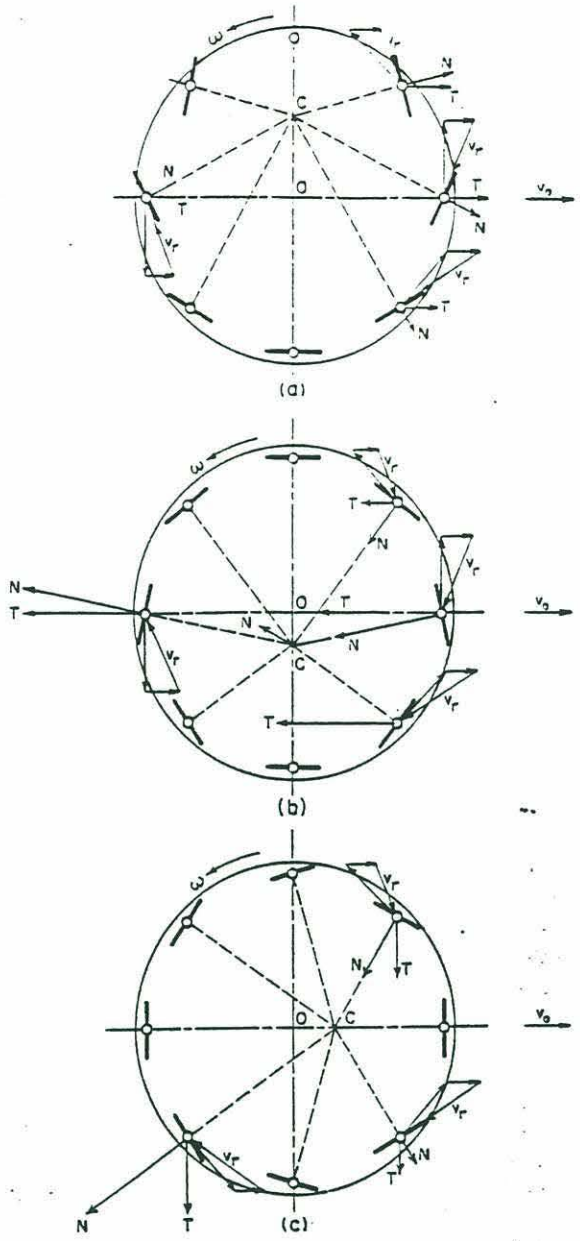

Fig. 3-6. Voith-Schneider Vertical Axis Propeller [13]

Chapter 4
DISCUSSION OF CONCEPTUAL DESIGNS

4.1 Modified Fixed-Pitch Propeller

Before deciding on a final design for improving thruster dynamic performance, we examined several different options. The simplest solution, mechanically speaking, is to redesign a conventional fixed pitch propeller blade to give a higher thrust bandwidth. Nearly all marine propellers are optimized for maximum efficiency at a given load and speed, a goal incompatible with dynamic performance. While there has been no well-publicized research in this field, it is conceivable that some increase in bandwidth could be seen in a propulsor expressly designed for that purpose. Design of this propulsor would, however, be very difficult. The lack of commercial interest in this aspect of propeller performance has meant an absence of computer models predicting dynamic response. Development of an improved conventional design would have to use a trial and error approach, or involve the development of a numerical model using hydrodynamics and propeller theory to predict results, a difficult task.

4.2 Pumpjet

The central problem of propulsor dynamic response is the time it takes to accelerate a mass of water to the point where it provides the desired reaction force. If some method were developed to provide nearly instantaneous acceleration of the fluid mass, a very high bandwidth actuator would be the result. One way to accomplish this would be through the use of a pumpjet and reservoir system (figure 4-1). A reservoir would keep a quantity of water at a given pressure, higher than ambient. To produce thrust, a solenoid valve in the direction of the desired thrust would open. The opening would present an area of higher pressure, and hence thrust, nearly instantly. This solenoid valve could be pulse-width modulated to produce a range of thrust. The reservoir would be resupplied by a continually operating pump, and its pressure would be regulated by a blow-out valve. The limiting factor in this design is the maximum flow rate of the resupply pump or pumps. Table 4-1 illustrates this problem for a hypothetical jet pump maneuvering system. It shows the reservoir pressure, flow rate, and power drawn by the resupply pump to operate a single 5 lbf thruster.

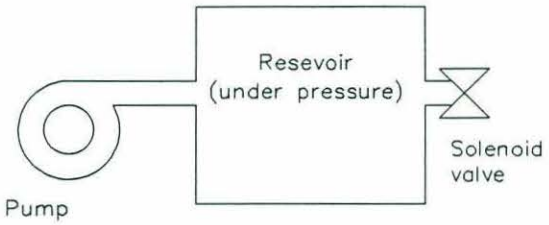

Fig. 4-1 Schematic of pumpjet thruster

Clearly, these flow rates are unacceptably high, and the efficiency very low. Another drawback to this design is the space required by the reservoirs. Nevertheless, this type of pumpjet could prove useful as a supplement to a conventional thruster system for use in maneuvering when precise control is required.

Power reqd in hp	Resevoir pressure (psi)	Resupply flowrate in gpm
1	43	40
0.95	39	42
0.9	35	44
0.85	31	47
0.8	28	50
0.75	24	53
0.7	21	57
0.6	16	66
0.5	11	79
0.4	7	99
0.3	4	132

Table 4-1. Power vs. flowrate for a pumpjet thruster producing 5 lbf of thrust

4.3 Vertical Axis Propeller

Another possibility is the utilization of a vertical axis propeller system. The gearing of the large commercial versions of this type of system, while complex, could be reduced to a size suitable for ROV use. Small Voith-Schneider vertical axis propellers, of the sort described in chapter 3, were mounted on the U.S. Navy manned submersible *Makakai* in the 1960's. These propellers, while giving the pilot enormous control over the vehicle, were prone to entanglement. This problem would only be exacerbated on an ROV designed to survey objects on or near the bottom. More importantly, the size of the disk

required to produce the necessary thrust were large enough to require the vehicle to be designed around them. To add to this mounting problem, the two disks needed to be mounted at an angle with respect to the vehicle sides in order to provide 6-axis force control. These factors, along with the daunting complexity of the gearing systems, make this type of propeller unacceptable for our application.

4.4 Controllable Pitch Stators

Many ducted propellers have small fixed blades, called stators, fore or aft of the main rotating propeller (fig. 4-2). Hughes et al. have shown that the pitch of these stator blades has an important impact on the performance of the thruster. Indeed, the level of thrust produced for a given propeller at a given rotation speed can be decreased by a factor of two for a small change in the angle of the stators. Altering the stator blade pitch rather than the propeller blade pitch has one major advantage: the stator blades are stationary. An actuator can be attached to the duct and can drive the stator blades through a direct mechanical linkage. One such design is shown in fig. 4-3. This design uses a beveled ring gear rotating around the duct meshing with small bevel gears on the base of the stator blades. The ring gear, in turn, is driven by a sealed servo motor through a bevel gear. To change stator pitch, the servo simply rotates the ring gear through a set angle. Another method of transmission might involve the use of a cable drive mechanism to eliminate backlash. A single loop of cable is wrapped around the shaft of the servo actuator and the shafts of the stator blades. The blades are driven by the friction of the cable around their shafts. Some type of tensioning method would also be required in this

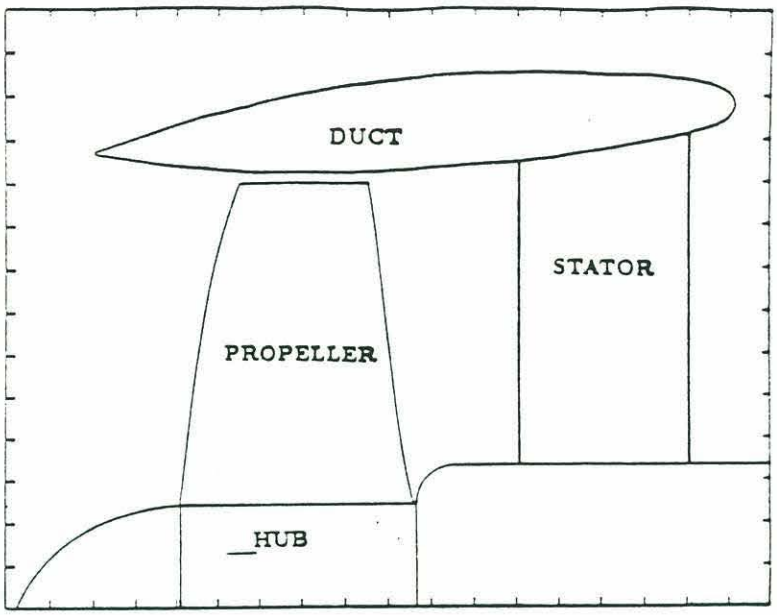

Fig. 4-2. Pre-swirl stators [7]

design. Another way to eliminate backlash would involve a sliding pin mechanism, similar to the pin-slot mechanism mentioned in the previous chapter. The stator blades would be free to revolve around their axis. On the hub end of the blades, an offset pin would fit into a socket on a moveable ring concentric with and sliding on the duct. The socket in this ring is free to move circumfrentially, but restrained axially and radially. To change the pitch of the blades, the ring is moved forward and aft, essentially acting as a hollow ram.

The variable stator concept has several significant liabilities. While, in theory, a higher bandwidth thrust can be generated, this thrust exists only within some finite range of a non-zero setpoint. This design cannot effectively achieve a zero thrust state with the propeller spinning, and would be incapable of reversing the thrust without reversing the propeller rotation. Because the prime mission of this actuator is to improve station-keeping performance, bandwidth at very low thrust levels is a requirement. Also, all the designs described above have transmission mechanisms exposed to the sea. Over time marine growth might well foul these mechanisms, making the propulsor inoperable.

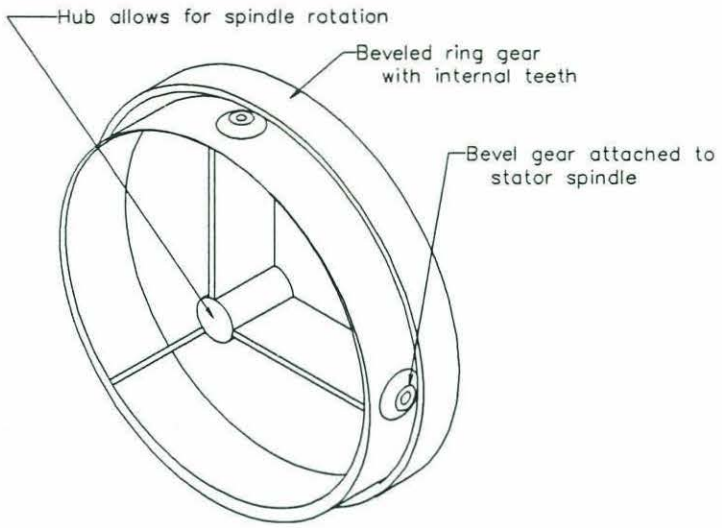

Figure 4-3. Variable pitch stators (propeller not shown) using beveled ring gear.

Enclosing these mechanisms in an oil-filled housing would most likely either involve unacceptable weight and bulk or a high level of complexity and expense.

4.5 Controllable Pitch Propeller

A proven method of controlling thrust at low levels is the CP propeller. While CP propellers in large vessels have a very low bandwidth, this is largely due to their high mass and the large forces involved. A small CP propeller suitable for ROV use could be designed to operate with a high bandwidth pitch actuator. A CP propeller for an ROV would also differ from a commercial CP propeller in its actuation method. Hydraulics, while providing easy coupling of rotating and non-rotating machinery and high forces, are not used in ROV's produced at Woods Hole Oceanographic Institution. To be practical, pitch actuation should utilize the same electrical power source as the rest of the onboard equipment. The problem is then to transmit torque from a servo, most likely mounted rigidly to the ROV, to a rotating propeller blade.

One conceptual design dealing with this transmission problem utilizes planetary gear sets. A planetary gear set, as shown in figure 4-4, uses a central pinion gear, called the sun, and an internal ring gear, between which revolve several pinion gears, called planets. The planet gears are attached to a common carrier revolving around the same axis as the sun and ring gears and located above or below the gearset. The speed of rotation of the carrier, N_C, is a function of the difference between the rotation speed of the sun, N_S, and that of the ring, N_R. If the pitch diameter of the sun and ring gears are given as D_S and D_R respectively, the rotation speed of the carrier, N_C, is given as

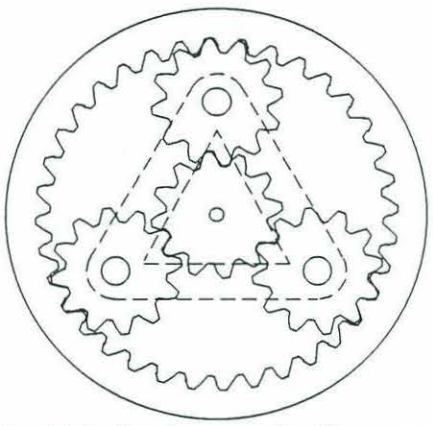

Fig. 4-4 A planetary, or epicyclic, gearset. The carrier is shown with broken lines.

$$N_C = \frac{D_S N_S + D_R N_R}{D_S + D_R}$$

This epicyclic transmission uses two such gearsets in conjunction with a reduction gear train to couple the stationary actuator to the rotating propeller blades (figure 4-5). One gearset is located in a non-rotating housing attached to the aft end of the propeller hub, while the other is in the propeller hub itself. A small pinion on the end of the servo motor shaft drives the ring gear in the first (stationary) epicyclic gear train. The sun in this gear train is rigidly attached to the propeller housing and rotates with the propeller at the propeller's speed of rotation.

$$N_{C1} = \frac{N_{S1} D_{S1} + N_{R1} D_{R1}}{D_{S1} + D_{R1}}$$

where

$$N_{R1} = \frac{N_{SERVO} D_{SERVO}}{D_{R1}}$$

N_{c1}...Rotational speed of the carrier

N_{S1},D_{S1}...Rotional speed and pitch diameter of the sun gear (same as speed of rotation of the propeller)

N_{R1},D_{R1}...Rotational speed and pitch diameter of the ring gear in the stationary gearset

N_{SERVO},D_{SERVO}...Rotational speed and pitch diameter of the pinion on the end of the servo shaft

This will produce a rotation in the planet gear carrier dependent upon the difference in the rotational velocity of the servo and the propeller. This carrier is attached to a gear train designed to step up its speed of rotation by some factor r_k. The final gear of this train is mounted to a hollow shaft concentric with the propeller shaft which passes through a coupling into the rotating hub. This shaft is attached to the ring gear of a second epicyclic gearset inside and rotating with the hub. The sun gear of this gearset is mounted rigidly to the hub and is stationary with respect to the rotating reference frame. The speed of rotation of the planet gear carrier of this gearset is given as

$$N_{C2} = \frac{N_{S2} D_{S2} + N_{R2} D_{R2}}{D_{S2} + D_{R2}}$$

N_{C2}...Speed of rotation of the second planet gear carrier, with respect to the rotating reference frame.

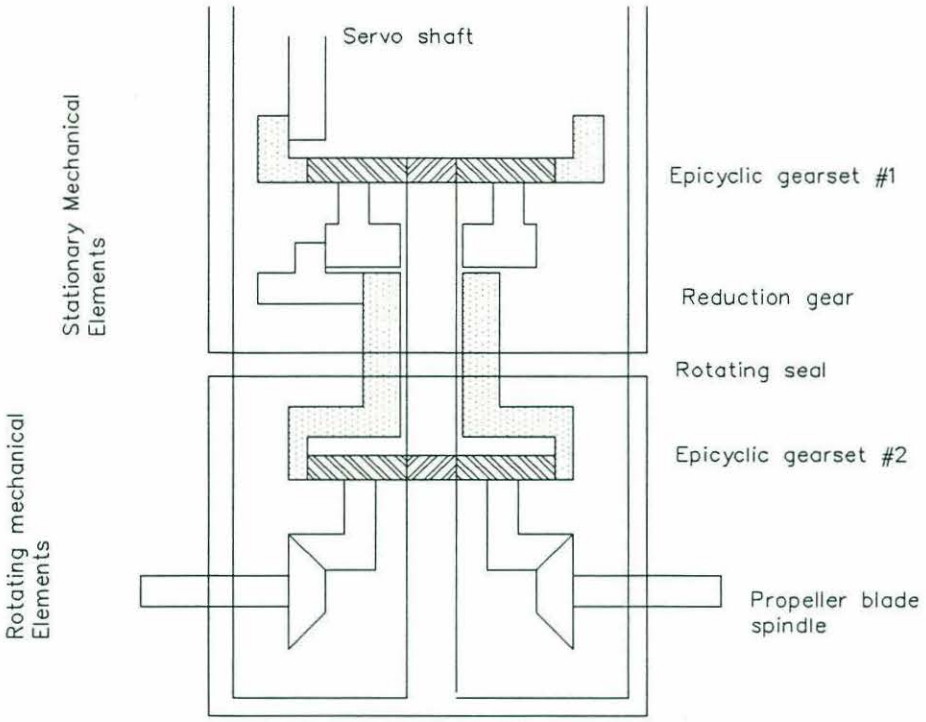

Fig. 4-5. Epicyclic CP transmission

D_S,N_S...Pitch diameter and speed of rotation of the sun gear with respect to the rotating reference frame. Because the sun is fixed to the propeller hub, N_S=0.

D_R,N_R...Pitch diameter and speed of rotation of the ring gear with respect to the rotating reference frame.

This second carrier is attached to a bevel gear meshing with bevel gears at the base of the propeller blade spindles. When the carrier rotates, the propeller blades rotate along their axis. To make this a practical design, the blades should be stationary when the servo is stationary. In other words, the ring gear in the second gearset should be stationary with respect to the rotating reference frame when the servo is stationary. This can be done by correctly setting the reduction ratio, r_k. This ratio can be shown to be

$$r_k = \frac{D_{S1} + D_{R1}}{D_{S1}}$$

The overall gear ratio between the servo and the propeller blades is then

$$\frac{N_{BLADES}}{N_{SERVO}} = \left(\frac{D_{SERVO}}{D_{S1}}\right)\left(\frac{D_{R2}}{D_{S2} + D_{R2}}\right) r_{K_{BLADES}}$$

N_{BLADES}...Speed of rotation of the blades about their spindle axes

$r_{k,BLADES}$...The ratio of the diameters of the bevel gears on the base of the propeller blades to the large bevel gear attached to the second pinion carrier.

The Achilles' heel of this design is backlash. With the small gears needed to fit this type of gear train in an ROV propeller hub backlash becomes excessive. In larger propellers backlash is reduced to an acceptable level only through the use of fine toothed, and therefore noisy and expensive, gears.

As a final footnote to this design, it should be noted that, by use of a continually variable transmission, no pitch actuating servo would be needed. The transmission could be placed between the sun and ring gears of the first gear train. By varying the gear ratio in this transmission, energy to change the pitch of the blades could be drawn from the propeller shaft. This design modification will have to await the development of a robust, compact, and submersible continually-variable transmission set.

Another approach to this design problem involves moving the entire thruster axially to effect a pitch change (figure 4-6). The thruster housing slides in a support sleeve and mates to a pinion gear on the end of the servo shaft by way of a rack mounted axially on its surface. The propeller blades are mounted in rotating housings in the hub and are surrounded by a ring. The blades mate to the ring by way of pins located off the blades' axes of rotation. The rotating ring is axially constrained by way of cam followers or sliding bearings. When the motor, shaft, and hub move axially, the axial position of the hub changes with respect to the rotating ring. The pins move with respect to the blade axis and cause the blades to change pitch.

This propeller has the advantage that there are no mechanisms or moving parts inside the hub. Also, blade support bearing forces are reduced with the blade supported at both ends. There are several important reasons why this design is unworkable. First and foremost, this design tasks the servo with resisting the entire thrust load of the propulsor. Indeed, the servo must work against this load to change pitch. Secondly, the bearings supporting the ring must operate at high surface speeds, with high stiffness, for extended periods of time. Additionally, the mechanism is exposed to the sea, with the attendant risks

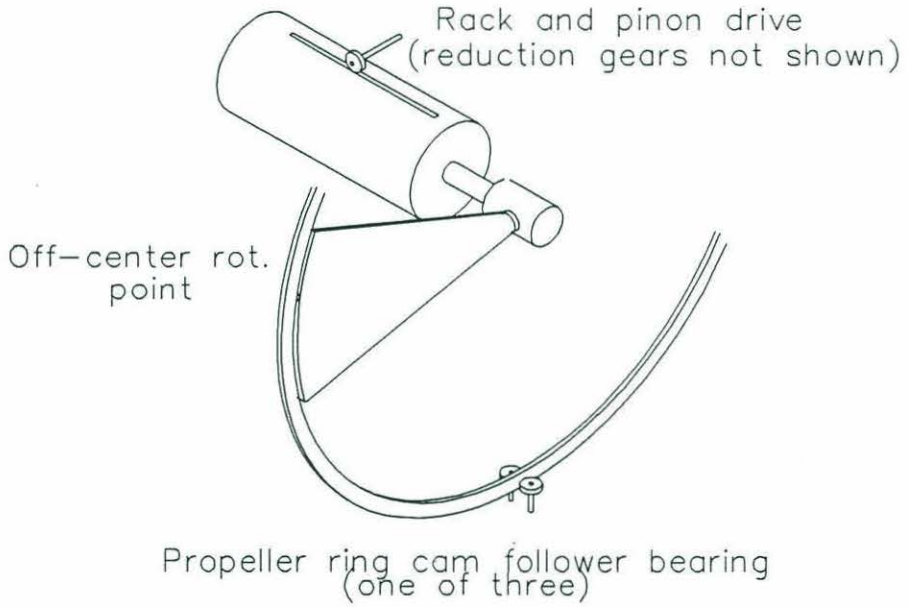

Fig. 4-6. CP mechanism requiring axial movement of the entire thruster

of entanglement and fouling.

A more traditional approach to pitch control yields a more practical design. An ROV CP propeller could utilize the same principles of operation as the larger commercial CP propellers. Instead of a hydraulic ram, an electrically driven leadscrew acts as the linear actuator, and the rotating and non-rotating elements of the mechanism are coupled through bearings rather than by hydraulic fluid. The propeller hub is split into two parts,

one rotating and the other fixed to the vehicle with a spider truss. The actuating servo is mounted to the stationary part located aft of the spinning elements. The pitch actuation could be accomplished using any of the principles illustrated in fig. 3-1. A simple example of such a CP system is shown in figure 4-7. This system uses the crank-slot principle, with a pin sliding in the linearly translating crosshead and mating to the base of the propeller

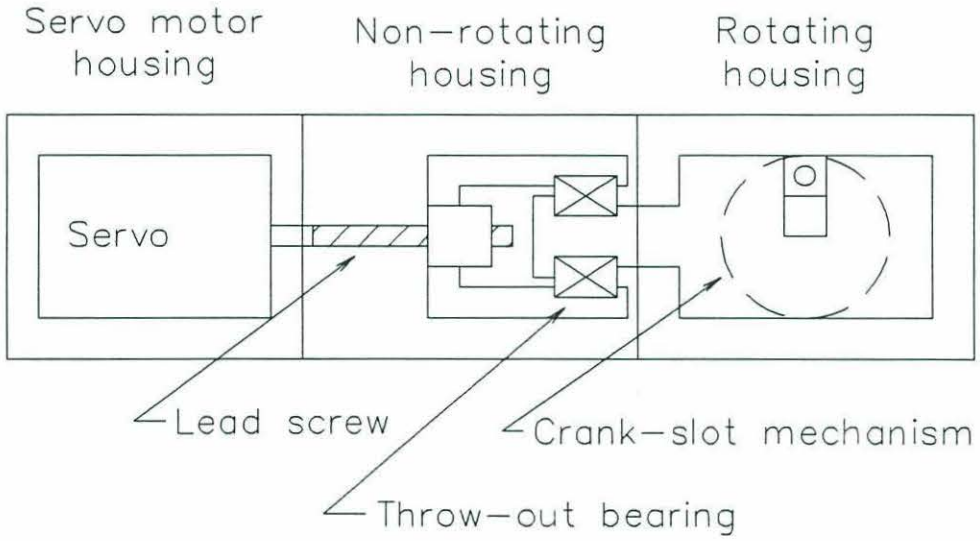

Fig. 4-7. Electrically actuated CP propeller using traditional pitch control mechanism

blade. One notable difficulty with such a sliding arrangement, is concerned with the space it occupies. The thrust load of the linear actuator is supported entirely by the two sliding edges of the block to which the pin is mounted. In a small ROV propeller hub, the area of the edges can be very small. The load supported by these edges may be quite high, particularly during operation with high spindle torque induced by a large pitch angle. The bearing pressure on these edges would likely exceed that of any practical bearing material, resulting in damage to the bearing surface or perhaps even seizure.

The crank rod is a more practical alternative. Not only does it eliminate linear sliding pins, but it also occupies less volume within the hub. The crank arms are attached

to the crosshead and mate with an ear attached to the spindle shaft. This ear can extend as far away from the spindle shaft as space permits to provide for a relatively large moment arm, reducing the actuation force required.

The crosshead and levers, of course, must rotate with the propeller blades. The spinning crosshead is coupled to the stationary lead nut through a throw-out bearing, a bearing which transmits axial force in both directions but allows for relative rotation. This concept is developed into the final design presented in the following chapter.

Chapter 5
DESIGN OF HUB MECHANISM

5.1 Design Requirements, Constraints and Objectives

The most important design requirements of our improved propulsor concern thrust performance. The propulsor must have comparable performance to existing fixed pitch propellers in the areas of steady-state thrust and shaft speed. This requirement ensures that the propulsor will be compatible with existing ROV systems, and, more specifically, existing thruster motors. To simplify steady-state control schemes, the device should deliver symmetric or nearly symmetric thrust in forward and reverse.

The improvement delivered by the propulsor, and the motivation of this thesis, should be in the area of dynamic performance. The propulsor should be able to deliver complete thrust reversal in 0.2 seconds. This is approximately one order of magnitude greater than typical fixed pitch propulsors [1]. In order to utilize an existing servo motor, the actuator driving this thrust change should consume less than 100 watts of power during peak operating load, and should use an electrical power source to be compatible

with electrically powered ROV's. During operation, no undesirable resonances should occur.

To be compatible with existing thruster motors the propeller should operate at speeds of up to 1200 rpm's and fit on the end of a propeller shaft. The non-rotating elements should mount securely to the vehicle. The blades themselves should have some measure of impact resistance, with a design maximum load set arbitrarily at 100 lbs and moment of 1,000 in-lbs per blade.

5.2 Discussion of basic mechanical design

The design consists of two controllable pitch propeller blades actuated by a crank-rod transmission originating from a crosshead. The crosshead is connected to a non-rotating lead nut through a throw-out bearing which transmits axial force while allowing relative rotation. The lead screw is connected to the shaft of a submersible servo motor. Each blade shaft is supported by two bushings, with a central bushing common to both shafts. The entire mechanism is sealed and oil-compensated.

The blade's shafts are milled flat where they attach to the propeller blades. A matching flat section is milled from each blade and the shaft rests in this depression, locating it and smoothing the flow across the blade surface. The two parts are secured using flat head machine screws countersunk to match the blade surface. A shaft ear, acting as the lever arm in the pitch actuation mechanism, is secured to the shaft between the two bushing surfaces using a shrink fit. The effective lever arm is 1.95 cm.

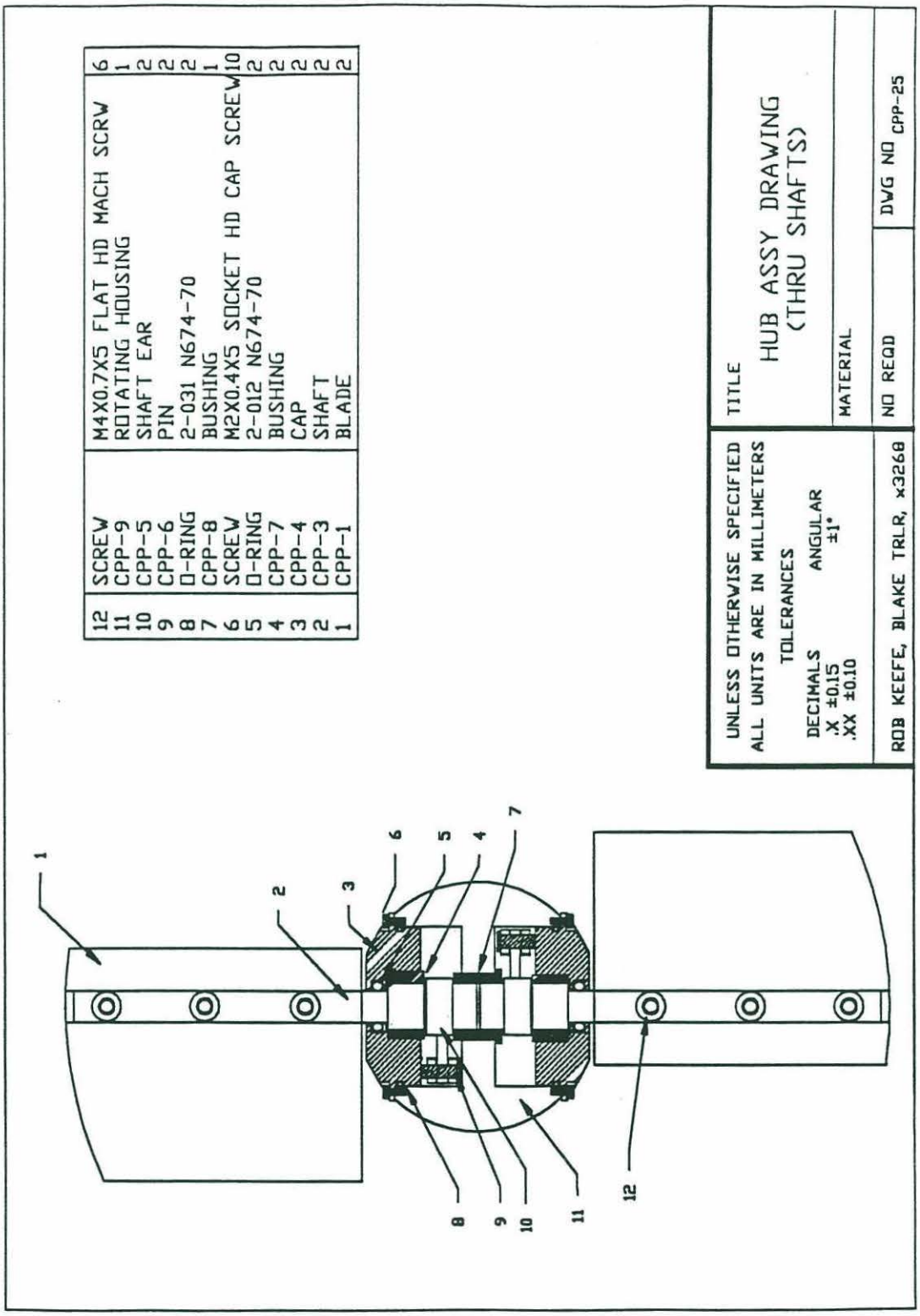

Fig. 5-1. Assembly drawing of the rotating housing of the hub, taken through the axis of the propeller blade spindles.

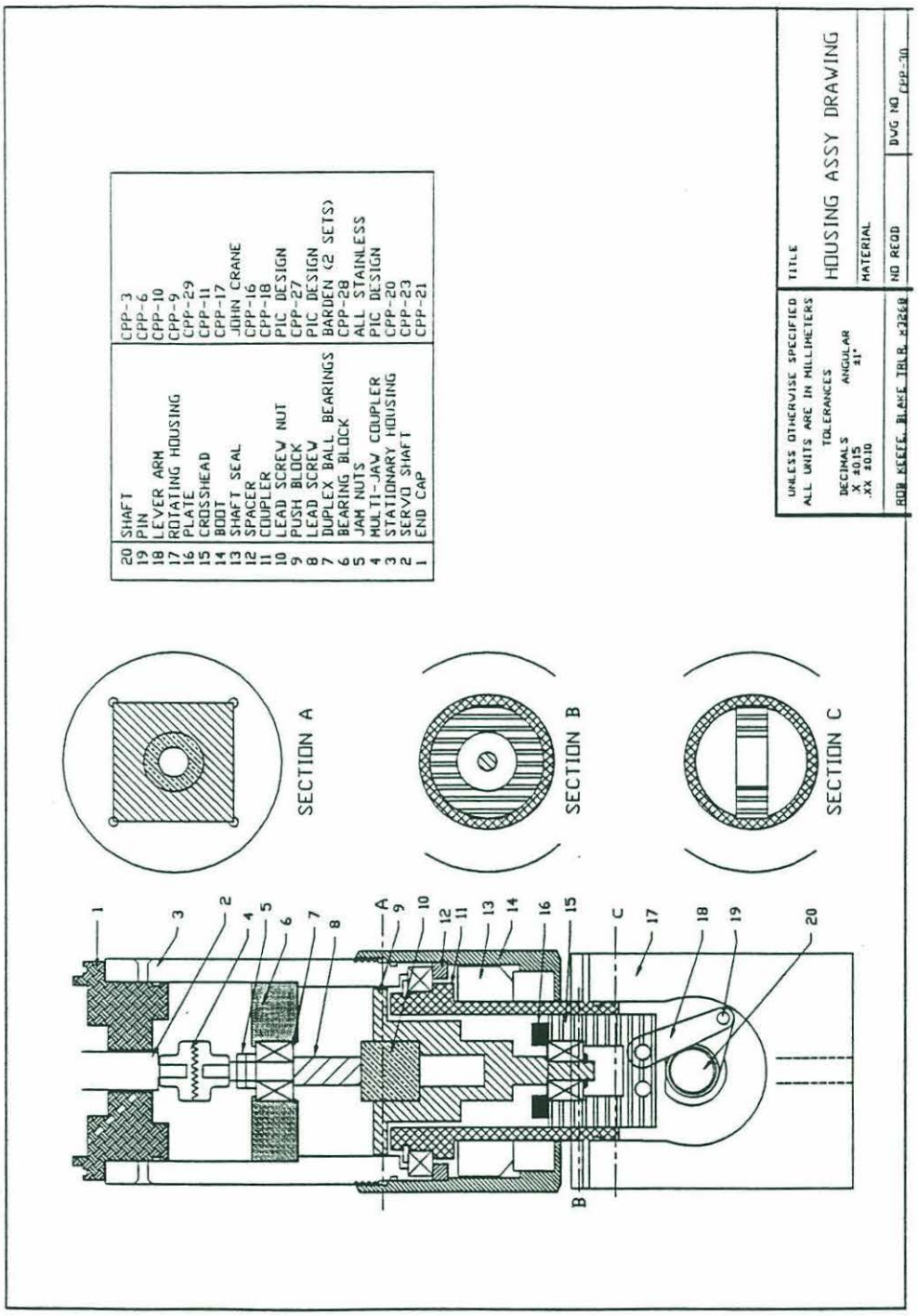

Fig. 5-2. Assembly drawing of the propeller hub mechanism taken through the lead screw axis and perpendicular to the propeller spindle axes.

The blade shafts and bushings are located in a cylindrical rotating housing. This housing supports the common central support bushing and encloses all rotating mechanical elements. The thrust motor shaft attaches to the base by means of a set screw and flat on the shaft.

Screwed to either side of the rotating housing are the caps. These caps permit access to the inside of the rotating housing for assembly and maintenance and simplify its fabrication. They support the outer propeller blade shaft bushings and house the shaft seals.

The shaft ears are attached to levers with sliding brass pins. These levers in turn attach to a crosshead also with sliding brass pins. The crosshead slides axially in grooves in the coupler, rotating with the propeller. It also comprises the rotating member of the throw-out bearing, providing the outer housing for the duplex angular contact bearing. The bearing is retained in the crosshead with a retainer plate, and rests against a shoulder.

The coupler is a tube-like part secured to the aft end of the rotating housing with cone point set screws. The coupler extends into the non-rotating housing and supports the main bearing between the rotating and non-rotating assemblies. It acts as the "shaft" for the main seal between the housings.

Supporting the non-rotating seal elements is the boot. The boot also houses the forward surface of the main bearing, with the aid of a spacer. It screws into the non-rotating housing, the screw thread preloading the seal and bearing.

The push-block transmits the axial force of the lead nut to the throw-out bearing. The inner race of the throw-out bearing is retained on one end, while the lead nut screws

into the other. A square cross-section on the aft end slides in a square opening in the non-rotating housing, preventing lead nut-induced rotation.

The lead screw is held in place by a duplex angular contact bearing set retained in the bearing retainer. The bearing retainer is secured by retaining ring inside the non-rotating housing aft of the square opening. The bearing retainer holds the outer races of the lead screw support bearings with a shoulder and retaining ring. The inner races of these bearings rests on a surface turned onto the end of the lead screw. A threaded section aft of the bearing surfaces allows for preload with jam nuts.

The endcap and servo shaft are modifications of the corresponding parts on an existing submersible servo motor. These modifications allow for a sealed connection between the servo housing and the non-rotating housing. The modified servo shaft is designed to allow for mounting of a multi-jaw coupler connecting the servo shaft to the lead screw.

5.3 Servo motor

A motor from the autonomous underwater vehicle ABE was used to actuate the pitch change. The motor, geared through a 10:1 planetary gearbox is capable of producing up to 100 in-lbs stall torque and has a maximum shaft speed of 90 rpm. This motor is sealed with all its control hardware in an oil-filled housing. Control of the motor is accomplished by sending ASCII command codes through a serial line to a translation box. This box is connected to the motor controller with two leads in a watertight cable. The

cable also accommodates the positive and negative power leads, which draw up to 2A at 50V nominal.

5.4 Material Selection

The majority of the machined parts in the design are constructed of 6061-T6 aluminum. This material is commonly used in underwater vehicles, largely due to its high machineability, low cost, and good corrosion resistance. Parts requiring high hardness are constructed of 303 stainless steel.

Galvanic corrosion is ignored in this design. This prototype will be tested in a fresh water test tank, and will not be submerged for extended lengths of time in any case. Were it to be placed into service in a marine environment, steps to retard corrosion, such as the use of sacrificial anodes and anti-seize compound, would be required.

5.5 Bearing Selection

Wherever practical, sliding contact bearings have been used to reduce complexity and cost and increase overall design ruggedness. The most significant set of bushings are those used to support the blade spindle shafts, with their small range of motion and potentially large shock loads. During pitch change, a great deal of friction is developed in these bushings accounting for the largest single sink of pitch actuator power. Since these bearings are required to resist large loads and moments, contact pressure becomes the dominant design constraint. To reduce the size of the spindle shaft bronze was chosen for the bearing material.

Duplex angular contact bearings (face-to-face) with a light factory preload are used to resist the axial actuation loads in the throw-out bearing and lead screw mount. A four-point contact thin section bearing is used to keep the rotating and non-rotating housing separate during both forward and reverse operation.

5.6 Environmental Insulation

All mechanical components of the design except the blades and part of the blade spindle shafts are enclosed in oil-compensated housings. All mating surfaces are equipped with O-ring seals, as are the spindle shafts where they penetrate the rotating housing. The servo motor housing is equipped with a flexible oil chamber to counteract any expansion or contraction of the oil during depth change. All enclosed areas, including the servo motor, are part of a single continuous oil volume.

5.7 Static Performance Analysis

The performance of this design is computed using an adaptation of methods described by Vassilopoulos and Ghosh [8]. First the loads and moments about the propeller blade spindle are analyzed. A schematic view of the propeller spindle support mechanism is shown in figure 5-3. The shaft diameter in the inner bearing, D_{IB}, in the outer bearing, D_{OB}, and at the shoulder, D_{OS}, are critical in bearing friction analysis. If we allow M_Y to represent the entire externally imposed moment load on the propeller blade spindle,

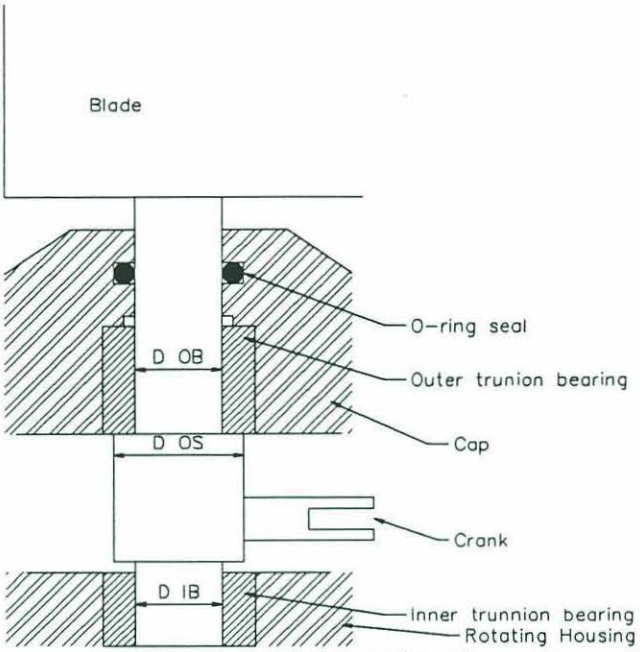

Fig. 5-3 Schematic of blade spindle and support mechanism.

we can develop an equation for the tangential force on the crank imposed by the crank rod.

$$M_Y + F_{LT}R_C \pm\left[\frac{1}{2}\mu_T\left(\sqrt{R_{OX}^2+R_{OZ}^2}\,D_{OB}+\sqrt{R_{IX}^2+R_{IZ}^2}\,D_{IB}\right)+\frac{1}{2}\pi f_S D_{RI}+\mu_B D_B F_L + M_{FA}\right]=0$$

$$M_{FA}=\frac{1}{3}\mu_T R_Y\frac{D_{OS}^3-D_{OB}^3}{D_{OS}^2-D_{OB}^2}$$

and

$$F_{LT}=F_L\cos\phi$$

where

R_C = Radius of the crank pin
μ_T = Coefficient of friction between bearing and shaft
R_{OZ},R_{OX} = Bearing reaction forces in z- and x-directions in outer bearing
R_{IZ},R_{IX} = Bearing reaction forces in z- and x-directions in inner bearing
f_S = Specific friction force of O-ring
D_{RI} = Diameter of inner surface of O-ring
μ_B = Coefficient of friction between crank pin and crank

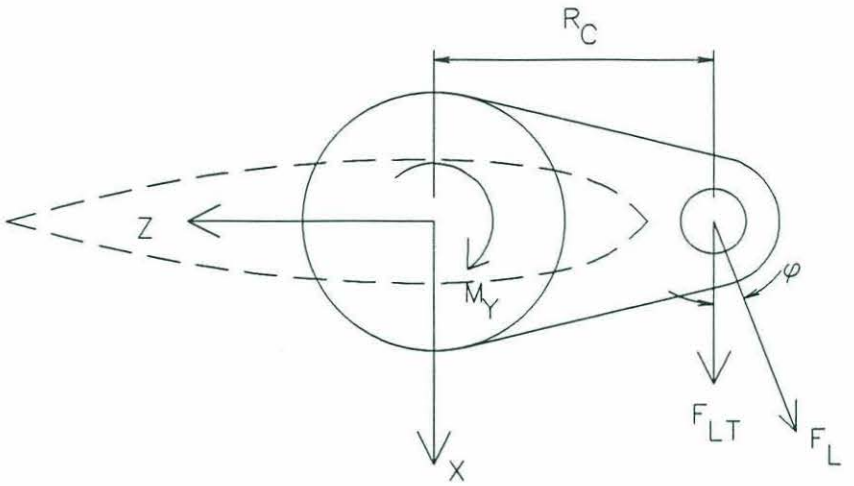

Fig. 5-4 **End-on view of propeller spindle shaft looking toward the hub. The crank ear is shown at right.**

D_B = Outer diameter of crank pin
F_L = Axial force in crank rod
R_Y = Centrifugal force of blade and spindle

This formula represents the summation of moments around the long axis of the propeller spindle shaft. The first term is the externally imposed moment caused by hydrodynamic forces, the second is the moment exerted by the crank rod, and the last term in parentheses is the sum of frictional moments. To evaluate this expression we must solve for the reaction forces exerted by the inner and outer bearing. This is done through examination of the sum of forces on the spindle shafts, and summation of the corresponding moments about the inboard ends of the shafts.

In the x-direction the balance of forces is

$$F_X - R_{OX} + R_{IX} + F_{LX} = 0$$

where

$$F_{LX} = F_L \cos\psi$$

ψ represents the angle between the main axis of the link and the x-axis. The balance of moments about the center of the hub is given as

$$-F_X R_{CP} + R_{OX} H_{OB} - R_{IX} H_{IB} - F_{LX} H_{LF} = 0$$

where

F_X = The externally imposed force on the blade in the x-direction
R_{CP} = The radius of the center of pressure on the blade from the center of the hub.
H_{OB} = The radius of the center of the outer bearing
H_{IB} = The radius of the center of the inner bearing
H_{LF} = The radius of the center of the crank pin

A similar balance of moments and forces can be done on the z-axis yielding

$$F_Z + R_{OZ} + R_{IZ} - F_{LZ} = 0$$

$$F_{LZ} = F_L \sin\psi$$

$$F_Z R_{CP} + R_{OZ} H_{OB} + R_{IZ} H_{IB} - F_{LZ} H_{LF} = 0$$

where

F_Z = Externally imposed force on blade in z-direction

The crank angles ψ, φ, and θ can be determined geometrically using figure 5-7.

$$\Delta X = X_{LF} - R_C \sin\theta$$
$$\Delta Z = R_C \cos\theta - Z_{LF}$$
$$\psi = \arctan\left(\frac{\Delta X}{\Delta Z}\right)$$
$$\phi = \psi - \theta$$

The force and moment equations are most easily solved by solving iteratively for F_L. The design was evaluated using these formulae under a variety of conditions. For evaluation of normal operating conditions, blade forces are drawn from theoretical data obtained in the following chapter. As covered in that chapter, the blades are designed such

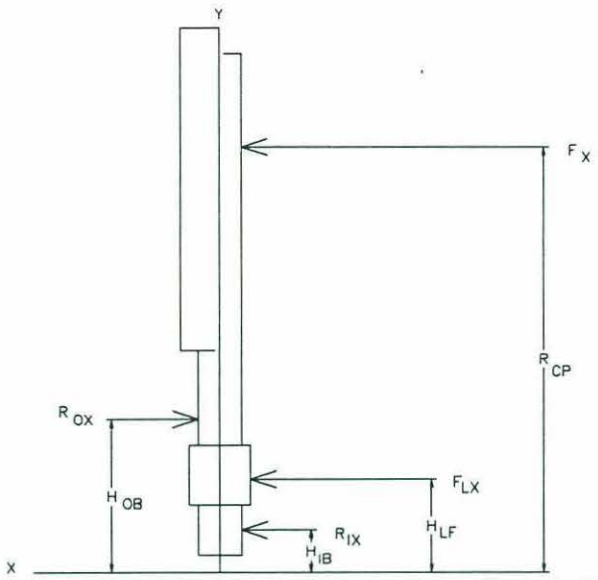

Fig. 5-5 Free body diagram of propeller spindle in x-y plane, pitch angle 0 deg.

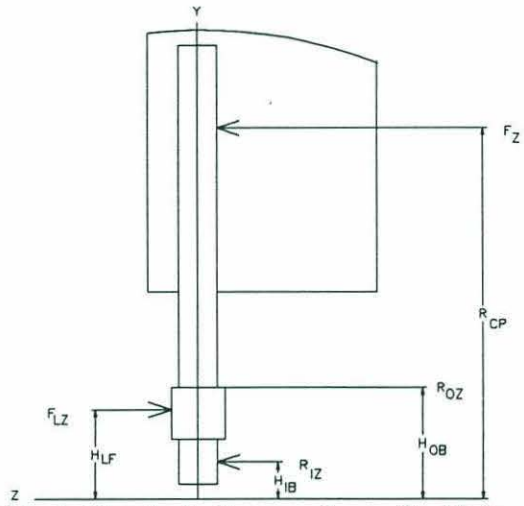

Fig. 5-6 Free body diagram of propeller blade spindle in y-z plane, pitch angle 0 deg.

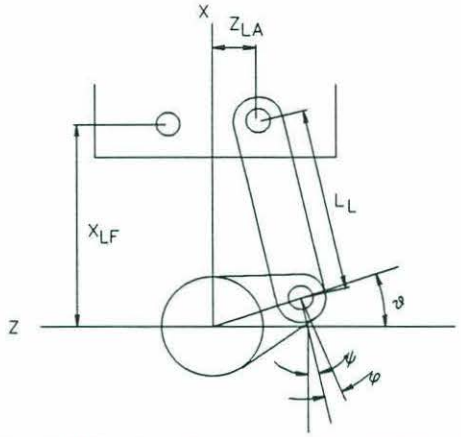

Fig. 5-7 Crank rod geometry in x-z plane, pitch angle of approximately 30 deg.

that no hydrodynamically induced moment about the spindle shaft axis occurs during operation. As a conservative assumption, hydrodynamic moments were applied by assuming a 1cm moment arm extending across the blade axis toward the leading edge of the blade.

Link forces were computed using the above formulae for several different angles of attack. The propeller forces were calculated using predicted values of thrust and torque

derived in the following chapter. The thrust was assumed to be concentrated at a radius of 10cm from the center of the hub. Since the thrust acts only along the x-axis the x-component of propeller force on each of the two blades is

$$F_X = \frac{Thrust}{2}$$

The torque predicted by the propeller force calculations represents the drag of the propeller blades as they rotate about the hub. This drag exists only tangential to the rotation of the blades, that is, along the z-axis. If we also assume the drag force to be concentrated at a point of 10cm radius from the hub, then the tangential force on each blade, F_z is

$$F_Z = \frac{1}{2}\frac{Torque}{10cm}$$

The values calculated and tabulated below in table 5-1 represent the link force due only to the forces and moments induced by hydrodynamic forces and the frictional resistance in the bearings. They can be thought of as the resistive force history as the blade changes pitch from +30 to -30 degrees, at a shaft speed of 900rpm.

Appendix A lists the constants used in these calculations with their symbols and values.

Pitch angle (degrees)	F_X (N)	F_Z (N)	F_{LX} (N)	F_L (N)
30	104	56.6	123	134
20	56.6	21.5	67.2	75
10	20	3.8	28.7	32.7
5	7.1	0.7	16	18
-5	-7.1	0.7	9.2	10.4
-10	-20	3.8	9.6	10.9
-20	-56.6	21.5	12.5	13.9
-30	-104	59.35	20	21.2

Table 5-1. Force history derived from static analysis of pitch change from +30 to -30 degrees.

Now that the reaction forces imposed from the bearings are known, the contact pressure between the bearing surface and the shaft can now be evaluated. The formulae for determining contact pressure of a cylinder in a cylindrical socket are

$$\sigma_{CB} = 0.789\sqrt{\frac{p}{K_D C_E}}$$

$$\delta_{BP} = \frac{2p(1-\nu^2)}{\pi E}\left(\frac{2}{3} + \ln\frac{2D_{CB}}{b} + \ln\frac{2D_P}{b}\right)$$

$$b = 1.60\sqrt{pK_D C_E}$$

$$K_D = \frac{D_{CB}D_P}{D_{CB} - D_P}$$

$$C_E = \frac{1-\nu_B^2}{E_B} + \frac{1-\nu_P^2}{E_P}$$

where

σ_{CB} = The contact stress between pin and socket
p = The load supported by the socket per unit length
δ_{BP} = The deflection of the pin axis due to compression
D_{CB} = The diameter of the socket
D_P = The diameter of the pin
E_P = The modulus of elasticity of the pin
ν_P = Poisson's ratio for the pin
E_B = The modulus of elasticity of the socket
ν_B = Poisson's ratio for the socket
b = The circumfrential length of contact

Using the values for the bearing reaction force at a pitch angle of +30 degrees, the maximum contact pressure is 3900psi, well within the operating range for a bronze bushing. The deflection of the spindle is less than 0.03mm.

Using the formulae developed for blade force, the expression for the axial lead screw force required can be developed as a function of angle and operating conditions. The axial (x-direction) force on the crosshead is simply the sum of the two x-components of the crank rod force.

$$F_{\text{crosshead}} = 2F_{LX}$$

This axial force is transmitted through the throw-out bearing to the push block and lead nut. The axial force on the lead nut is identical to the force on the crosshead, assuming no friction in the sliding surfaces between the coupler and crosshead and between the push block and non-rotating housing. This force is transmitted to the lead screw which is secured axially to the non-rotating housing through the lead screw support bearings and bearing block.

5.8 Dynamic Performance Analysis

To construct a dynamic model of the system, the lead screw force equation is solved at a number of different blade pitch angles. The results are used to construct a

polynomial relating link force to pitch angle for that specific shaft speed. Using the previous calculations for a shaft speed of 900 rpm the following formulae are found by curve fit.

$$F_{LX} = 0.6877\alpha^{1.5} + 9.0 \quad for \quad \alpha \geq 0$$
$$F_{LX} = 0.00223|\alpha|^{2.5} + 9.0 \quad for \quad \alpha < 0$$

where

α = pitch angle in degrees
F_{LX} in units of N

All damping is considered to occur at the square cross-section flange on the push-block as the oil flows through the four vent holes.

If the push-block moves axially at a speed, v, and the area of the square opening is A_{SQ}, the volumetric flowrate of oil is simply

$$\dot{V} = vA_{SQ}$$

The flow of the oil through the holes in the push-block can be approximated as flow through an orifice plate in a pipe. The head loss incurred by this flow is given graphically in Fox and McDonald as a function of the ratio of the area of the pipe to the area of the orifice hole [9]. A conservative assumption is to assume that the area of the orifice hole is equal to one half the total area of the holes in the orifice block. The ratio of one half the area of the holes in the push block to the area of the square opening in which the push-block slides is .026. The resultant head loss is 98.5%. Head loss is related to pressure drop by

$$h_l = \frac{\Delta p}{\rho}$$

The head of the flow is

$$h = \frac{p}{\rho} + \frac{v^2}{2} + gz$$

If we disregard any change in height and take the pressure as absolute pressure this equation simplifies to

$$h = \frac{p}{\rho}$$

Assuming a complete reversal of thrust in 0.2 seconds, the maximum velocity of the push-block is around 0.1 m/s. The resultant pressure differential is approximately 5 Pa. Multiplying by the area of the square hole, the total resistive force is less than 7 mN.

The effective mass as seen by the actuator is comprised of the mass of the linear sliding components, the effective mass of the rotating components, and the added mass of the oil surrounding the push-block. The mass of the linear components "downstream" of the lead nut is estimated at 600g. The estimated mass moment of inertia of the rotating components about the spindle axis is .001 kg-m^2. Mapping this through a 1.95cm moment arm yields an effective linear mass of around 2.5 kg. The added mass of the oil surrounding the push-block can be estimated by simply using the mass of the entire volume of oil in the square section of the non-rotating housing. This mass is approximately 600g. The total effective mass seen by the lead screw is therefore estimated as 3.7kg. Because the total range of travel of the push-block is quite small (less than 2 cm) and hence the velocities low, we will assume that the system is undamped. If we define x as the displacement of the push-block from some initial position, the equation of motion for the system downstream of the push-block is

$$3.25kg(\ddot{x}) = F_{\text{applied}} - F_{resistive}$$

where $F_{resistive}$ is the equation for resistive force derived from the static model, encompassing friction and hydrodynamic forces on the blade. Since the applied force comes from a rotating lead screw, the following equation can be used relating lead nut force, $F_{applied}$, to lead screw torque, τ.

$$\tau = \frac{F_{applied} d_m}{2}\left(\frac{l + \pi\mu d_m}{\pi d_m - \mu l}\right)$$

where

dm = Major diameter of leadscrew = 3/8"

l = Lead = 1"

μ = Dynamic coefficient of friction between lead screw and nut = 0.12

Solving for this equation yields

$$\tau = F_{applied}(0.0052\text{m})$$

The resultant equation of motion for the entire system as seen by the servo motor shaft is then

$$3.25\text{kg}(\ddot{x}) + F_{resistive}(\alpha) - \frac{\tau}{0.0052\text{m}} = 0$$

This equation was analyzed using numerical techniques. Assuming a perfect servo motor, i.e. torque developed by the motor appears instantly, the mechanism is capable of very high bandwidth. A 1 N-m step torque command produces a change in blade position from +30 to -30 degrees in less than 0.1 second. The actual response will be heavily dependent on characteristics of the motor and controller.

Chapter 6
PROPELLER BLADE DESIGN

For this propulsor to be practical in an ROV, it must produce adequate thrust and operate with some measure of efficiency under normal operating conditions. This requires properly designed blades. This chapter sets forth the operating requirements of the propulsor, details a brief review of propeller theory, and utilizes that theory to analyze several blade designs. The most suitable design is presented in detail.

6.1 Operating requirements

To allow for successful retrofitting of this propulsor into existing ROV platforms, it should produce steady-state thrust comparable to existing fixed-pitch propellers of similar diameter and power consumption. It should produce at least 40 lbf of thrust at a shaft speed of 900 rpm and maximum blade pitch. To allow the propeller to idle while the shaft continues to spin, the blades should have some repeatable pitch at which they produce negligible thrust regardless of shaft speed. While efficiency is somewhat less important than dynamic performance for our application, it should not be prohibitively low. If we assume that the maximum blade pitch angle routinely used will be at 80% of its

maximum, the efficiency of the thruster (defined later in this chapter) should be no lower than 15% at this pitch angle. This value is arbitrarily chosen as one half the efficiency of a typical reversible ROV propeller.

Blades in a CP propeller system are generally optimized for a certain pitch angle and operating conditions. For example, a CP propeller on a tug might be optimized for a high pitch angle, low advance speed, and high shaft speed. The propeller is most efficient at the angle to which it is optimized and progressively less efficient as the pitch departs from this optimum. Were this propeller to be used primarily for forward motion or to keep a positively buoyant vehicle submerged, choice of an optimum pitch angle would be proper. However, the mission of this system is to provide high-bandwidth maneuvering thrust in both forward and reverse directions. Arguably, the average pitch angle encountered during maneuvering is 0. This propeller will then be optimized for a 0 pitch angle, and the resultant blade shape is a flat plate. The flat plate blade shape sacrifices efficiency for symmetry of thrust response in the forward and reverse directions. Another advantage to the flat plate design is its ease of manufacture. Standard blade shapes require costly 5-axis milling machine time to produce. A flat plate with a standard thickness profile to smooth flow can easily be produced on any CNC milling system, provided the blade is not excessively long.

6.2 Review of propeller theory[1]

Propeller blade analysis begins with an examination of foil sections. Consider a flat foil in a uniform flow. Due to some physical characteristic of the foil, at some point the velocity of the flow on the top of the plate, $\vec{V_u}$, and the velocity on the bottom of the plate $\vec{V_l}$ differ. If we define a mean velocity such that

$$\vec{V_m} = \frac{1}{2}\left(\vec{V_u} + \vec{V_l}\right)$$

The velocities on either side of the foil differ from the mean velocity by some difference vector, $\vec{V_d}$.

$$\vec{V_d} = \frac{1}{2}\left(\vec{V_u} - \vec{V_l}\right)$$

The presence of a velocity difference implies the existence of a vortex sheet, whose strength at this point is

$$\gamma = 2V_d$$

directed perpendicular to $\vec{V_d}$ in the plane defined by $\vec{V_u}$ and $\vec{V_l}$. We can define some angle, δ, representing the angle between the mean velocity and the direction of the vortex sheet strength vector.

This velocity differential also produces a pressure differential across the plate, defined by Bernoulli as

---

[1] This section is adapted from Prof. Justin Kerwin's Hydrofoils and Propellers (13.04) Lecture Notes, 1993.

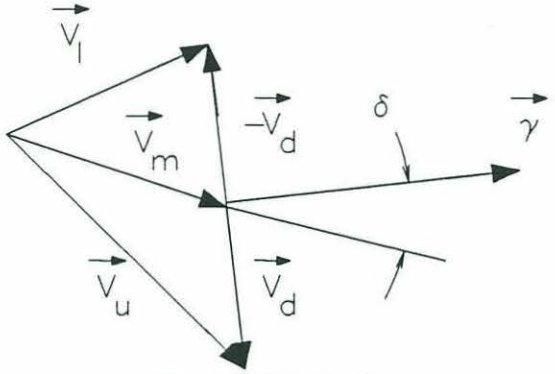

Fig. 6-1. Velocity diagram

$$\Delta p = p_l - p_u = \frac{1}{2}\rho\left(V_u^2 - V_l^2\right)$$

By using the law of cosines to relate the upper and lower velocities to the mean and difference velocities, the pressure equation can be simplified to

$$\Delta p = \rho V_m \gamma \sin\delta$$

To further simplify this equation, the vorticity is divided into free vorticity, γ_f, and bound vorticity, γ_b, in such a way that only bound vorticity contributes to the pressure differential.

$$\gamma_f = \gamma \cos\delta$$
$$\gamma_b = \gamma \sin\delta$$

$$\Delta p = \rho V_m \gamma_b$$

The bound vorticity always acts perpendicular to the mean velocity and the free vorticity parallel to it. On a foil, the bound vorticity points along the span of the foil, while

the free vorticity points from the nose of the foil to the tail. By integrating the area of the foil, we arrive at some total vortex strength, Γ.

This vortex representation of pressure drop is used in two different numerical schemes to analyze propeller blades. The simplest of the two is called the lifting line theory. It states that the lift and drag produced by an infinite foil can be represented by an infinitely long two-dimensional vortex about the spanwise centerline of the foil. The vortex induces velocities at points in space, as indicated by Biot-Savart's law. A momentum flux examination of the wake far downstream of the foil demonstrates that lift and drag are an effect of flow parallel to the z-axis, represented by a velocity component, w [10]. The momentum flux equation at a point infinitely far downstream is

$$F_z(y)\delta y = -\rho U \iint_{-\infty}^{+\infty} w(\infty, y, z)dzdy$$

Simplification of the above equation, and evaluation of the integral leads to the final equation for lift force

$$F_z = \rho U \Gamma(y)$$

The total lift force on the foil is the same as would result if the bound circulation over the chord were concentrated in a single vortex of strength $\Gamma(y)$.

Drag can be evaluated for a foil of length, s, through an examination of the kinetic energy added to the flow in the wake as the foil advances some unit distance. This force is found to be

$$F_x(total) = -\frac{\rho}{2}\int_{-s/2}^{+s/2} \Gamma(y)w(\infty, y, 0)dy$$

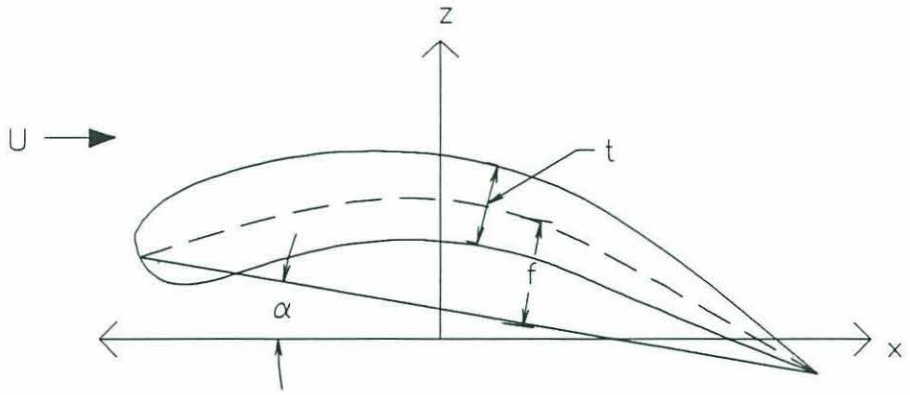

Fig. 6-2. Propeller blade geometry.

The lifting line numerical model treats each blade as this type of two-dimensional vortex emanating from the center of the hub. Since the velocities induced by each blade will affect the flow over all other blades, an iterative method is used in flow calculations. The final result is a reasonably-accurate preliminary analysis of the propeller's basic performance characteristics. A lattice of vortex segments, arranged spanwise in two-dimensions, may be used to increase the accuracy (and complexity) of the calculations. For propellers of high aspect ratio, and low rake and skew (defined later in this chapter) this method is quite accurate.

For propellers of more complex geometry, the lifting surface method is employed. This method also involves the application of a lattice, however this lattice is arranged in

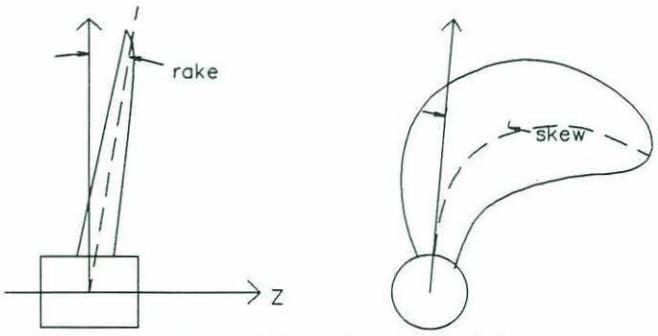

Fig. 6-3. Propeller rake and skew.

three-dimensional space along the surface of the propeller blade itself. The result is the ability to properly account for blade curvature, or camber, and odd propeller geometries.

A number of terms are used to describe specific properties of propellers. A new propeller coordinate system is introduced, which is not to be confused with the coordinate system used in the previous section. The chord length, *c*, is defined as the length of a line drawn from the nose of a propeller blade section to the tail, called the nose-tail line. The angle this line makes with the mean flow is the angle of attack, α. Camber, *f*, is the distance between the nose-tail line and a line drawn through the middle of the section dividing the section's thickness, *t*, into two equal parts (fig. 6-2). On a propeller blade we can draw a line over the span of the blade, at the middle of the chord and passing through the middle of the blade's thickness. The distance between this line and a line emanating radially from the center of the hub in parallel to the z-axis is the rake, and the distance between the two lines in the x-y plane is called the skew (fig. 6-3).

Analysts of propellers have found a number of non-dimensional values useful in their studies. Thrust, T, and torque, Q, produced by a rotating propeller are non-dimensionalized into coefficients of thrust and torque, K_t and K_q.

$$K_T = \frac{Thrust}{\frac{1}{2}\rho n^2 D^4}$$

$$K_Q = \frac{Torque}{\frac{1}{2}\rho n^2 D^5}$$

where ρ represents the medium density, n the shaft speed in turns per second, and D the diameter of the propeller. Thrust can also be non-dimensionalized with respect to the forward speed of the vessel, V_s, and the propeller radius, R.

$$C_T = \frac{Thrust}{\frac{1}{2}\rho V_S^2 \pi R^2}$$

The speed of the vessel is also non-dimensionalized with respect to the shaft speed, n.

$$J = \frac{V_S}{n\pi D}$$

The efficiency of the propeller is defined as the ratio of power put out by the propeller, to the power drawn by the propeller.

$$\eta = \frac{Thrust \bullet V_S}{Torque \bullet n\pi} = J\frac{K_T}{K_Q}$$

Most propellers exhibit typical thrust and torque behavior over their expected range of operating conditions. Both K_T and K_Q are at their maximum values at J=0, a condition called bollard pull. They decrease at an increasing rate until they vanish. The efficiency is 0 at bollard pull, increases to some maximum value, then decreases until it vanishes.

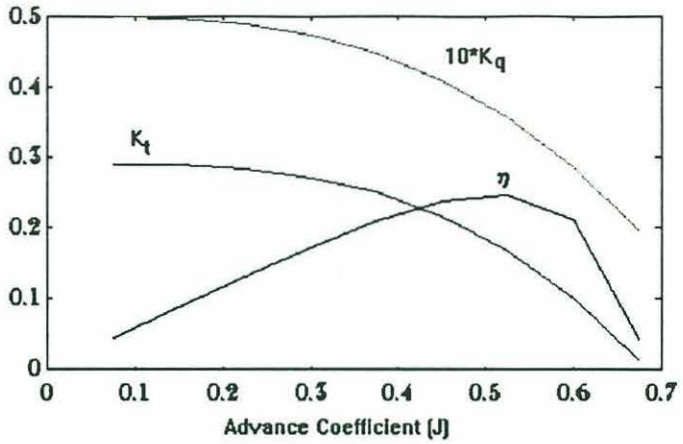

Fig. 6-4. Graph showing K_t, K_q, and efficiency plotted against advance coefficient for a typical fixed pitch propeller.

6.3 Pre-swirl Stators

Addition of pre-swirl stators to a ducted propeller has a significant effect upon all operating parameters. Table 1, reproduced from Hughes [7], shows the variation in four non-dimensional parameters as the pitch of the stator blades is altered at J=0.8. $K_{t\ (total)}$ takes into account the drag force on the duct and stator blades, whereas K_t concerns only the force generated by the propeller blades. In the example shown, from a starting stator pitch angle of 6 degrees, thrust can be increased or decreased by 50% solely through the alteration of stator pitch. Increasing the pitch of the stators increases the thrust produced, while simultaneously increasing the torque required. At some point the resultant efficiency reaches a maximum, in this case at around 9 degrees stator pitch angle [7].

Stator pitch angle	K_t	$K_{t(total)}$	K_q	η
-7.000	0.140	0.139	0.035	0.505
0.000	0.201	0.199	0.046	0.561
3.000	0.221	0.248	0.049	0.577
6.000	0.255	0.258	0.054	0.603

9.000	0.295	0.310	0.057	0.654
14.000	0.352	0.349	0.071	0.632

Table 1. The effect of stator pitch angle on a ducted propeller at J=0.8.

6.4 Controllable Pitch Blades

Alteration of the pitch of the propeller blades has a similar effect. Increasing the blade pitch increases both the thrust and drag. At some point the resultant efficiency reaches a maximum value then decreases sharply reaching zero at the blade's stall angle.

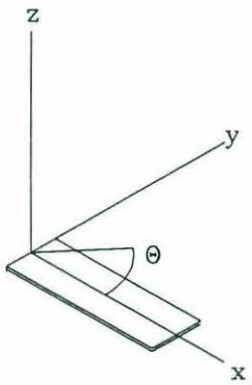

Coordinate System for Propeller

To determine the camber distribution of a flat bladed propeller at some non-zero angle of attack we must define a cylindrical coordinate system (r,θ,z). For convenience we will also define

$$x = r\cos\theta \quad y = r\sin\theta$$

The propeller rotates about the *z*-axis with one propeller blade lying along the θ=0 line (the *x*-axis). This blade is represented as a zero-thickness surface of width, *c*, at an angle of a from the *y*-axis in the *y*-*z* plane. The intersection of this plate with a cylinder of radius *r* is derived below. On the plate

$$z = y\tan\alpha = r\sin\theta\tan$$

This is valid between $\pm\theta_{max}$ given by

$$\theta_{max} = \arcsin\left(\frac{c\csc\alpha}{2r}\right)$$

We can now define a nose-tail line on the surface of the cylinder. This line will be at some angle ϕ given by

$$\tan\phi = \frac{\Delta z}{r\Delta\theta} = \frac{2r\tan\alpha\sin\theta_{max}}{2r\theta_{max}} = \tan\alpha\frac{\sin\theta_{max}}{\theta_{max}}$$

The camber is then simply the difference between the meanline of the plate and the nose-tail line.

$$f(\theta) = r\tan\alpha\left(\sin\theta - \frac{\theta\sin\theta_{max}}{\theta_{max}}\right)$$

We wish to express this camber as a function of x_p the distance from the centerline of the blade along the nose-tail line.

$$x_p = \frac{r\theta}{\cos\phi}$$

$$f(x_p) = r\tan\alpha\left[\sin\left(\frac{x_p\cos\phi}{r}\right) - \frac{\sin\theta_{max}}{\theta_{max}}\left(\frac{x_p\cos\phi}{r}\right)\right]$$

The result is a camber profile closely resembling a full sinusoid (figure 6-5). The amount of camber decreases with increasing radius and increase with increasing chord length and angle of attack.

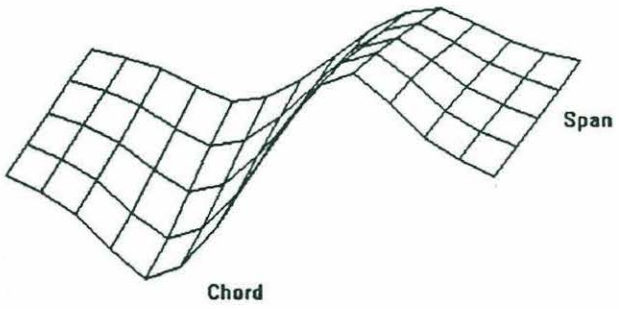

Fig. 6-5. Effective camber profile of a flat propeller blade looking outward from hub.

Also, the effective chord length changes with the radius. If we define the chord length as the length of the nose-tail line, then the chord length *c(r)* is derived as

$$c(r) = \frac{2r\theta_{max}}{\cos\phi}$$

6.5 Analysis of CP Propeller Designs

We can use the lifting surface program PSF-10 to evaluate the performance of flat plate propellers. This program accepts an administrative file and a propeller geometry file as inputs and produces a detailed output including the non-dimensional thrust and torque coefficients K_T and K_Q, the overall propeller efficiency η, and the thrust coefficient C_T.

First, the optimum number of blades was determined. From a purely practical standpoint, a smaller number of blades is preferable to a larger number. However, if great gains in performance were to occur with a larger number of blades, the increased complexity might be justified.

Separate blade geometry was generated for each run. To allow adequate room for pitch changing mechanisms, the propeller had to have a hub of at least 3.5cm radius. A maximum propeller diameter of 25cm is chosen so that the propeller will fit within existing propeller shrouds. The chord length was set as the maximum which would allow all blades to contact the hub at a zero angle of attack. This chord length is simply equal to the length of one side of an *n*-sided polygon circumscribed about the circle. For two and three bladed propellers, a chord length of twice the hub radius was used. The blade was given a NACA66 thickness profile with a maximum thickness of 1/4 inch to allow sufficient

material for mounting the blade to its spindle. These propellers were analyzed at an advance coefficient, J_S, of 0.137.

The results of these runs (table 6-2) shows that efficiency actually decreases slightly as the number of blades increases.

Number of blades	Chord	Blade length	A_P	K_T	K_Q	η	C_T
2.000	7.000	8.500	0.250	0.170	0.020	0.200	22.700
3.000	7.000	8.500	0.370	0.220	0.030	0.193	29.800
4.000	7.000	8.500	0.496	0.260	0.030	0.190	34.700
5.000	5.080	8.740	0.440	0.220	0.030	0.189	30.200
6.000	4.040	8.840	0.410	0.210	0.030	0.189	27.800
7.000	3.370	8.890	0.400	0.210	0.020	0.188	27.800
8.000	2.900	8.920	0.390	0.200	0.020	0.188	27.500

Table 6-2. Results of multiple blade PSF-10 runs.

The two-bladed propeller has the best efficiency and is easy to build. The K_T of 0.168 translates to a thrust of 33.2 lbf at 900rpm. This is a reasonable value for an underwater vehicle under normal operating conditions. Also, this occurs at the rather moderate pitch angle of 15 degrees. More thrust could likely be generated by increasing the blade pitch.

A second set of PSF-10 runs were performed for the two-bladed propeller and this time the pitch was varied. The results of these runs show that after what seems almost like

a dead zone for pitch angles of less than 5 degrees, K_T and C_T increase nearly linearly up to a pitch angle of 30 degrees, while K_Q increases in a parabolic manner. Propeller efficiency increases rapidly to a maximum at a pitch angle of 10 degrees then decreases again.

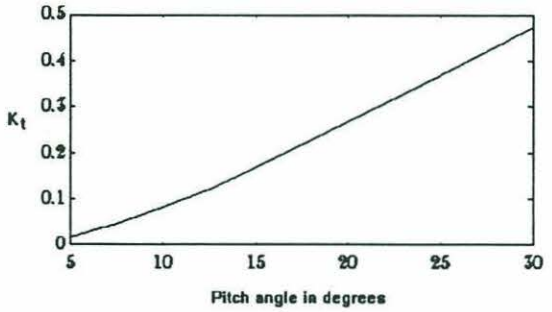

Fig. 6-6. The non-dimensional thrust, K_t, of the two-bladed propeller plotted against pitch angle

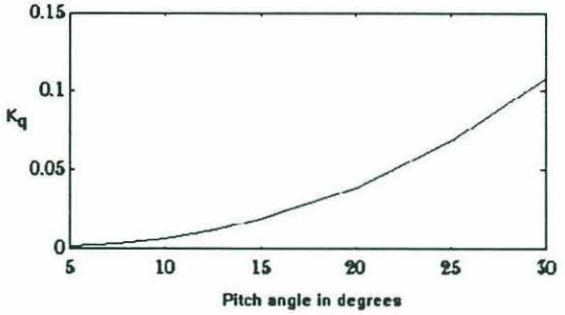

*Fig. 6-7.*Non-dimensional torque, K_q, plotted against pitch angle for the two-bladed propeller design.

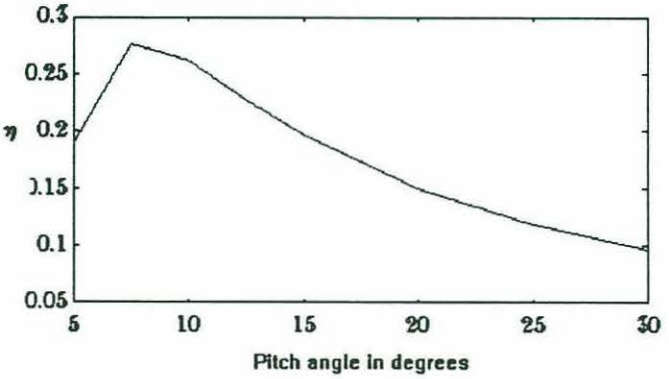

Fig. 6-8 Efficiency plotted against pitch angle for the two-bladed propeller design.

This thrust response is very well suited toward use in a variable pitch propeller. It allows a high resolution response in the low-thrust range and a linear response for the rest of the pitch range. The high resolution could be useful during hover and the linear response is easily modeled in a control scheme.

Analysis of the pressure distribution over the chord of a flat plate at a non-zero angle of attack indicates that the chordwise center of pressure is located at or near the quarter-chord point, that is, the point located a distance of c/4 from the leading edge of the blade. To minimize the moment around the spindle axis induced by hydrodynamic forces, the spindle axis is located at the quarter-chord point. While this produces an unusual-looking propeller, it has little effect on the overall thrust, torque, or efficiency.

The final blade design is presented in the appendix. It is nearly identical to the blade shape analyzed with the two bladed propeller above. The blade uses a NACA66 thickness profile to smooth the flow and retard separation. These blades were produced for the prototype using a CNC milling machine, with the end mill profiling the blade shape along the propellers spanwise axis. Figure 6-9 shows the completed blades mounted on the assembled propeller system.

Fig. 6-9. Photo of the propeller blades.

Chapter 7
IMPLEMENTATION AND RECOMMENDATIONS

The machined parts were fabricated at a local machine shop from the mechanical drawings shown in appendix B. The propeller system was assembled at Woods Hole incorporating the machined parts and a number of off-the-shelf parts and fasteners. Figures 7-1 and 7-2 show the final assembled device with and without the attached servo motor unit.

7.1 Recommended testing procedure

This propeller system is ready to undergo testing to determine dynamic thrust response. The following recommendations are made for this testing

1. The servo motor gains should be adjusted to give a higher torque bandwidth. Currently, the system bandwidth is limited by the servo motor controller.

2. Computer code should be generated to control the pitch angle of the blades during testing.

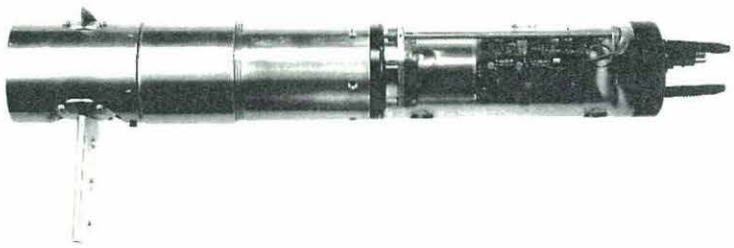

Fig. 7-1 The assembled propeller system with the pitch actuating servo motor attached.

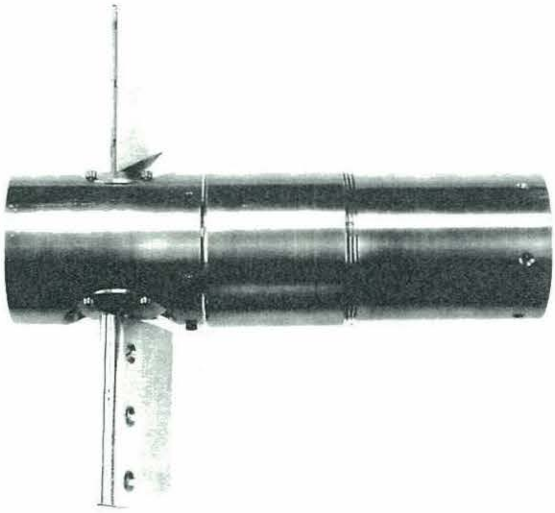

Fig. 7-2. The assembled propeller system without the servo motor.

3. The propeller system should be tested using a speed-controlled thruster motor capable of supplying at least 0.5 hp.

4. The propeller should be mounted such that the stationary housing and servo motor housing are rigidly supported and prevented from rotating during operation. The thruster motor shaft should not support the weight of the propeller and servo.

5. Dynamic tests should be conducted to determine the step response of thrust resulting from a step in blade pitch angle. The blade pitch angle steps should occur over a wide range of starting and stopping angles.

6. A dynamic model describing the transient response of the system should be generated.

7. This model should be used to design a control system utilizing the propeller system. The control system could be tested over a variety of trajectories to determine the tracking error. This error could be compared against that of existing control systems to validate or invalidate the use of this CP propeller system to improve dynamic thrust performance.

7.2 Recommendations for redesign

The propeller system would benefit from a mechanical redesign. A number of components were difficult to assemble and required material modification during debug as described in Appendix C.

1. The interference problems between the links and the rotating housing, coupler, and inner bushing should be addressed.

2. A larger value for the compressed thickness of wave washers should be used.

3. Fastener size should be standardized to the greatest degree possible. Inch series fasteners could be used to ease acquisition problems.

4. A different method of securing the boot to the stationary housing should be found. The idea of using a threaded connection arose from the need to preload the seal spring and the main bearing. This proved problematic in practice. The spacer tended to jam as the boot was screwed into place. The stiff spring in the seal generated a great deal of friction in the threads during preloading. Most troubling was the difficulty in getting the threaded surface to pass over the O-ring in the stationary housing without causing it to bind in the threads.

5. A method of hardening O-ring sealing surfaces, such as hard-coat anodization, should be found. The soft aluminum surfaces were easily scratched during repeated assembly and disassembly.

6. Use of teflon hard coating of the crosshead to reduce friction as it slides in the coupler should be considered.

7. The caps could be made to better conform with outside surface of the hub.

7.3 Summary

As vehicle control systems become increasingly advanced, overall vehicle control is becoming limited by mechanical actuators. Clearly, fixed pitch propeller actuation systems are less than optimal in those situations requiring the most precise vehicle control. The device presented in this thesis has the potential to provide a significant advance in thrust bandwidth at low thrust levels, while retaining the capacity to perform adequately at larger thrust levels.

The thesis first demonstrated the problems of fixed pitch propellers using several numerical models. These models revealed the highly non-linear nature of fixed-pitch propeller dynamic response. Different types of propulsors were examined to determine a suitable alternative. Several prospective designs for improved dynamic response were generated and from these the controllable pitch propeller was chosen. The design for the pitch changing mechanism was presented and modeled. Dynamic modeling predicted very fast response to a step torque input from the pitch actuator. Next the blades were designed after a short section covering the basics of propeller theory. Precise equations for the camber profile of the blades at different angles of attack were derived, and the operating characteristics of the propeller were determined numerically. The device was built and debugged.

While this device remains to be tested, it has the possibility of making a significant advance in the area of underwater vehicle control. This system represents the next generation of underwater thrust actuators. Where fixed-pitch propellers were adequate for the missions and control schemes of the past, they are often unable to satisfy the requirements of modern vehicle systems. When implemented, this system will provide future designers with a valuable alternative in their underwater propulsion toolbox.

7.4 Recommendation for Future Work

There are a number of subjects addressed in this thesis which are appropriate topic for future research.

- Work could be done to improve upon existing propeller thrust models and perhaps incorporate controllable pitch propeller systems into those models.

- The hydrodynamic forces and flows occurring during a pitch change on a controllable pitch propeller could be investigated.
- A functional controllable pitch stator system could be designed and built.
- A vertical axis propeller system for an ROV could be designed and built.
- A fixed-pitch propeller optimized for dynamic response could be designed.
- Different blades with different shapes and cambers could be tested with this propeller system.

REFERENCES

[1] Cooke, J.G., "Incorporating Thruster Dynamics in the Control of an Underwater Vehicle," Master's Thesis, Massachusetts Institute of Technology and Woods Hole Oceanographic Institution, 1989.

[2] McLean, M.B., "Dynamic Performance of Small Diameter Tunnel Thrusters," Master's Thesis, Naval Post Graduate School, Monterey, Ca., March 1991.

[3] Crandall, S.H., D.C. Karnopp, E.F. Kurtz and D.C. Pridmore-Brown, *Dynamics of Mechanical and Electromechanical Systems.* New York: McGraw-Hill, 1968.

[4] Wind, J. ,Principles of mechanisms used in controllable pitch propellers, 1st Propeller Symposium, Feb. 1971, Rotterdam.

[5] Haselton, Ted and John Goode, *A retrofit ROV modular thruster system.* Imagineering, Cookeville, TN.

[6] *Principles of Naval Architecture*, John Comstock, ed., SNAME, NY, 1967.

[7] Hughes, Michael J., "An Experimental Analysis of Adjustable Pitch Pre-Swirl Stators in Combination with a Ducted Propeller", Presented at New England SNAME meeting, January, 1991.

[8] Vassilopoulos, Lyssimachos and Pranab Ghosh," Simplified Structural Analysis Techiniques for Trunnion-Type Hub Mechanism of Controllable Pitch Propellers," Propellers '84 Symposium, SNAME, NY, 1984.

[9]Fox, Robert and Alan McDonald, *Introduction to Fluid Dynamics*, New York: John Wiley and Sons, 1985.

[10] Kerwin, J.E., "Hydrofoils and Propellers (13.04) Lecture Notes," 1993.

[11] Beek, G.H.M. and J. Heidemans, "Strength Considerations in Controllable Pitch Propeller Design", 3rd Lips Propeller Symposium, Drunen, The Netherlands, 1977.

[12] Fay, John, *The Helicopter: History, Piloting, and How It Works*, New York: Hippocrene Books, 1987.

[13] *Principles of Naval Architecture*, John Comstock, ed., New York: SNAME, 1967.

Appendix A

SYMBOLS USED IN STATIC ANALYSIS

Geometric Dimensions

D_{OB}	Diameter of the propeller spindle at the outer bushing	14mm
D_{OS}	Diameter of the shoulder on the propeller spindle contacting the outer bushing	15mm
D_{IB}	Diameter of the propeller spindle at the inner bushing	14mm
D_{RI}	Diameter of the propeller spindle at the O-ring	9.5mm
R_C	Radius of the crank arm	19.5mm
D_S	Diameter of the crank pin	4mm
H_{IB}	Radius from the center of the hub to the center of the inner bushing	6.5mm
H_{OB}	Radius from the center of the hub to the center of the outer bushing	24.5mm
H_{LF}	Radius from the center of the hub to the center of the line of force of the crank arm along the propeller spindle	13.5mm
L_L	Effective length of the link	27.97mm
X_{LF}	The *x*-coordinate of the aft pivot of the link	5.56mm

Material Properties

μ_T Coefficient of friction between bushings and propeller spindle 0.16

μ_S Coefficient of friction between pin and propeller spindle shaft ear 0.16

f_S' Specific friction of the O-ring against the propeller spindle 1.5 lbf/in

Derived Quantities

R_{OX} Reaction force from outer bushing along the *x*-axis

R_{OZ} Reaction force from outer bushing along the *z*-axis

R_{IX} Reaction force from the inner bushing along the *x*-axis

R_{IZ} Reaction force from the inner bushing along the *z*-axis

R_Y Reaction force from the outer bushing resistive the centripetal force along the *y*-axis

F_X Hydrodynamic force on the blade acting along the *x*-axis

F_Z Hydrodynamic force on the blade acting along the *z*-axis

M_X Externally imposed moment on the spindle about the *x*-axis

M_Y Externally imposed moment on the spindle about the *y*-axis

F_L Force acting along the main axis of the link

F_{LX} Component of link force along the *x*-axis

F_{LZ} Component of link force along the *z*-axis

Z_{LF} The *z*-coordinate of the aft pivot of the link

Angles

ψ	Angle between the main axis of the link and the x-axis
θ	Pitch angle of the blade

Appendix B
MECHANICAL DRAWINGS

Parts for the prototype were produced from these mechanical drawings. The drawings do not reflect the minor changes made during debugging and shake-down.

Drawing title	Number
Blades	CPP-1
Shaft	CPP-3
Shaft Assembly Drawing	CPP-3A
Cap	CPP-4
Cap Assembly Drawing	CPP-4A
Shaft Ears	CPP-5
Pin	CPP-6
Bushing	CPP-7
Bushing	CPP-8
Rotating Housing	CPP-9
Rotating Housing Assy. Drawing	CPP-9A
Lever Arm	CPP-10
Crosshead	CPP-11

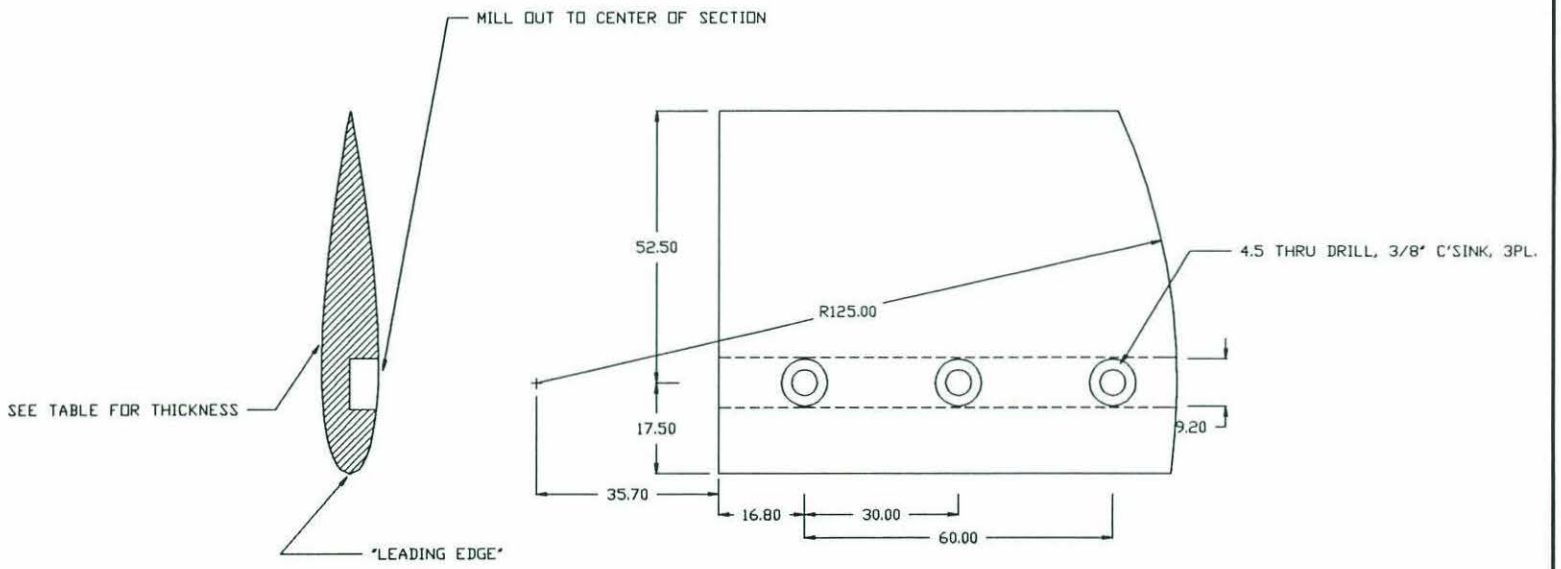

UNLESS OTHERWISE SPECIFIED ALL UNITS ARE IN MILLIMETERS TOLERANCES DECIMALS .X ±0.15 .XX ±0.10 ANGULAR ±1°	TITLE: BLADE #1
	MATERIAL: 6061-T6 ALUMINUM
ROB KEEFE, BLAKE TRLR, x3268	NO REQD: 1 — DWG NO: CPP-1

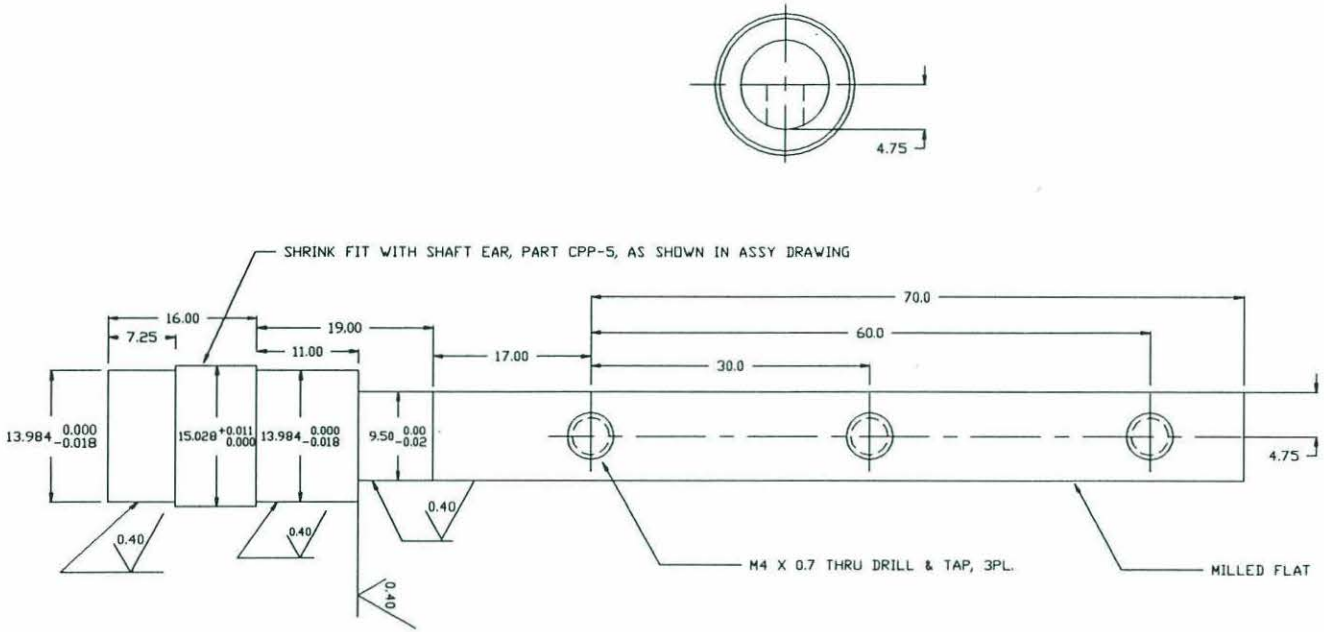

UNLESS OTHERWISE SPECIFIED ALL UNITS ARE IN MILLIMETERS TOLERANCES DECIMALS .X ±0.15 .XX ±0.10 ANGULAR ±1°	TITLE SHAFT
	MATERIAL AISI 316 STAINLESS STEEL
ROB KEEFE, BLAKE TRLR, x3268	NO REQD 2 / DWG NO CPP-03

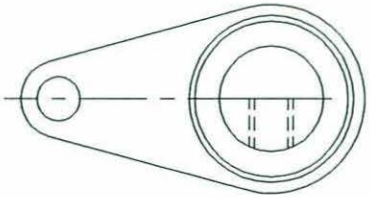

FLAT ON END OF SHAFT MUST ALIGN WITH
CENTER LINE OF RING ON SHAFT EAR

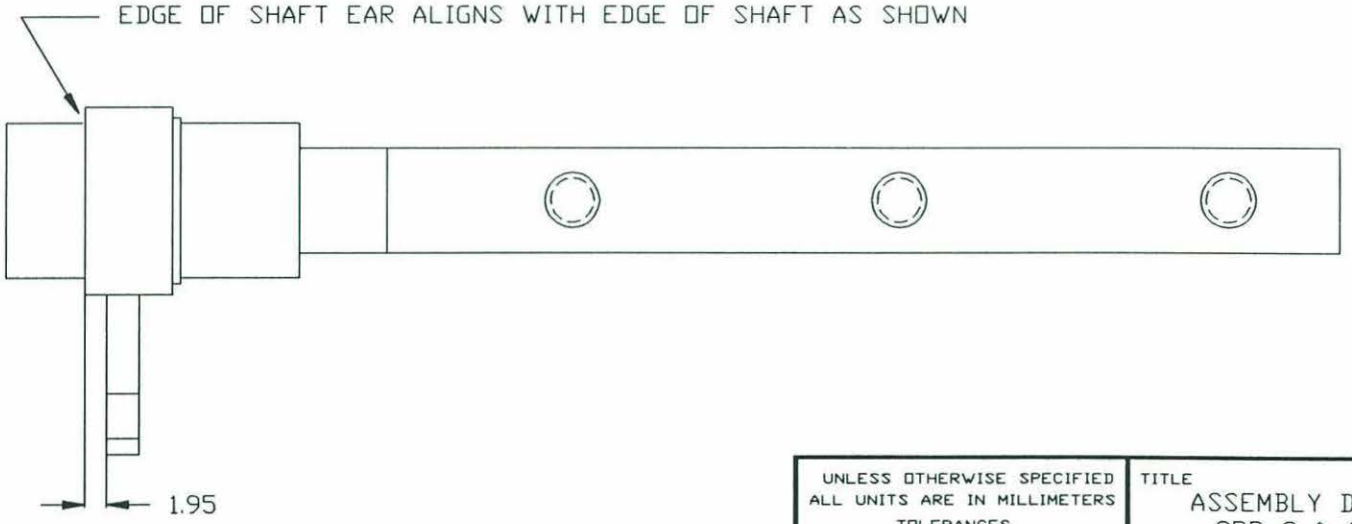

UNLESS OTHERWISE SPECIFIED ALL UNITS ARE IN MILLIMETERS TOLERANCES DECIMALS .X ±0.15 .XX ±0.10 ANGULAR ±1°	TITLE ASSEMBLY DRAWING CPP-3 & CPP-5
	MATERIAL PARTS CPP-3 AND CPP-5
ROB KEEFE, BLAKE TRLR, x3268	NO REQD 2 ASSY. / DWG NO CPP-3A

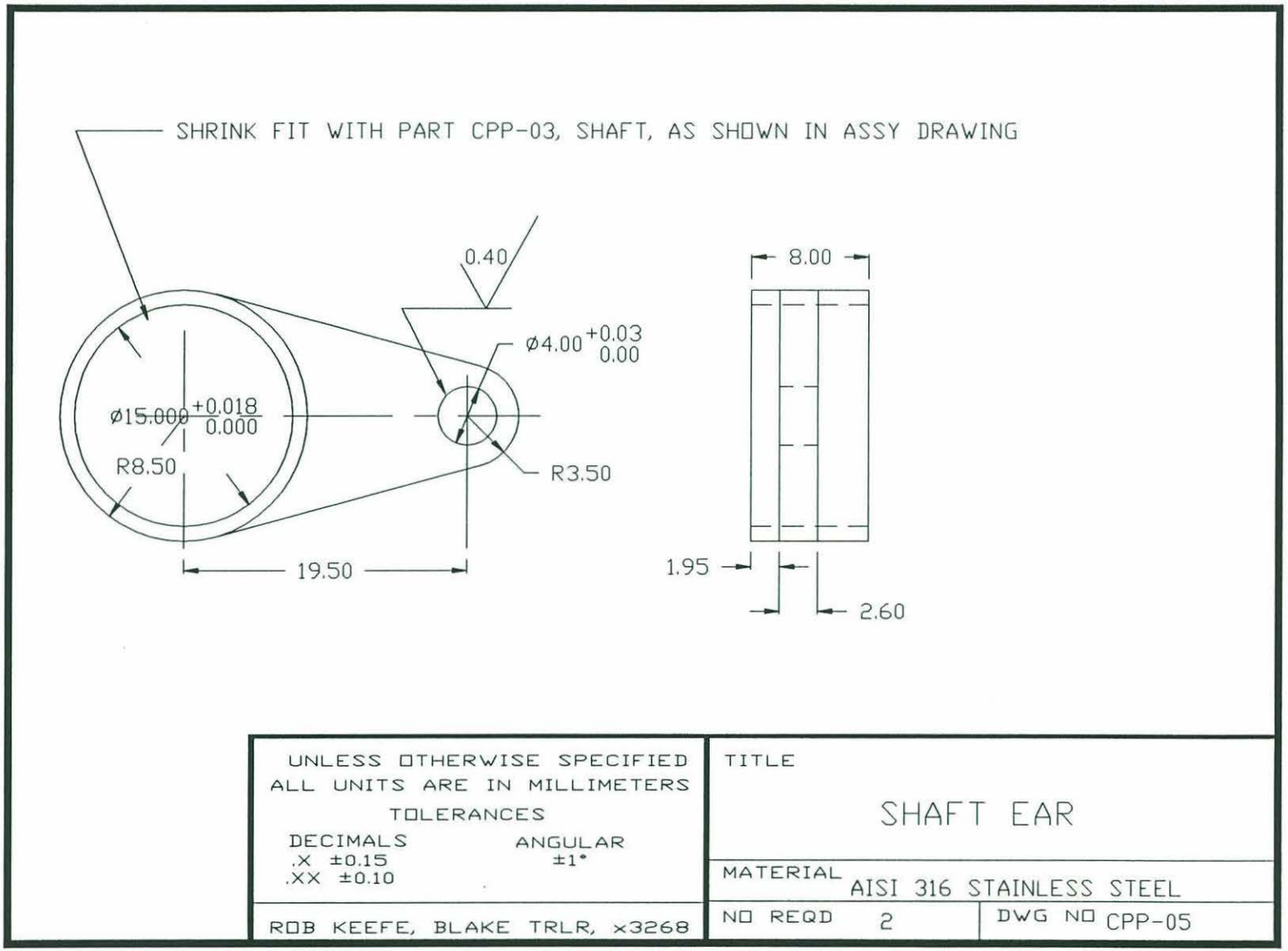

UNLESS OTHERWISE SPECIFIED ALL UNITS ARE IN MILLIMETERS TOLERANCES DECIMALS .X ±0.15 .XX ±0.10 ANGULAR ±1°	TITLE SHAFT EAR
	MATERIAL AISI 316 STAINLESS STEEL
ROB KEEFE, BLAKE TRLR, x3268	NO REQD 2 / DWG NO CPP-05

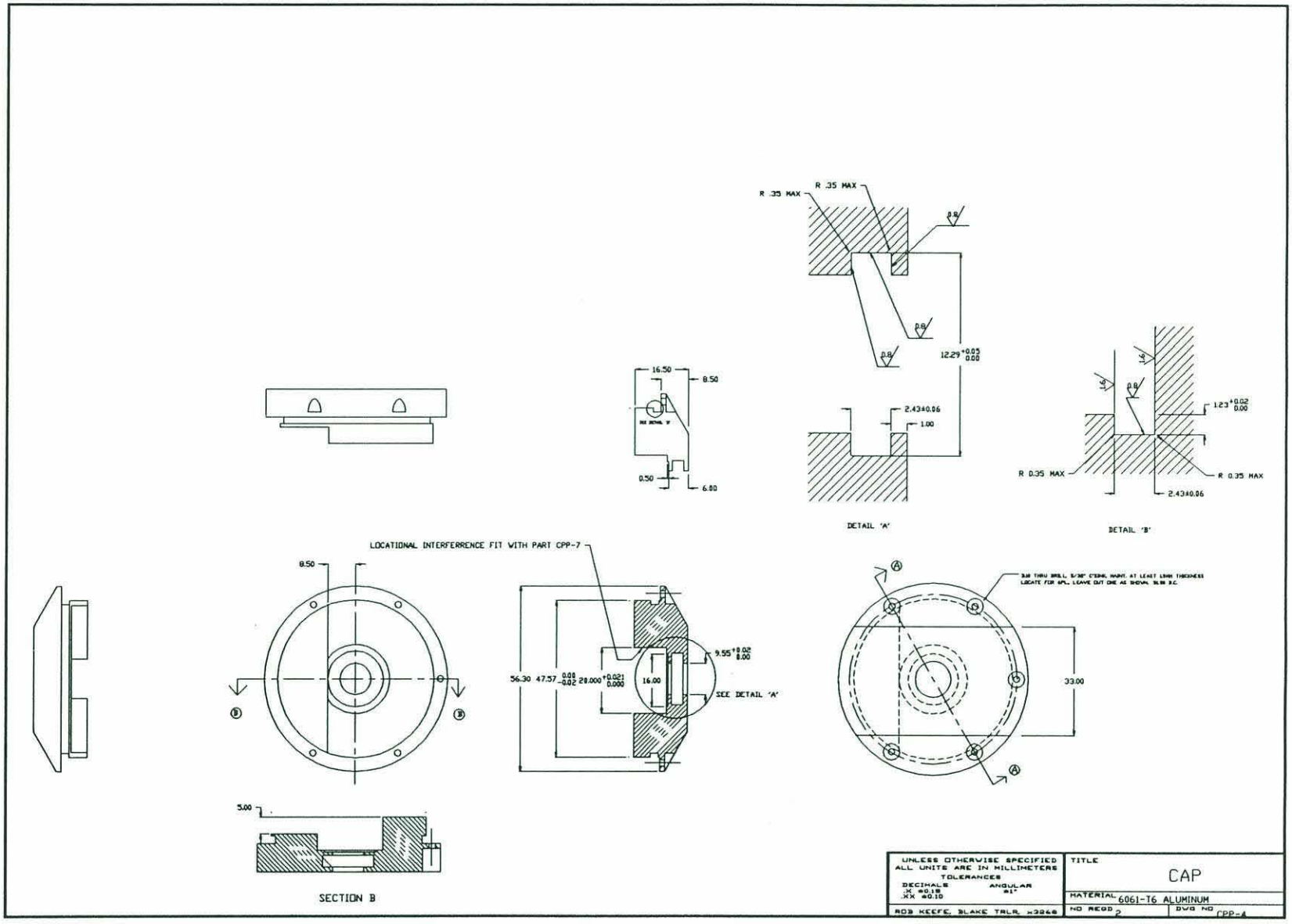
R .35 MAX
R .35 MAX
0.8
0.8
0.8
12.29 +0.05 0.00
2.43±0.06
1.00
16.50
8.50
0.50
6.00
1.6
1.6
0.8
1.23 +0.02 0.00
R 0.35 MAX
R 0.35 MAX
2.43±0.06
DETAIL 'A'
DETAIL 'B'
LOCATIONAL INTERFERRENCE FIT WITH PART CPP-7
8.50
56.30
47.57 0.08 -0.02
28.000 +0.021 0.000
16.00
9.55 +0.02 0.00
SEE DETAIL 'A'
33.00
3.00
SECTION B
UNLESS OTHERWISE SPECIFIED
ALL UNITS ARE IN MILLIMETERS
TOLERANCES
DECIMALS
.X ±0.1
.XX ±0.10
ANGULAR
±1°
ROB KEEFE, BLAKE TALR, x3268
TITLE
CAP
MATERIAL 6061-T6 ALUMINUM
NO REQD 2
DWG NO CPP-A

INSERT BUSHING IN AS FAR AS IT GOES

SOME OF BUSHING MAY BE VISIBLE IN GAP IN BORE CAUSED BY MILLED FLAT AREA. BUSHING PROTRUSION IN THIS AREA IS ACCEPTABLE.

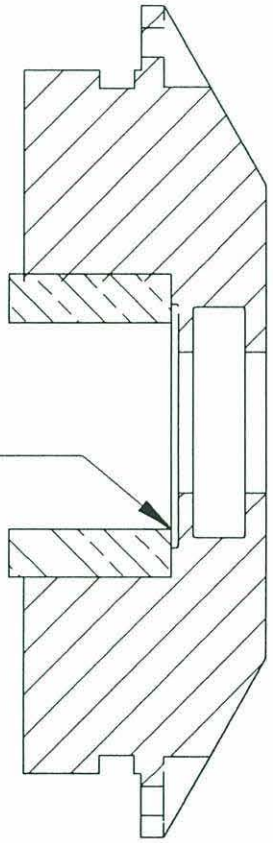

UNLESS OTHERWISE SPECIFIED ALL UNITS ARE IN MILLIMETERS TOLERANCES DECIMALS .X ±0.15 .XX ±0.10 ANGULAR ±1°	TITLE CAP ASSY DRAWING
	MATERIAL PARTS CPP-4 & CPP-7
ROB KEEFE, BLAKE TRLR, x3268	NO REQD 2 ASSY. DWG NO CPP-4A

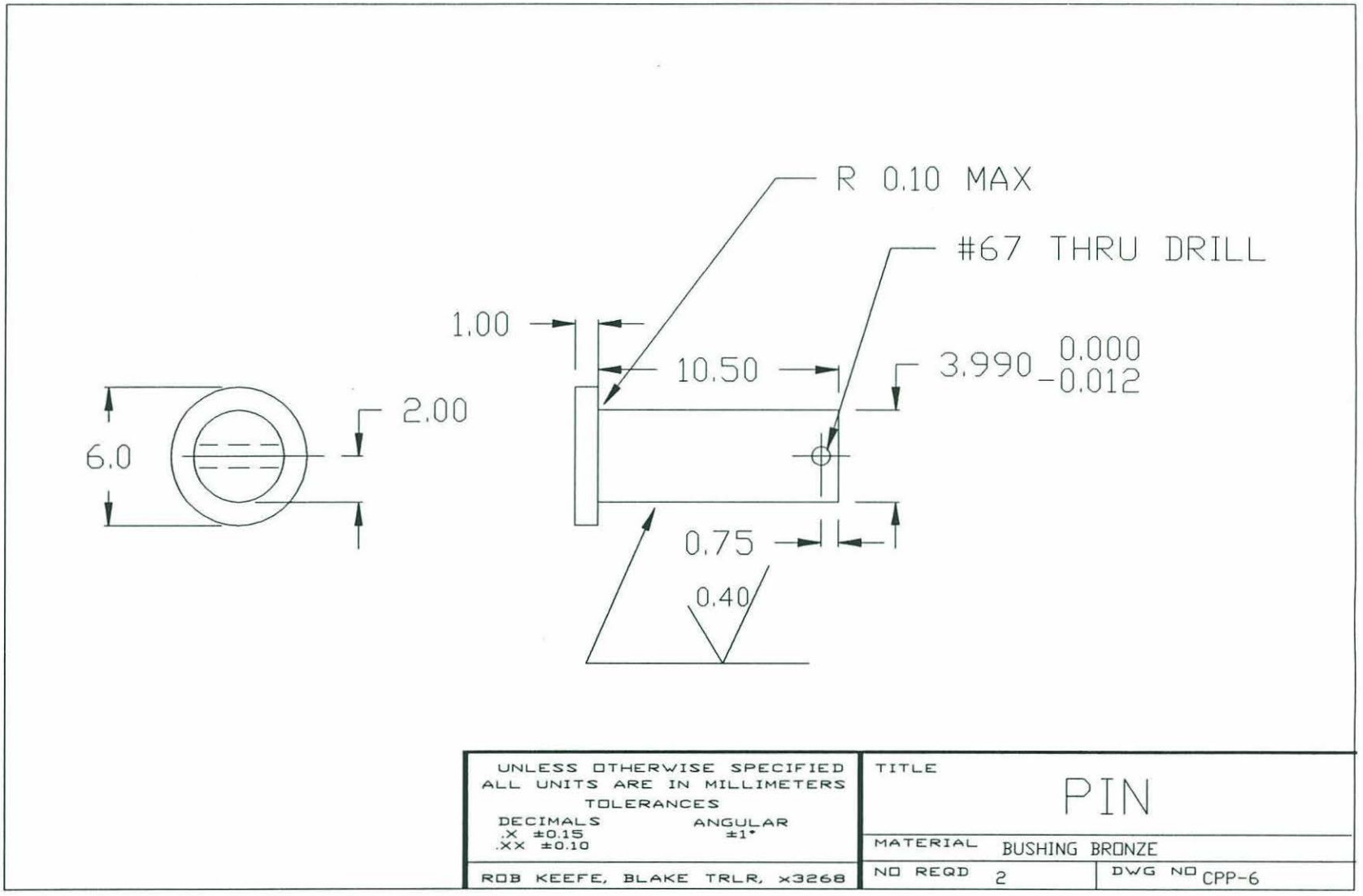
R 0.10 MAX
#67 THRU DRILL
1.00
10.50
3.990 0.000 -0.012
2.00
6.0
0.75
0.40
UNLESS OTHERWISE SPECIFIED
ALL UNITS ARE IN MILLIMETERS
TOLERANCES
DECIMALS
.X ±0.15
.XX ±0.10
ANGULAR
±1°
ROB KEEFE, BLAKE TRLR, x3268
TITLE
PIN
MATERIAL BUSHING BRONZE
NO REQD 2
DWG NO CPP-6

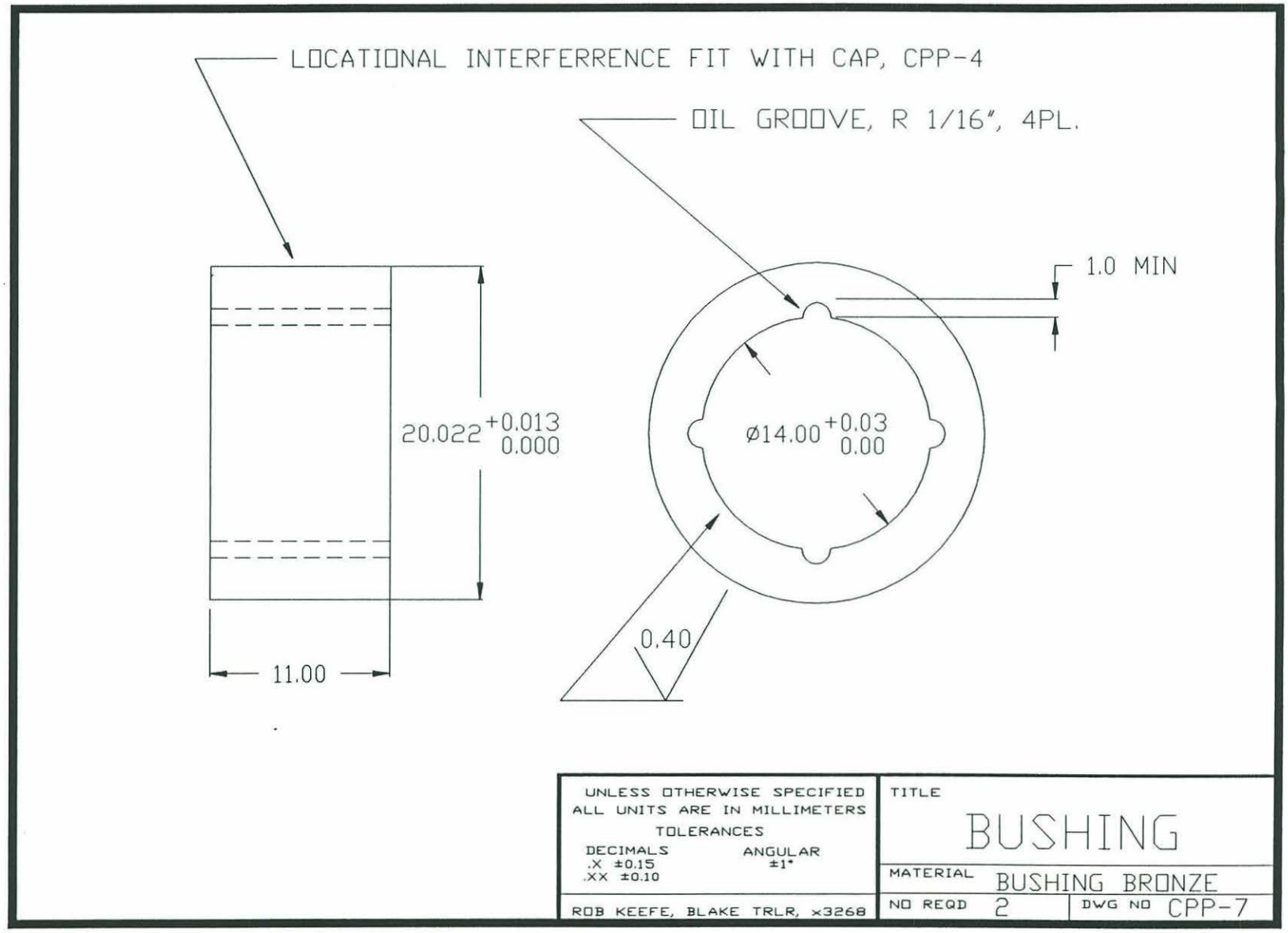
LOCATIONAL INTERFERRENCE FIT WITH CAP, CPP-4
OIL GROOVE, R 1/16", 4PL.
1.0 MIN
20.022 +0.013 0.000
Ø14.00 +0.03 0.00
0.40
11.00
UNLESS OTHERWISE SPECIFIED
ALL UNITS ARE IN MILLIMETERS
TOLERANCES
DECIMALS
.X ±0.15
.XX ±0.10
ANGULAR
±1°
ROB KEEFE, BLAKE TRLR, x3268
TITLE
BUSHING
MATERIAL BUSHING BRONZE
NO REQD 2
DWG NO CPP-7

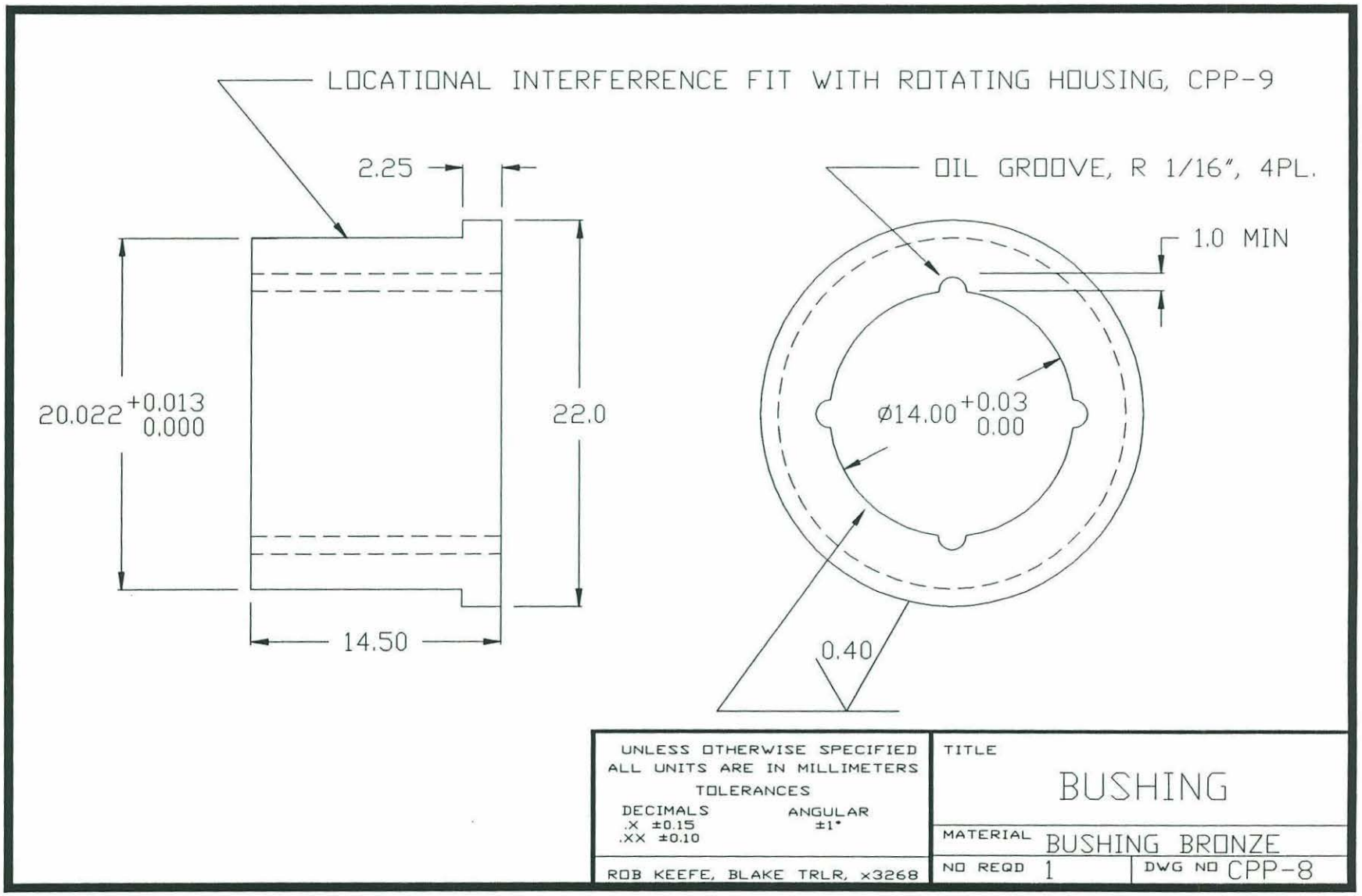
LOCATIONAL INTERFERRENCE FIT WITH ROTATING HOUSING, CPP-9
2.25
OIL GROOVE, R 1/16", 4PL.
1.0 MIN
20.022 +0.013 0.000
22.0
Ø14.00 +0.03 0.00
14.50
0.40
UNLESS OTHERWISE SPECIFIED
ALL UNITS ARE IN MILLIMETERS
TOLERANCES
DECIMALS
.X ±0.15
.XX ±0.10
ANGULAR
±1°
ROB KEEFE, BLAKE TRLR, x3268
TITLE
BUSHING
MATERIAL BUSHING BRONZE
NO REQD 1
DWG NO CPP-8

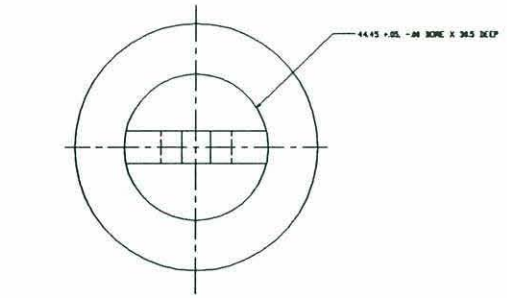

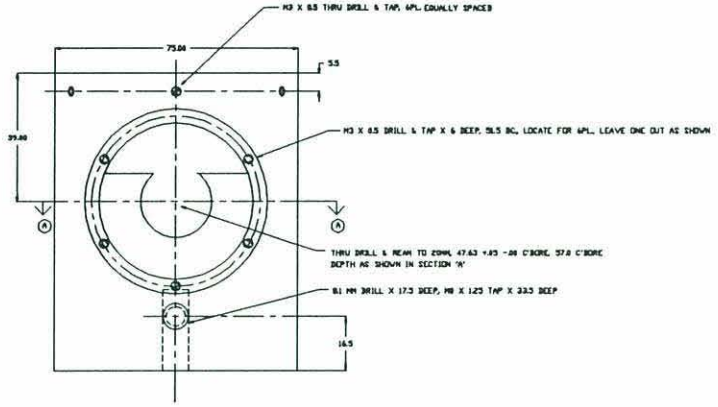

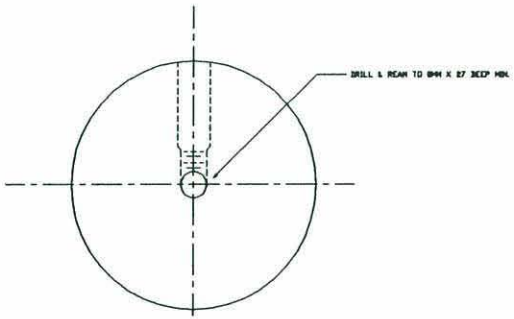

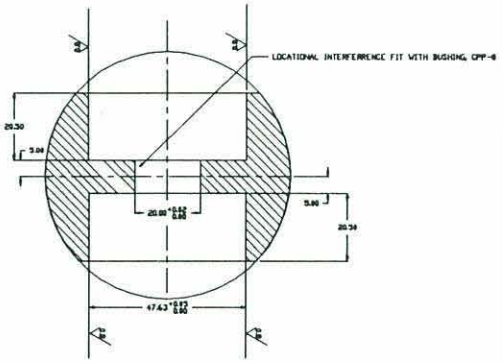

UNLESS OTHERWISE SPECIFIED ALL UNITS ARE IN MILLIMETERS TOLERANCES DECIMALS .X ±0.15 .XX ±0.10 ANGULAR ±1°	TITLE ROTATING HOUSING
	MATERIAL 6061-T6 ALUMINUM
ROB KEEFE, BLAKE TRLR, x3268	NO REQD 1 / DWG NO CPP-9

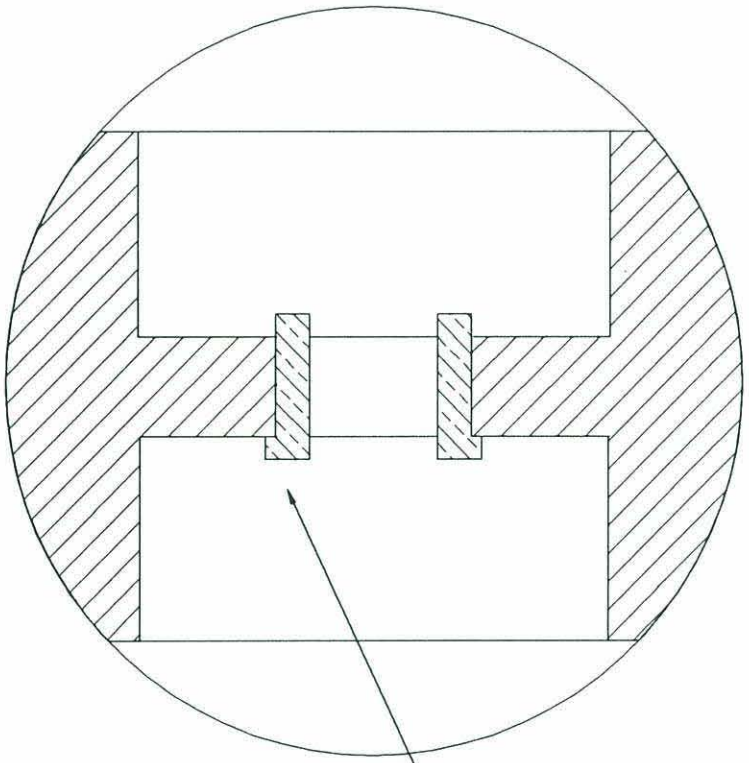

INSERT INTO THRU BORE UNTIL FLANGE CONTACTS HOUSING

THE SIDE THE FLANGE IS ON IS UNIMPORTANT

UNLESS OTHERWISE SPECIFIED ALL UNITS ARE IN MILLIMETERS TOLERANCES DECIMALS .X ±0.15 .XX ±0.10 ANGULAR ±1°	TITLE HOUSING ASSY DRAWING
	MATERIAL PARTS CPP-9 & CPP-8
ROB KEEFE, BLAKE TRLR, x3268	NO REQD 1 ASSY. / DWG NO CPP-9A

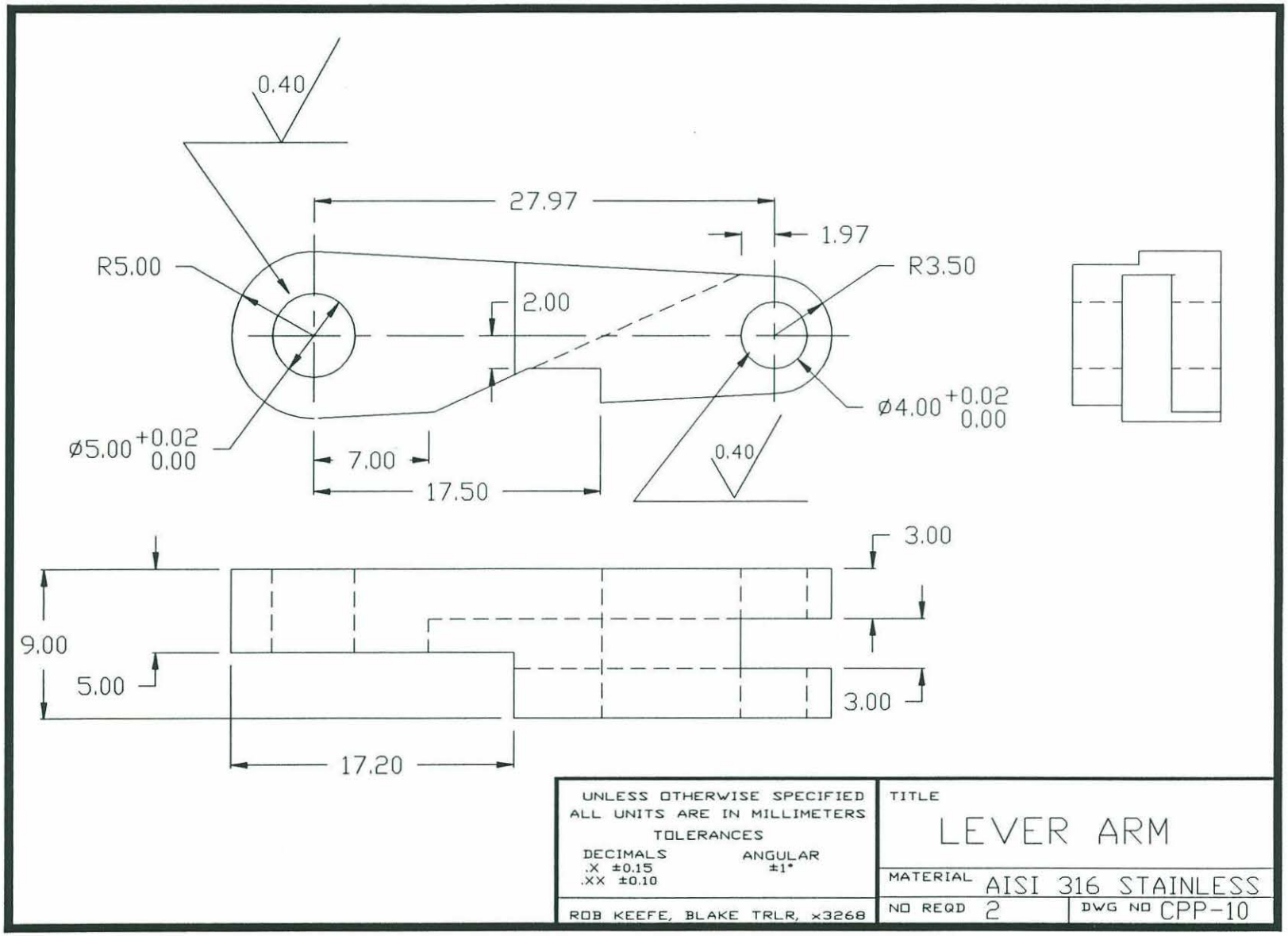
0.40
27.97
1.97
R5.00
R3.50
2.00
ø5.00 +0.02 0.00
ø4.00 +0.02 0.00
7.00
17.50
0.40
3.00
9.00
5.00
3.00
17.20
UNLESS OTHERWISE SPECIFIED
ALL UNITS ARE IN MILLIMETERS
TOLERANCES
DECIMALS
.X ±0.15
.XX ±0.10
ANGULAR
±1°
ROB KEEFE, BLAKE TRLR, x3268
TITLE
LEVER ARM
MATERIAL AISI 316 STAINLESS
NO REQD 2
DWG NO CPP-10

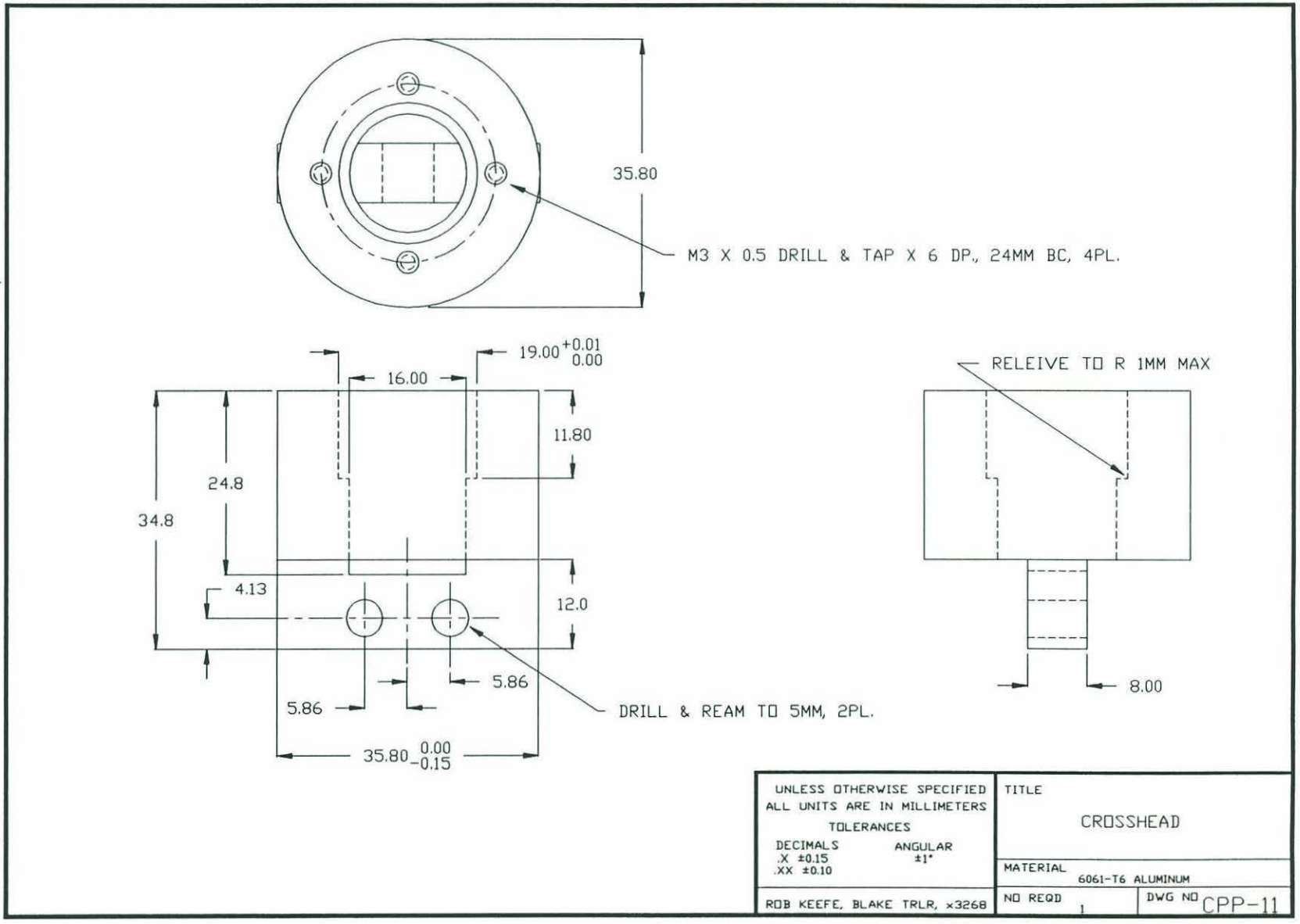
35.80
M3 X 0.5 DRILL & TAP X 6 DP., 24MM BC, 4PL.
19.00 +0.01 0.00
16.00
11.80
24.8
34.8
4.13
12.0
5.86
5.86
DRILL & REAM TO 5MM, 2PL.
35.80 0.00 -0.15
RELEIVE TO R 1MM MAX
8.00
UNLESS OTHERWISE SPECIFIED
ALL UNITS ARE IN MILLIMETERS
TOLERANCES
DECIMALS
.X ±0.15
.XX ±0.10
ANGULAR
±1°
ROB KEEFE, BLAKE TRLR, x3268
TITLE
CROSSHEAD
MATERIAL
6061-T6 ALUMINUM
NO REQD
1
DWG NO
CPP-11

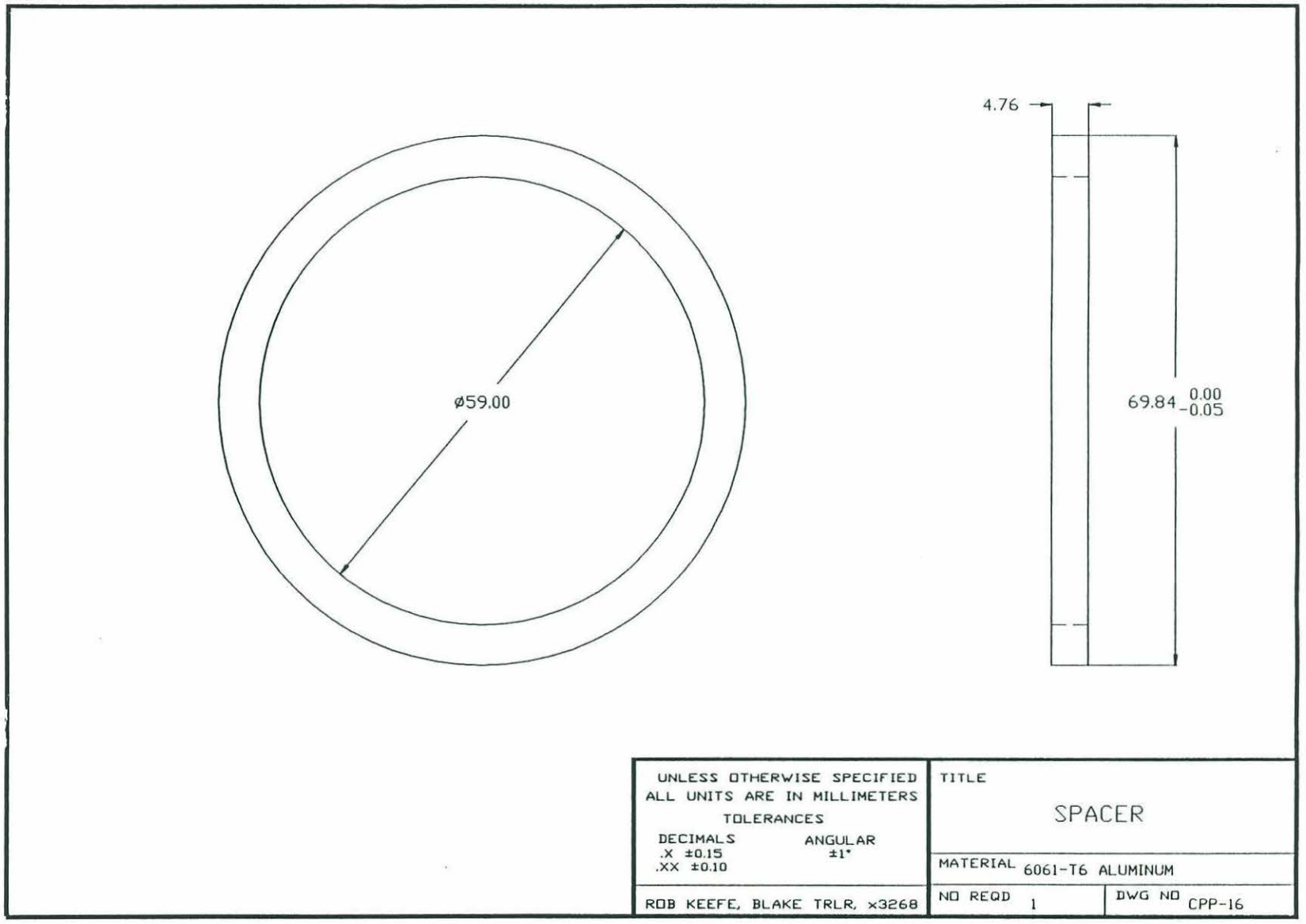

UNLESS OTHERWISE SPECIFIED ALL UNITS ARE IN MILLIMETERS TOLERANCES DECIMALS .X ±0.15 .XX ±0.10 ANGULAR ±1°	TITLE SPACER
	MATERIAL 6061-T6 ALUMINUM
ROB KEEFE, BLAKE TRLR, x3268	NO REQD 1 / DWG NO CPP-16

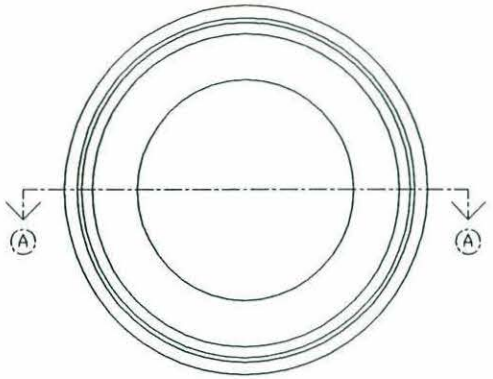

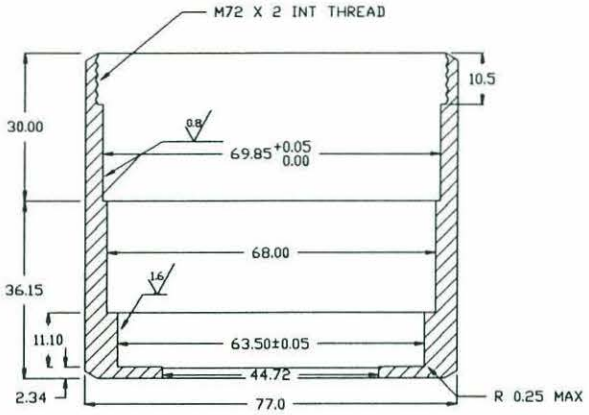

SECTION A

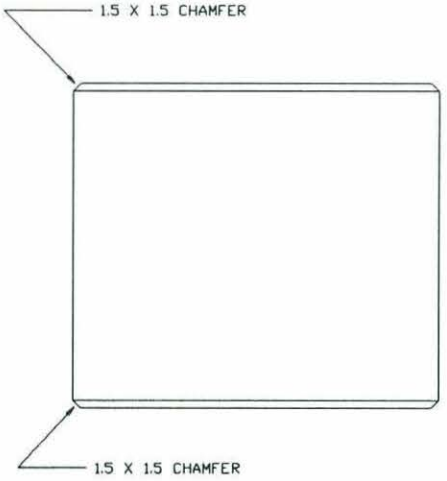

UNLESS OTHERWISE SPECIFIED ALL UNITS ARE IN MILLIMETERS TOLERANCES DECIMALS .X ±0.15 .XX ±0.10 ANGULAR ±1°	TITLE BOOT
	MATERIAL 6061-T6 ALUMINUM
ROB KEEFE, BLAKE TRLR, x3268	NO REQD 1 / DWG NO CPP-17

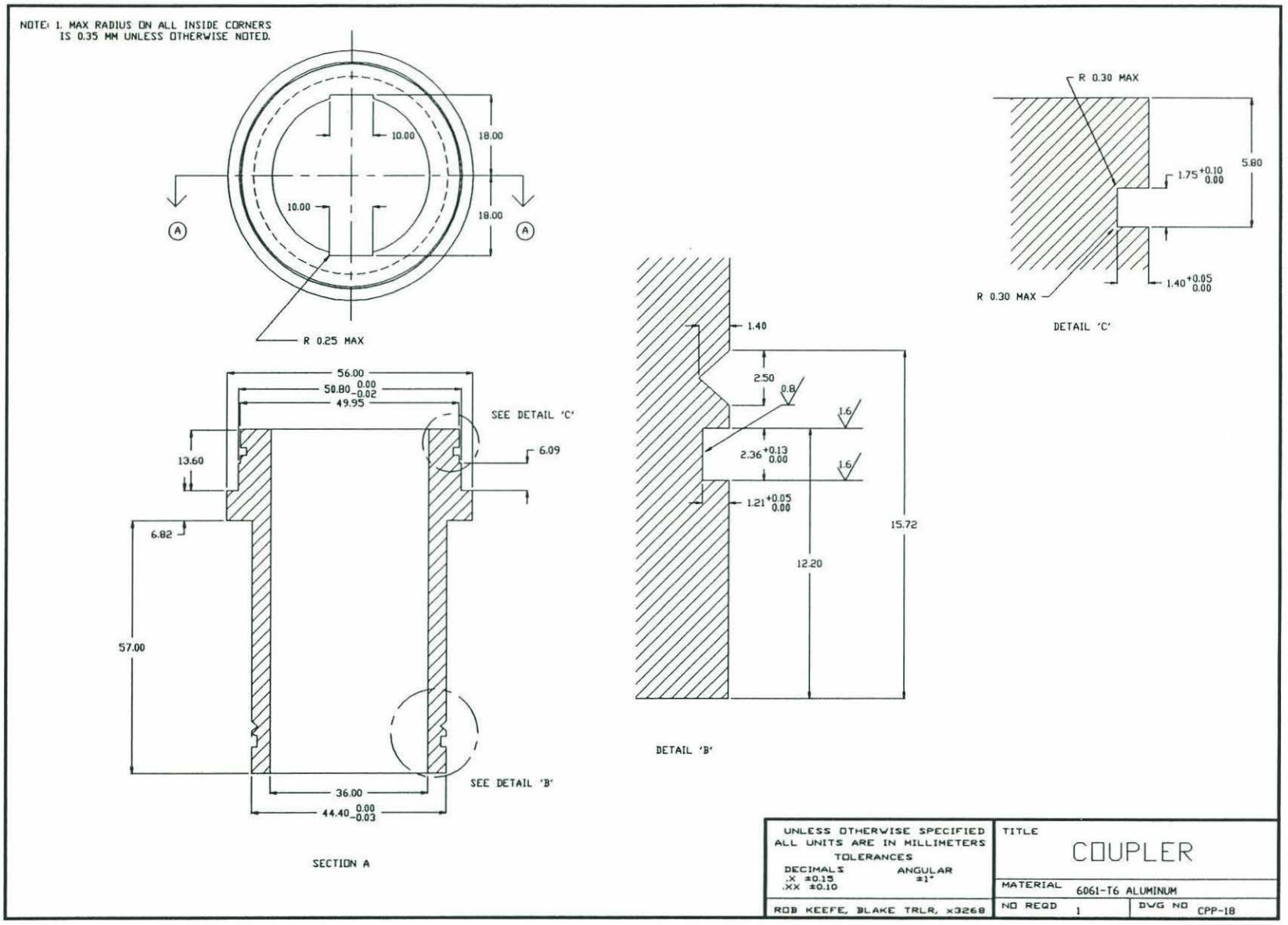
NOTE: 1. MAX RADIUS ON ALL INSIDE CORNERS IS 0.35 MM UNLESS OTHERWISE NOTED.
10.00
18.00
10.00
18.00
A
A
R 0.25 MAX
56.00
50.80 0.00 -0.02
49.95
SEE DETAIL 'C'
6.09
13.60
6.82
57.00
SEE DETAIL 'B'
36.00
44.40 0.00 -0.03
SECTION A
R 0.30 MAX
1.75 +0.10 0.00
5.80
1.40 +0.05 0.00
R 0.30 MAX
DETAIL 'C'
1.40
2.50
0.8
1.6
2.36 +0.13 0.00
1.6
1.21 +0.05 0.00
15.72
12.20
DETAIL 'B'
UNLESS OTHERWISE SPECIFIED
ALL UNITS ARE IN MILLIMETERS
TOLERANCES
DECIMALS
.X ±0.15
.XX ±0.10
ANGULAR
±1°
ROB KEEFE, BLAKE TRLR, x3268
TITLE
COUPLER
MATERIAL 6061-T6 ALUMINUM
NO REQD 1
DWG NO CPP-18

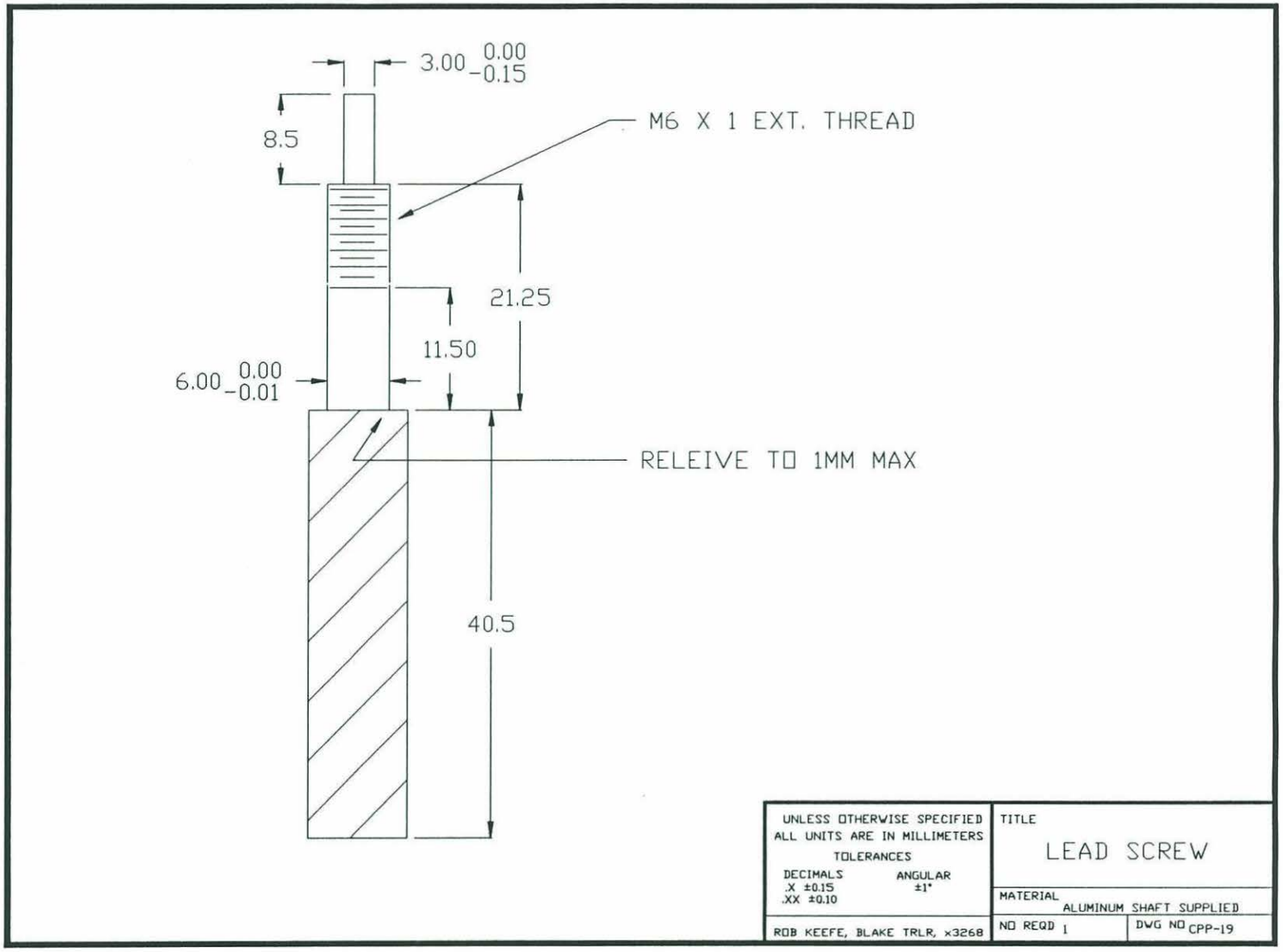
3.00 0.00 -0.15
8.5
M6 X 1 EXT. THREAD
21.25
11.50
6.00 0.00 -0.01
RELEIVE TO 1MM MAX
40.5
UNLESS OTHERWISE SPECIFIED
ALL UNITS ARE IN MILLIMETERS
TOLERANCES
DECIMALS
.X ±0.15
.XX ±0.10
ANGULAR
±1°
ROB KEEFE, BLAKE TRLR, x3268
TITLE
LEAD SCREW
MATERIAL
ALUMINUM SHAFT SUPPLIED
NO REQD 1
DWG NO CPP-19

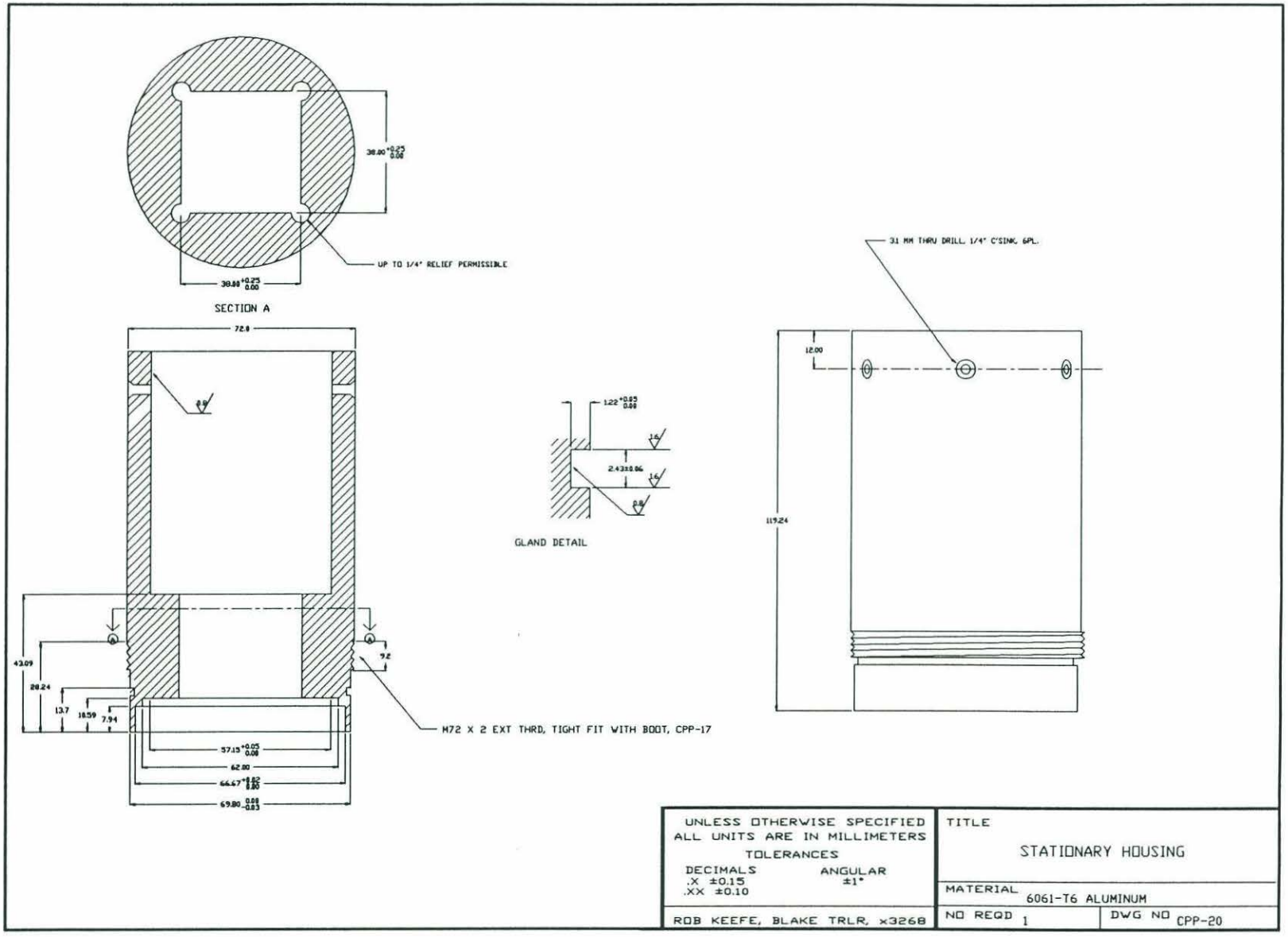
UP TO 1/4" RELIEF PERMISSIBLE
SECTION A
72.8
43.09
28.24
13.7
18.59
7.94
9.2
M72 X 2 EXT THRD, TIGHT FIT WITH BOOT, CPP-17
GLAND DETAIL
31 MM THRU DRILL 1/4" C'SINK, 6PL.
12.00
119.24
UNLESS OTHERWISE SPECIFIED
ALL UNITS ARE IN MILLIMETERS
TOLERANCES
DECIMALS
.X ±0.15
.XX ±0.10
ANGULAR
±1°
ROB KEEFE, BLAKE TRLR, x3268
TITLE
STATIONARY HOUSING
MATERIAL
6061-T6 ALUMINUM
NO REQD 1
DWG NO CPP-20

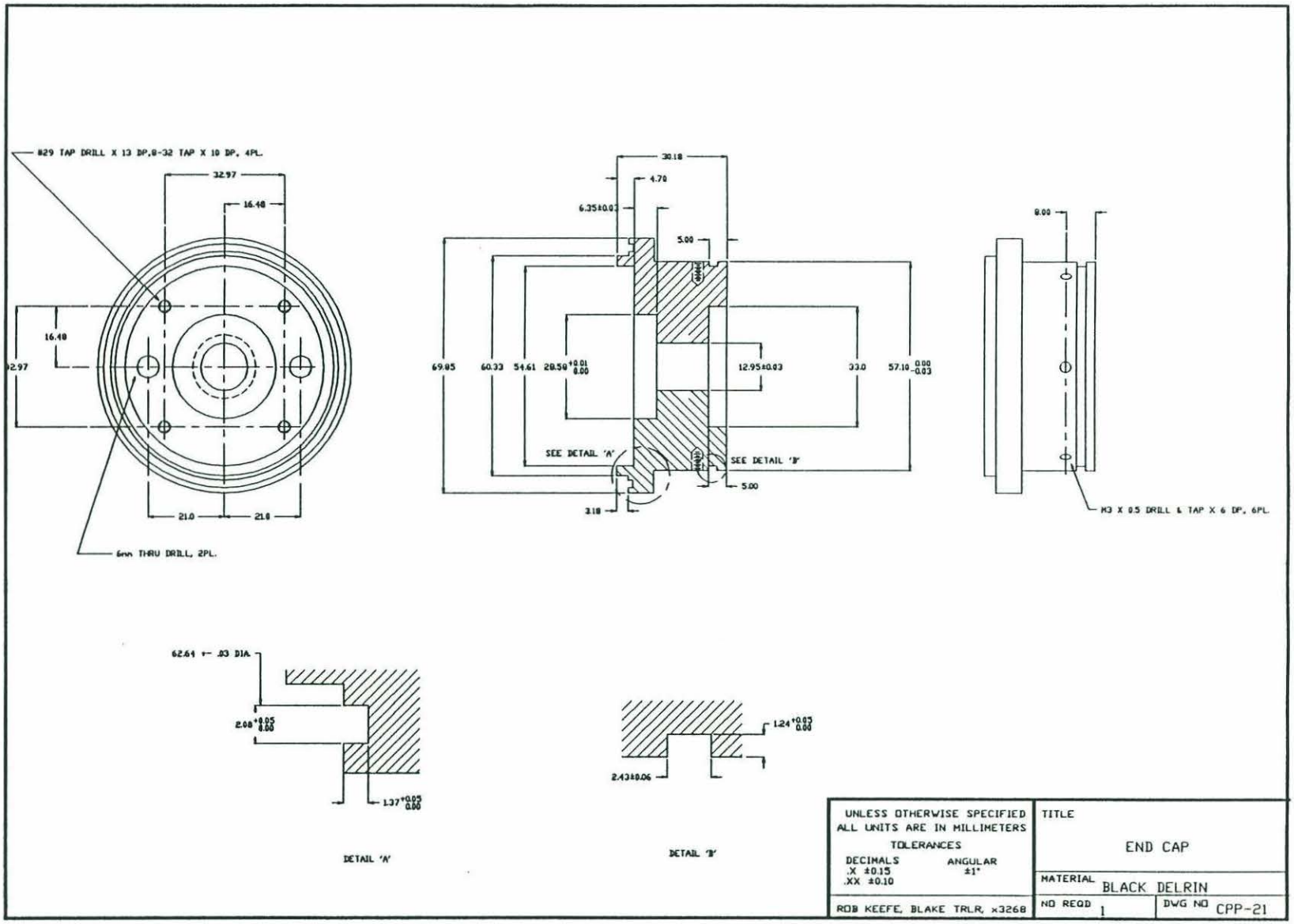
Ø29 TAP DRILL X 13 DP, 8-32 TAP X 10 DP, 4PL.
32.97
16.48
16.48
32.97
21.0
21.0
6mm THRU DRILL, 2PL.
30.18
4.70
6.35±0.03
5.00
69.85
60.33
54.61
28.50 +0.01 0.00
12.95±0.03
33.0
57.10 0.00 -0.03
SEE DETAIL 'A'
SEE DETAIL 'B'
5.00
3.18
8.00
M3 X 0.5 DRILL & TAP X 6 DP, 6PL.
62.61 +- .03 DIA.
2.08 +0.05 0.00
1.37 +0.05 0.00
DETAIL 'A'
1.24 +0.05 0.00
2.43±0.06
DETAIL 'B'
UNLESS OTHERWISE SPECIFIED
ALL UNITS ARE IN MILLIMETERS
TOLERANCES
DECIMALS
.X ±0.15
.XX ±0.10
ANGULAR
±1°
ROB KEEFE, BLAKE TRLR, x3268
TITLE
END CAP
MATERIAL
BLACK DELRIN
NO REQD
1
DWG NO
CPP-21

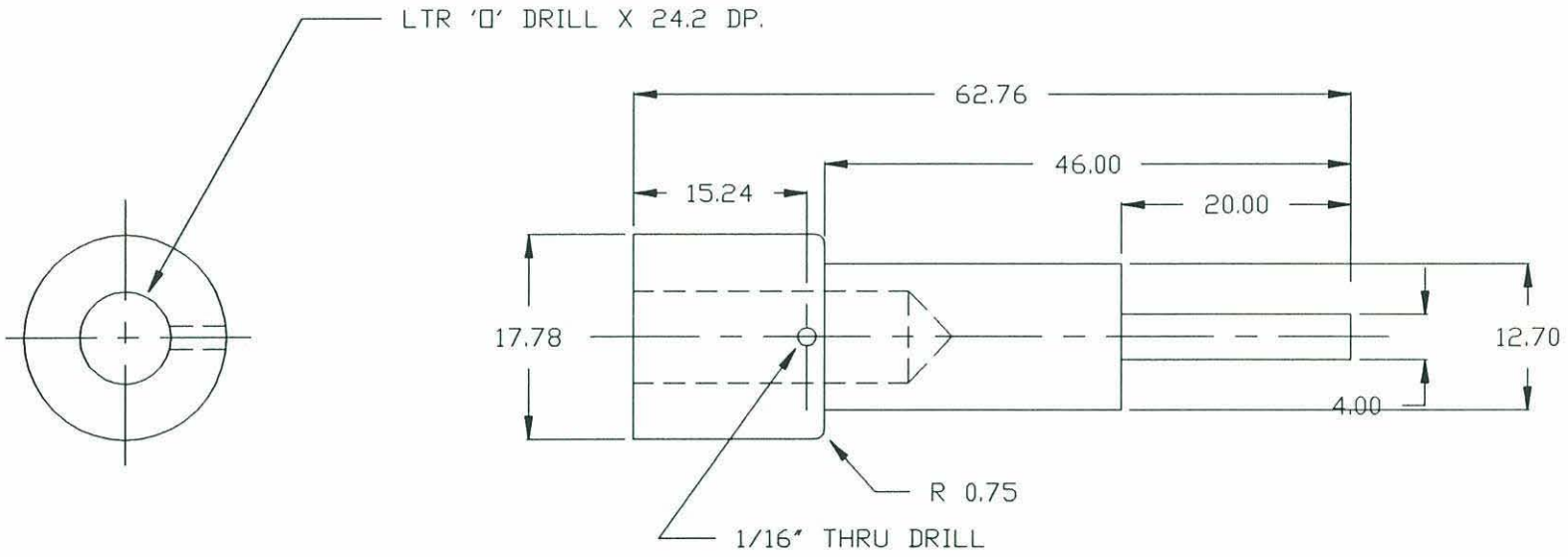

UNLESS OTHERWISE SPECIFIED ALL UNITS ARE IN MILLIMETERS TOLERANCES DECIMALS .X ±0.15 .XX ±0.10 ANGULAR ±1°	TITLE SERVO SHAFT
	MATERIAL 316 STAINLESS STEEL
ROB KEEFE, BLAKE TRLR, x3268	NO REQD 1 / DWG NO CPP-22

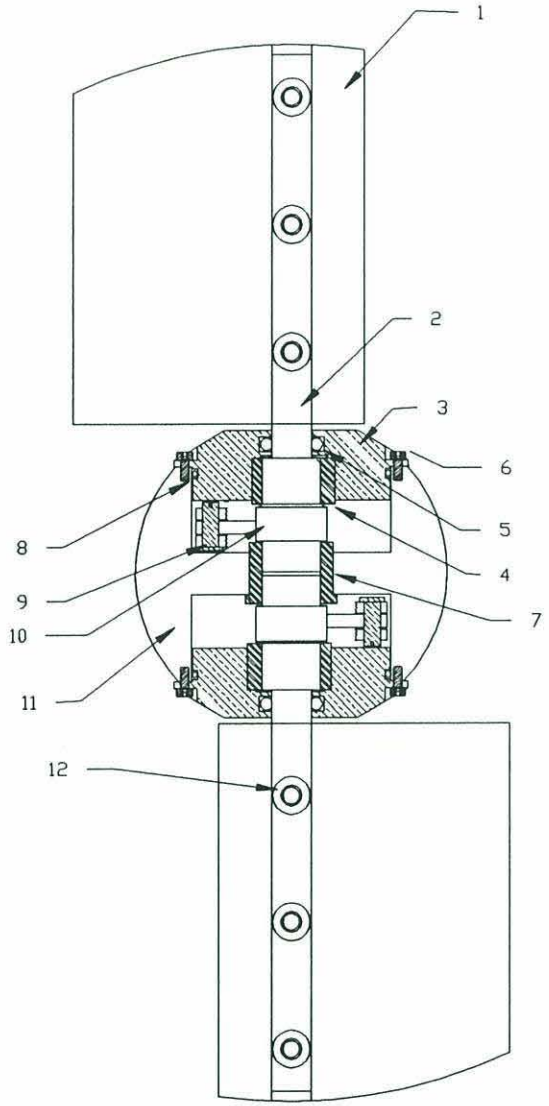

12	SCREW	M4X0.7X5 FLAT HD MACH SCRW	6
11	CPP-9	ROTATING HOUSING	1
10	CPP-5	SHAFT EAR	2
9	CPP-6	PIN	2
8	O-RING	2-031 N674-70	2
7	CPP-8	BUSHING	1
6	SCREW	M2X0.4X5 SOCKET HD CAP SCREW	10
5	O-RING	2-012 N674-70	2
4	CPP-7	BUSHING	2
3	CPP-4	CAP	2
2	CPP-3	SHAFT	2
1	CPP-1	BLADE	2

UNLESS OTHERWISE SPECIFIED
ALL UNITS ARE IN MILLIMETERS

TOLERANCES

DECIMALS
.X ±0.15
.XX ±0.10

ANGULAR
±1°

ROB KEEFE, BLAKE TRLR, x3268

TITLE

HUB ASSY DRAWING
(THRU SHAFTS)

MATERIAL

NO REQD

DWG NO CPP-25

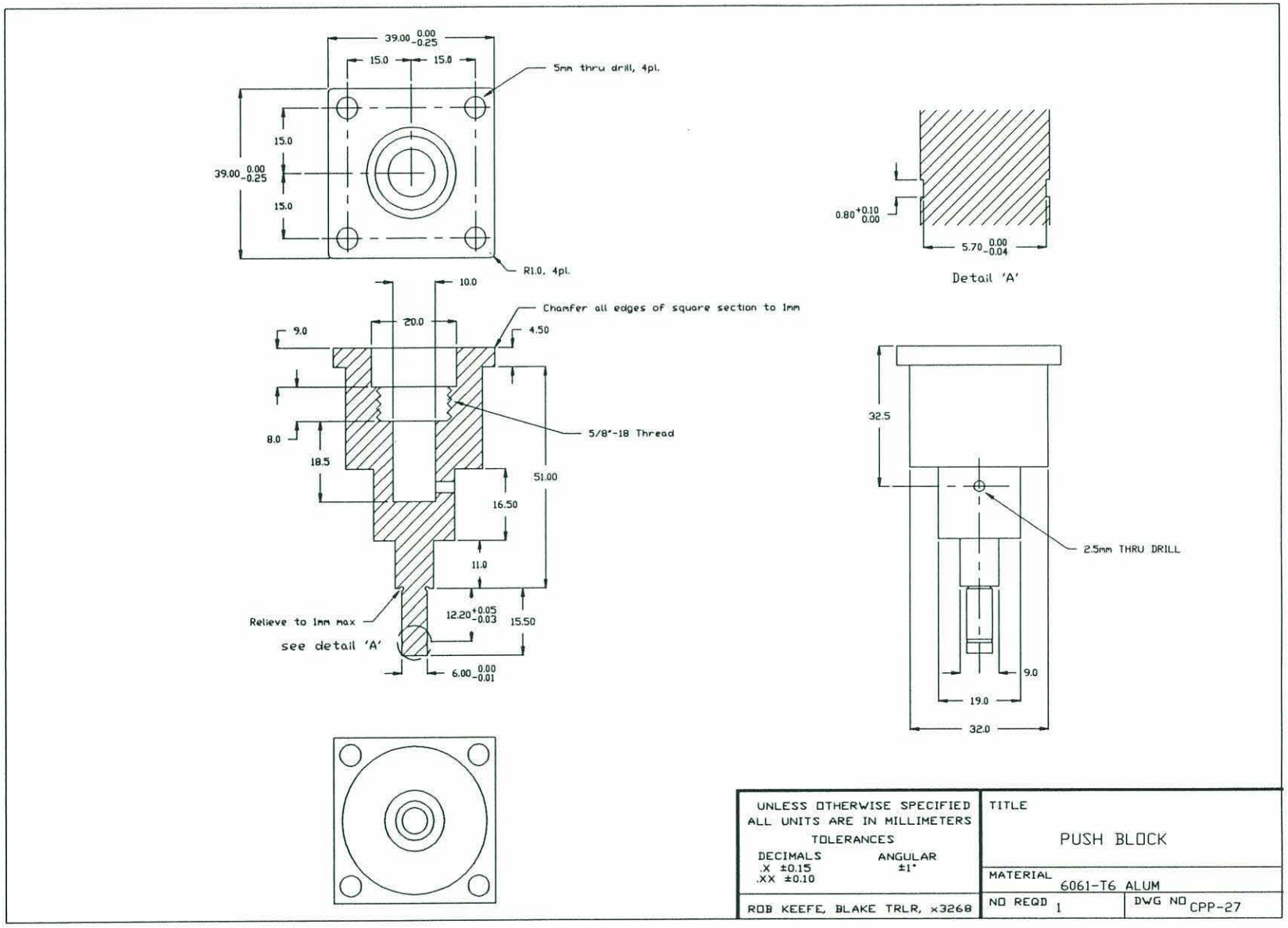
39.00 0.00 -0.25
15.0
15.0
5mm thru drill, 4pl.
15.0
39.00 0.00 -0.25
15.0
R1.0, 4pl.
10.0
Chamfer all edges of square section to 1mm
9.0
20.0
4.50
5/8"-18 Thread
8.0
18.5
51.00
16.50
11.0
Relieve to 1mm max
see detail 'A'
12.20 +0.05 -0.03
15.50
6.00 0.00 -0.01
0.80 +0.10 0.00
5.70 0.00 -0.04
Detail 'A'
32.5
2.5mm THRU DRILL
9.0
19.0
32.0
UNLESS OTHERWISE SPECIFIED
ALL UNITS ARE IN MILLIMETERS
TOLERANCES
DECIMALS
.X ±0.15
.XX ±0.10
ANGULAR
±1°
ROB KEEFE, BLAKE TRLR, x3268
TITLE
PUSH BLOCK
MATERIAL
6061-T6 ALUM
NO REQD 1
DWG NO CPP-27

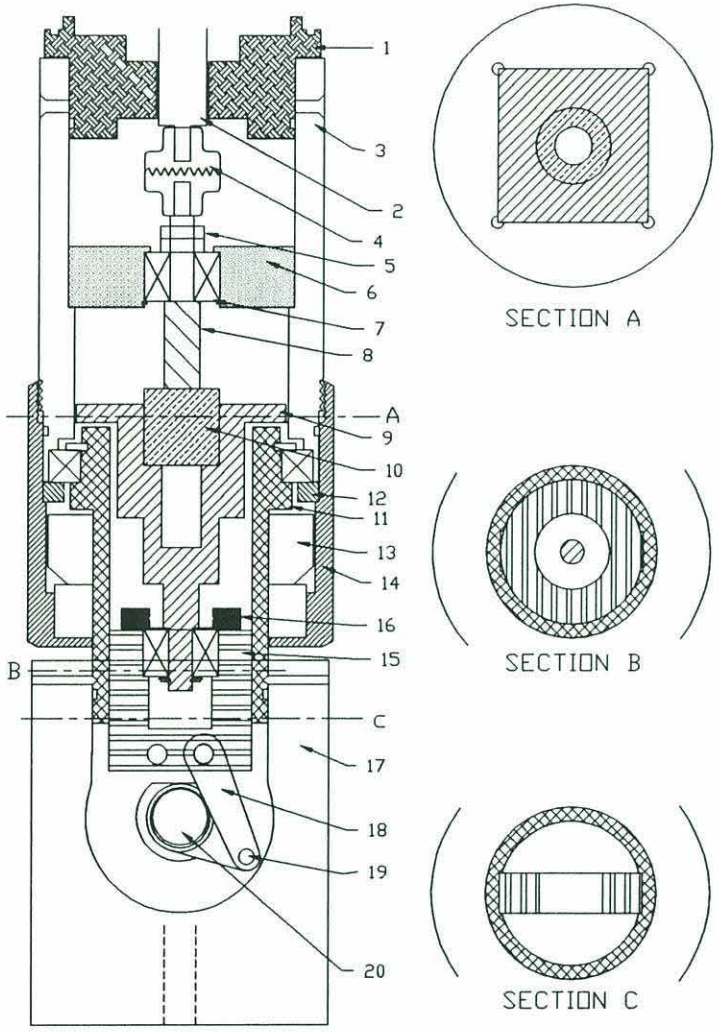

SECTION A

SECTION B

SECTION C

20	SHAFT	CPP-3
19	PIN	CPP-6
18	LEVER ARM	CPP-10
17	ROTATING HOUSING	CPP-9
16	PLATE	CPP-29
15	CROSSHEAD	CPP-11
14	BOOT	CPP-17
13	SHAFT SEAL	JOHN CRANE
12	SPACER	CPP-16
11	COUPLER	CPP-18
10	LEAD SCREW NUT	PIC DESIGN
9	PUSH BLOCK	CPP-27
8	LEAD SCREW	PIC DESIGN
7	DUPLEX BALL BEARINGS	BARDEN (2 SETS)
6	BEARING BLOCK	CPP-28
5	JAM NUTS	ALL STAINLESS
4	MULTI-JAW COUPLER	PIC DESIGN
3	STATIONARY HOUSING	CPP-20
2	SERVO SHAFT	CPP-23
1	END CAP	CPP-21

UNLESS OTHERWISE SPECIFIED
ALL UNITS ARE IN MILLIMETERS
TOLERANCES
DECIMALS .X ±0.15 .XX ±0.10
ANGULAR ±1°

ROB KEEFE, BLAKE TRLR, x3268

TITLE
HOUSING ASSY DRAWING

MATERIAL

NO REQD

DWG NO CPP-30

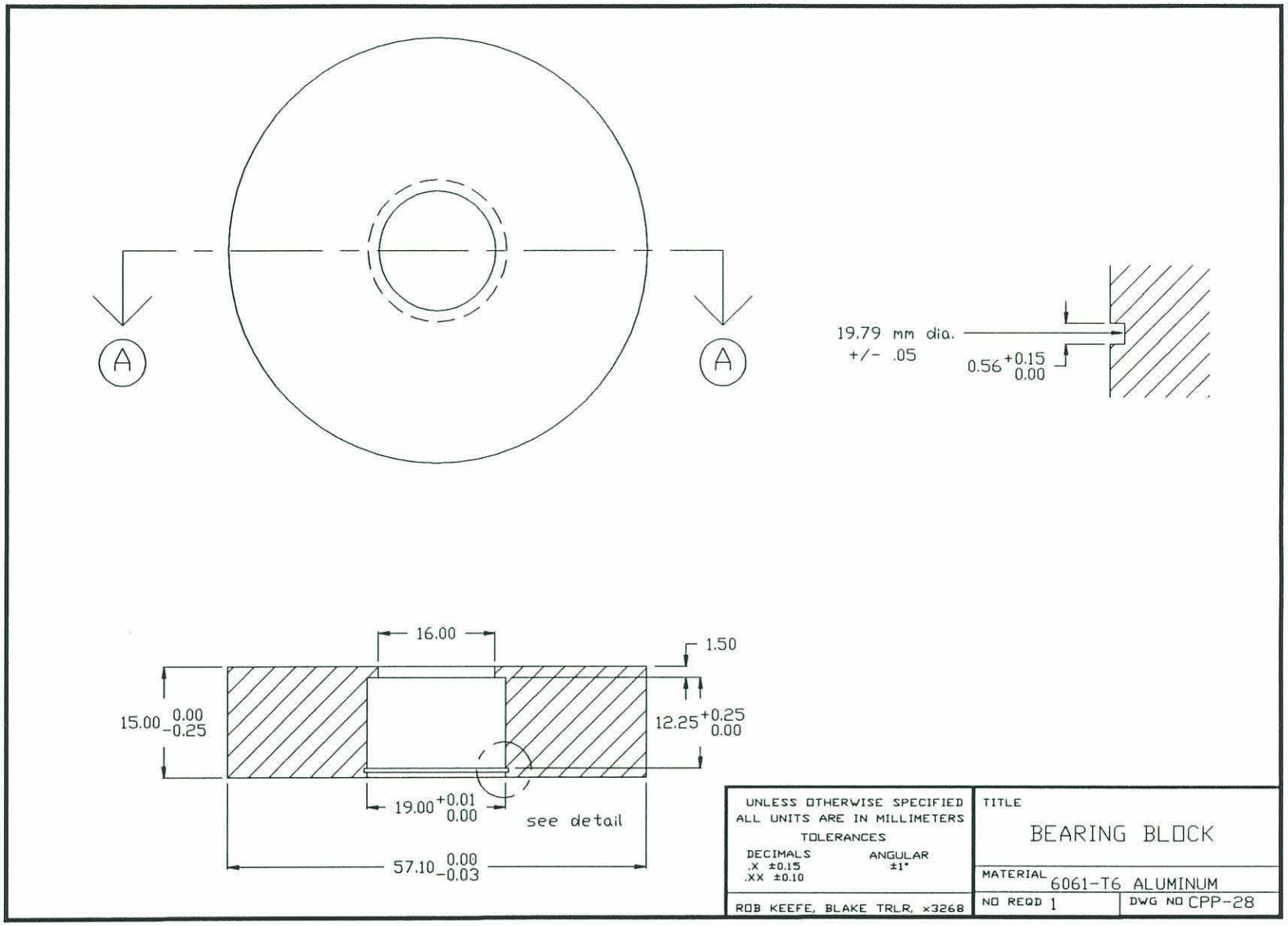
A
A
19.79 mm dia.
+/- .05
0.56 +0.15 0.00
16.00
1.50
15.00 0.00 -0.25
12.25 +0.25 0.00
19.00 +0.01 0.00
see detail
57.10 0.00 -0.03
UNLESS OTHERWISE SPECIFIED
ALL UNITS ARE IN MILLIMETERS
TOLERANCES
DECIMALS
.X ±0.15
.XX ±0.10
ANGULAR
±1°
ROB KEEFE, BLAKE TRLR, x3268
TITLE
BEARING BLOCK
MATERIAL 6061-T6 ALUMINUM
NO REQD 1
DWG NO CPP-28

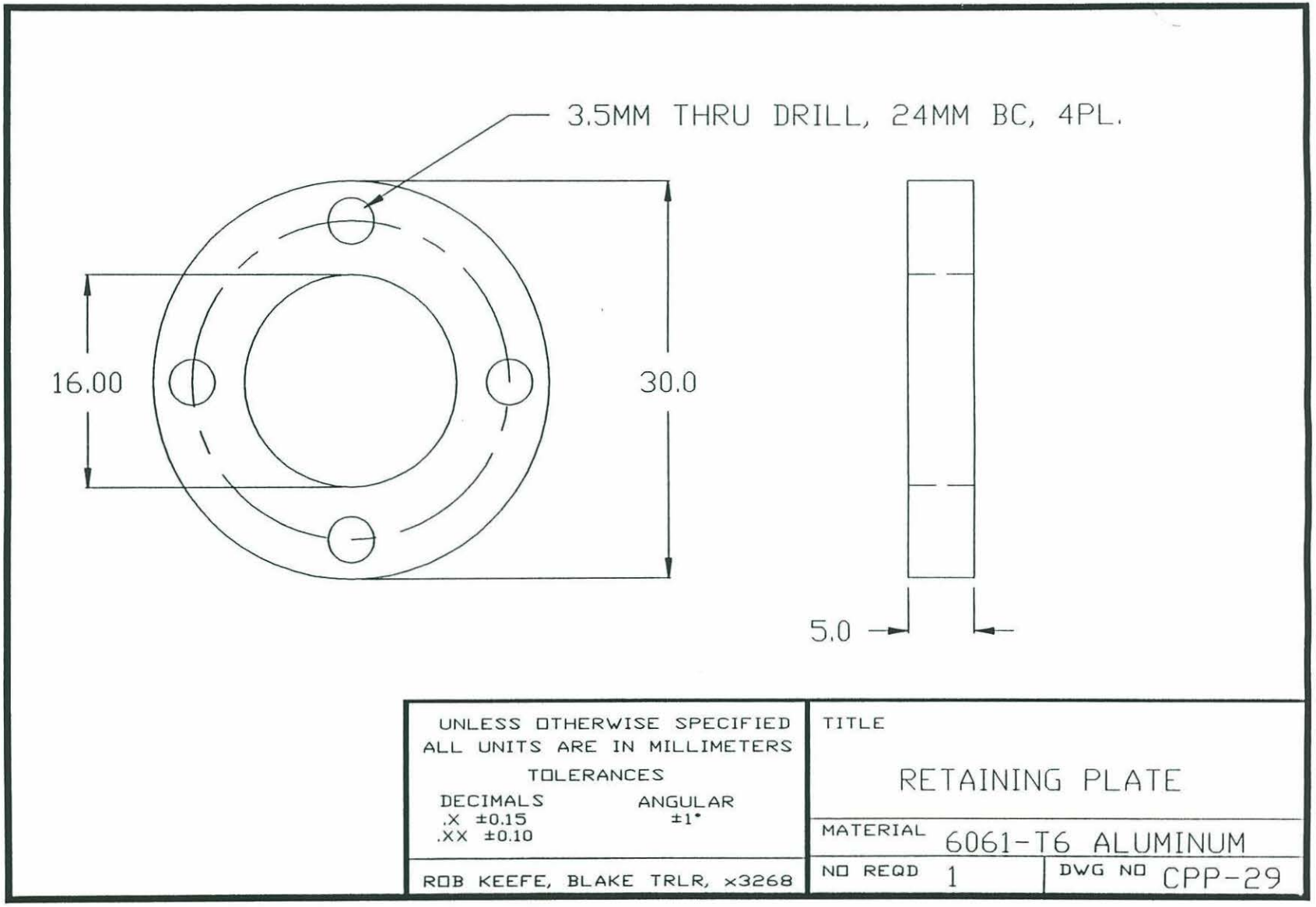

UNLESS OTHERWISE SPECIFIED ALL UNITS ARE IN MILLIMETERS TOLERANCES DECIMALS .X ±0.15 .XX ±0.10 ANGULAR ±1°	TITLE RETAINING PLATE
	MATERIAL 6061-T6 ALUMINUM
ROB KEEFE, BLAKE TRLR, x3268	NO REQD 1 / DWG NO CPP-29

Appendix C
DEBUGGING PROCEEDURE

Subsequent debugging revealed a number of minor design flaws.

1. The propeller blades failed to meet their designed range of motion. When first constructed, the blades were barely able to exceed 10 degrees in either direction. This was caused by interferrence between the crank arms, or links, and the coupler in one direction, and between the links and inner bushing in the other. The link was not sufficiently offset from the center of the housing and when the crosshead moved toward the rotating housing, the link would contact the part of the inner bushing protruding from its socket. When the crosshead moved away from the rotating housing, the links would contact the end of the coupler. To solve the first problem, washers were inserted between the links and the crosshead, allowing the links to clear the inner bushing. This worsened the interference between the link and the coupler. This problem was eased by milling away a portion of the end of the coupler to allow the links to attain their maximum angle. However, this led to interference between the links and the rotating housing. Filing away a small amount of material from both sides of the rotating housing eventually allowed the blades to attain their maximum angle.

2. Insufficient space was allowed for the wave washers in the two bearing sets. During design, the compressed thickness of the wave washer was assumed to be the thickness of the washer material with tolerance error acting only to ease washer compression. In practice, this thickness was very difficult to attain.The snap ring groove on the end of the push-block was widened by 0.5 mm to accomodate additional expansion of the washer. The bearing block was also modified to allow for additional expansion. Because the snap ring groove in the bore of this part was already very close to the edge of the bore, the expansion was accomplished by thinning the shoulder on the opposite end of the bore by 0.5 mm. Due to the difficulty of modifying the snap ring groove in the bore of the stationary housing, the wave washer used to secure the bearing block in place was omitted.

3. The snap ring groove in the bore of the bearing block was too shallow. Its diameter was increased by 1 mm.

4. The bearing block lacked holes for oil to flow through. Four holes were added matching the four holes on the push-block. The holes were countersunk to a depth of about 5 mm to ease oil flow.

The debugged system was connected to its servo motor and was operated under computer control. Testing revealed the aparatus to have approximately 3 degrees of backlash measured at the lead screw. Nearly 2 of the 3 degrees can be accounted for in axial play of the bearing block resulting from omission of the wave washer designed to

preload it. The remainder likely comes from small amounts of play in the link pivots and in the lead nut.

While the blade pitch was easy to control using the servo, the speed of the pitch change was limited by the servo motor controller. The gains for this controller were encoded on ROM on the controller board and not easily modified, and thus maximal pitch change speed was not realized.